Viral Sensitizers Potentiate the Infection of Cancer Cells via NF-κB

Submitted by
Michael Phan

A thesis submitted to the University of Ottawa in partial fulfillment of the requirements for the degree of

Master of Science, Specialization in Microbiology and Immunology

In

Faculty of Medicine
Department of Biochemistry, Microbiology, and Immunology

University of Ottawa
Ottawa, Ontario

Supervisor
Dr. Jean-Simon Diallo, PhD

© Michael Phan, Ottawa, Canada, 2020

Abstract

Genetically engineered oncolytic viruses (OVs) have been proven to be effective anti-cancer agents. However, the heterogeneity of tumours and obligate attenuation of OVs to achieve safety can limit their efficacy. Our lab has previously shown that diverse small molecules, which we have termed “Viral Sensitizers”, used in combination with OVs can potentiate the infection of cancer cells by OVs over 1000-fold in some cases, resulting in cancer-specific killing in both *in vitro* and *in vivo* tumour models. We observed that a subset of viral sensitizer compounds ultimately act by reducing the expression of IFNβ, thereby inhibiting antiviral signaling. Here, we aimed to further refine the mechanism of action of this class of compounds. Our results suggest that VSe1 and more stable analogs such as VSe1-28 inhibit nuclear accumulation of NF-κB p65 and expression of various antiviral cytokines including, TNFα, IL-6, IFITM1, and MX2 in multiple oncolytic VSV-resistant cancer cell lines but not in normal cells. This was also observed *in vivo* in CT26wt immune-competent mouse tumour models, where our group has already demonstrated the therapeutic benefit of combining VSe1-28 with oncolytic VSV. Using various biochemical methods, we have determined that VSe1 and its analog VSe1-28 lead to these effects at least in part through covalent modification of NF-κB p65. In sum, this study provides a new understanding of how these novel viral sensitizers work at the molecular level. This new understanding will not only aid in the discovery and development of improved molecules but also their clinical translation in combination with oncolytic viruses.

Acknowledgement

First I would like to thank Dr. Jean-Simon Diallo for this amazing opportunity to pursue graduate studies in his lab. Thank you for all the guidance and mentorship you have offered me in the past two years, not only for experiments and science but also in regards to my career goals. Thank you for always having your office door open and being so willing to stop everything you are doing to answer my questions.

Second I would like to thank everyone who has collaborated with me on this project, without whom this project would have been impossible to complete. To Dr. Ramya Krishnan and Nader El-Sayes, thank you for welcoming me with open arms when I first joined the lab and teaching me everything I needed to know, without the both of you, the transition would have been much more challenging. To Dr. Rozanne Arulanandam and Dr. Nicole Forbes, thank you for always being available to listen to my complaints about failed experiments and offering every piece of knowledge you have to help me complete this project. Thank you to all my fellow lab members, Anna Jirovec, Mohsen Hooshyar, Anabel Bergeron, Harsimrat Birdi, Adrian Pelin and others, for always being willing to offer your assistance for experiments and forming lifelong friendships that we can one day look back on. Thank you to the members of the Boddy and Smith labs with all their contributions to this project. We would not have completed this project without them. Thank you to my committee members Dr. Tommy Alain and Dr. John Pezacki for offering all your advice and guidance throughout my Masters. Also thank you Dr. John Pezacki and Geneviève Desrochers for welcoming me into their lab to conduct the click-chemistry experiments, without whom may not have ever worked.

Finally, a huge thank you to my parents, Charles and Doedoe, and Leah Clarke for all their love and support. Thank you for always being full of encouragement through challenges I have encountered not only during my education but also through life. To Leah, thank you for always pushing me to my full potential and believing in me, even when I stop believing in myself.

Table of Contents

Abstract ii

Acknowledgement iii

Table of Contents iv

List of Abbreviations vii

List of Figures ix

List of Tables x

List of Appendices x

1 Chapter: Introduction 1

1.1 Cancer History 1

1.2 Cancer Statistics 1

1.3 Hallmarks of Cancer 2

1.4 Cancer Immunoediting 2

1.5 Type 1 Interferon Pathway 3

1.6 Nuclear Factor-κB 4

1.6.1 Nuclear Factor-κB Signalling Pathway 4

1.6.2 NF-κB in Cancer 11

1.6.3 NF-κB Inhibitors 11

1.7 Current Cancer Therapy 17

1.8 Oncolytic Viruses 18

1.8.1 Development of Oncolytic Viruses 18

1.8.2 Oncolytic Vesicular Stomatitis Virus 20

1.9 Combination Therapy with Oncolytic Viruses 21

1.9.1 Small-Molecule Combination Therapy 21

1.9.2 Viral Sensitizers 28

1.9.3 VSe1 28
1.9.4 VSe1-28 29
1.10 Deducing the mechanism of action of VSe1 and VSe1-28 32
1.11 GSTP1-1 33
1.12 Rationale and Hypothesis 36
2 Chapter: Material and Methods 38
2.1 Drugs, Chemicals, and Cytokines 38
2.2 Viruses 38
2.3 Cell Lines 38
2.4 Isolate of Murine Hepatocytes 39
2.5 siRNA Transfection 39
2.6 Luciferase Reporter-Based Viral Titration Assay 40
2.7 Cell Viability Assay 40
2.8 Bradford Assay 41
2.9 Immunoblotting 41
2.10 Nuclear and Cytoplasmic Protein Extraction 42
2.11 Standard Plaque Assay 42
2.12 Activity-Based Protein Profiling 43
2.13 RNA Extraction 44
2.14 Quantitative Real Time PCR 45
2.15 *In vivo* Tumour Models 48
2.16 *In vivo* Imaging 48
2.17 Statistical Analysis 48
3 Chapter: Results 49
3.1 Identification of GSTP1-1 as an interacting molecule through ligand based affinity chromatography 49

3.2 VSe1 and VSe1-28 reduce nuclear accumulation of NF-κB and expression of NF-κB induced ISGs in various cancer cell lines 52
3.3 Covalent modification of NF-κB p65 identified as molecular target 66
3.4 VSe1-28 inhibits NF-κB target genes and interferon stimulated genes in mouse tumours 79
4 Chapter: Discussion 84
4.1 GSTP1-1 is not the molecular target of VSe compounds 84
4.2 VSe1 and VSe1-28 suppress p65 nuclear-translocation and inhibit target gene expression in various cancer cell lines 85
4.3 VSe1 analogs do not sensitize normal cells to viral infection 87
4.4 NF-κB p65 identified as a molecular target 88
4.5 VSe1-28 decrease expression of NF-κB target genes in mouse tumour models 91
5 Chapter: Conclusion 92
Appendices 93
Appendix A : Draft: Viral sensitizers suppress innate immunity to sensitize cancer cells to oncolytic virotherapy: Manuscript In Preparation 93
A.1 Manuscript in Preparation Text 93
A.2 Manuscript In Preparation Figures 125
References 136
Contributions from Collaborators 142
Curriculum Vitae 143

List of Abbreviations

ANK	Ankyrin repeats	**MS**	Multipe sclerosis
APC	Antigen-presenting cell	**MX2**	MX dynamin like GTPase 2
ATF-2	Activating transcription factor 2	**NDV**	Newcastle disease virus
CTLA-4	Cytotoxic T lymphocyte-associated antigen 4	**NEMO**	NF-κB essential modulator
DAMP	Damage associated molecular pattern molecules	**NF-κB**	Nuclear factor-κB
DHMEQ	Dehydoroxymethyl-epoxyquinomicin	**NIK**	NF-κB inducing kinase
DMD	Duschenne Muscular Dystrophy	**NRF2**	Nuclear factor (erythroid-derived 2)-like
DMF	Dimethyl fumarate	**OV**	Oncolytic virus
DMSO	Dimethylsulfoxide	**PAMP**	Pathogen associated molecular pattern molecules
ECM	Extracellular matrix	**PD-1**	Programmed cell death protein 1
Fluc	Firefly luciferase	**PD-L1**	Programmed death ligand 1
GFP	Green fluorescent protein	**PFU**	Plaque forming units
GLUT3	Glucose transporter 3	**RHD**	Rel homology domain
GM-CSF	Granulocyte-macrophage colony-stimulator factor	**RIG-I**	Retinoic acid-inducible gene I
GRR	Glycine rich region	**STAT**	Signal transducer and activator of transcription
GSH	Glutathione	**T-Vec**	Talimogene laherparepvec

GSTP1-1	Glutathione S-transferase π-1	**TAD**	Transactivation domain
HDACi	Histone deacetylase inhibitor	**TBTA**	Tris[1-benzyl-1H-1,2,3-triazol-4-yl)methyl]amine
HSV	Herpes Simplex Virus	**TCEP**	Tris(2-carboxyethyl)phosphine
IAP	Inhibitor of apoptosis	**TME**	Tumour microenvironment
IFITM1	Interferon induced transmembrane protein 1	**TNFα**	Tumour necrosis factor α
IFN	Interferon	**TNFR**	Tumour necrosis factor receptor
IKKs	Iκ*B* kinases	**TRAF**	TNF receptor associated factor
IL	Interleukin	**VEGF**	Vascular epithelial growth factor
IRF	Interferon regulator factor	**VEU**	Viral expression unit
ISG	Interferon stimulated genes	**VSe1**	Viral sensitizer 1
ISRE	Interferon stimulated response element	**VSe1-28**	Viral sensitizer 1-28
JAK	Janus kinases	**VSV**	Vesicular stomatitis virus
JNK	c-Jun N-terminal kinase	**WHO**	World Health Organization
MAPK	Mitogen activated protein kinase pathway	**WT VSV**	Wildtype Vesicular stomatitis virus

List of Figures

Figure 1. Schematic view of NF-**κ**B subunits. 8

Figure 2. Structure of NF-**κ**B p65/p50 heterodimer bound to PRDII element of IFN**β** promoter. 10

Figure 3. Mechanism of action of compounds combined with OVs. 25

Figure 4. Small molecule enhancers of oncolytic viruses..... 27

Figure 5. Chemical structure of VSe1 and VSe1-28..... 31

Figure 6. Schematic view of ligand based-affinity profiling. 35

Figure 7. GSTP1-1 fails to abrogate the viral sensitizing effects of VSe1. 51

Figure 8. VSe1 and VSe1-28 sensitize various cancer cell lines to VSVΔ51 infection. 55

Figure 9. VSe1 and VSe1-28 inhibit nuclear translocation of NF-**κ**B in multiple cancer cell lines. 57

Figure 10. VSe1 and VSe1-28 inhibit NF-**κ**B targeted genes and interferon stimulated genes.. 59

Figure 11. VSe1-28 does not enhance viral efficacy of VSV**Δ**51-fluc in primary murine hepatocytes..... 61

Figure 12. VSe1-28 does not inhibit expression of NF-**κ**B targeted genes and ISGs in primary murine hepatocytes. 63

Figure 13. Baseline expression of p65 induced genes higher in primary murine hepatocytes. 65

Figure 14. Schematic workflow of activity based protein profiling. 70

Figure 15. VSe and DMF probes still retain viral enhancement activity..... 72

Figure 16. Comparative Binding of DMF and VSe1-54 active probe. 74

Figure 17. DMF and VSe-1-54 active probe increase binding to heat inactivated lysate. 76

Figure 18. VSe1-28 blocks binding of DMF probe to NF-**κ**B p65. 78

Figure 19. VSe1-28 inhibits NF-κB target gene expression in mouse tumours. 81

Figure 20. VSe1-28 enhance VSVΔ51-Fluc infection in mouse tumour model. 83

List of Tables

Table 1. Classes of NFκB Inhibitors..... 16

Table 2. Primer sequences for quantitative RT-PCR. 47

List of Appendices

Appendix A: Draft: Viral sensitizers suppress innate immunity to sensitize cancer cells to oncolytic virotherapy: Manuscript in Preparation.……....93

A.1 Manuscript in Preparation Text…….93

A.2 Manuscript in Preparation Figures……..125

1 Chapter: Introduction

1.1 Cancer History

Cancer has afflicted humans for thousands of years, with one of the earliest documented records of cancer found in ancient Egyptian manuscripts[1]. Notably, the Smith papyrus written between 1500-1600 BC documented what is believed to be the first reference to breast cancer[1]. Along with those records, cancerous growths have been found in Egyptian and Peruvian mummies, with the oldest identified in a king found in Southern Siberia[1]. Hippocrates is credited for defining such malignant growths as "cancer". He has been documented to describe these ulcerating, non-healing lumps that range from benign to malignant tumours as *karkinos* and suggested surgery as a method to cure these *karkinomas*[1].

1.2 Cancer Statistics

In 2018, the World Health Organization (WHO) ranked cancer as the 2nd leading cause of death in the world with 1 in 6 deaths attributable to cancer [2]. In Canada today, it has become the number one cause of death in 2019 with 1 in every 2 Canadians developing the disease in their lifetime[3]. Additionally, treatments such as chemotherapy and radiation present a significant economic burden with costs increasing every years; in 2012, cancer care cost Canadians $7.5 billion, rising from $2.9 billion in 2005[3]. Further, cancer not only contributes to taxing the Canadian economy, it also represents significant emotional challenge for patients and families, incurring unexpected expenses including medical equipment, childcare, homecare, and transportation fees among others[3].

1.3 Hallmarks of Cancer

Cancer cells evolve through the accumulation of mutations that lead to characteristics defined by Hanahan and Weinberg as the "Hallmarks of Cancer". These include uncontrolled cellular metabolism, resistance to cell death, genomic instability, dysregulated angiogenesis, tissue invasion and metastasis, tumour-promoted inflammation, replicative immortality, bypassing of growth suppressors, uncontrolled proliferation, and evasion of immune recognition[4]. Tumour structure and growth are supported by the tumour microenvironment (TME) which consists of many players including the extracellular matrix (ECM), fibroblasts, neuroendocrine cells, adipose cells, immune-inflammatory cells, blood, and lymphatic networks[5]. Cancer-associated fibroblasts have been associated with tumour progression and direct stimulation of cancer cell proliferation through remodeling of the ECM, stimulation of angiogenesis, recruitment of inflammatory cells, and secretion of growth factors and cytokines [5]. Essentially all cancer therapies leverage the hallmarks of cancer as a basis of their cancer-selectivity, and modifying the supporting TME is increasingly popular as an approach to stop the growth of cancer cells.

1.4 Cancer Immunoediting

The immune system plays an important role in the progression of cancer. Originally, the immune surveillance theory suggested that the immune system recognizes and eliminates mutated cells[6]. Later this concept was refined as "Cancer immunoediting," recognizing the interaction and co-evolutionary relationship between the immune system and cancer [6]. The immune system can suppress and kill tumour cells but in doing so also helps shape the immune profile of the tumour[7]. From an immunological perspective, cancer occurs in three stages: elimination, equilibrium, and escape[6,7]. In the elimination stage, the immune system acts as a surveillance system, detecting and

eliminating mutated cells[6,7]. In the equilibrium stage, the growth of cancer cells that are not effectively eliminated by the immune system is in equilibrium wherein the immune system controls the net growth of tumours but also leads to alterations in cancer cell immunogenicity[7]. Eventually, this leads to one of the "Hallmarks of Cancer," escape from the immune system which leads these immunologically altered tumours to grow and establish their own immunosuppressive microenvironment[7]. During this stage, continuous rounds of immunoediting may take place. It is during this immunoediting stage where genes encoding for proteins and cytokines that can be detrimental to a growing tumour, such as interferon, are downregulated as they can stimulate the immune system, stop cell growth, and induce apoptosis[8].

1.5 Type 1 Interferon Pathway

Type 1 Interferons (IFN) are cytokines that include IFNβ, IFNα, IFNε, IFNκ, and IFNψ which all bind type 1 IFN receptor[9,10]. They are often activated following viral infection and have antiviral, anti-proliferative and immune-modulatory effects[9–11]. Type 1 interferons become activated after viral nucleic acids and proteins bind toll-like receptors or RNA helicase enzymes like retinoic acid-inducible gene I (RIG-I)[9]. IFNβ transcriptional activation requires a tri-partite activation of three signaling pathways forming an enhanceosome consisting of activating transcription factor 2 (ATF-2)/c-jun, interferon regulatory factor (IRF)-3/7, and nuclear-factor κB (NF-κB)[12]. This enhanceosome then plays a part in recruiting coactivators and chromatin remodelling proteins to the IFNβ promoter, resulting in IFNβ transcription, translation, and secretion[12]. The initial activation of the Type I IFN response requires IFNβ and IFNα4[13,14]. This first wave of Type I IFN acts in both an autocrine and paracrine fashion through interferon alpha receptor to induce a second wave of Type I IFN response that includes all members of the IFNα

family and IFNβ to further enhance the Type I IFN response[13,14]. Type 1 IFN activates the antiviral response through the JAK-STAT pathway. Type 1 IFN binds to the IFN alpha receptor which is associated with Janus kinases (JAKs)[15]. This leads to the downstream phosphorylation of both signal transducer and activator of transcription 1 (STAT1) and signal transducer and activator of transcription 2 (STAT2) which then associates with IFN-regulatory factor 9 (IRF9). This protein complex translocates into the nucleus and binds the IFN stimulated response elements (ISREs) leading to transcription of interferon stimulated genes (ISGs) and activation of the second wave of IFNβ and IFNα[13–15]. Activation of the type I IFN pathway stimulates over 300 ISGs that prevent viral replication within target cells and induces activation of innate immune cells[16]. These ISGs are able to inhibit the viral life cycle through multiple mechanisms including the prevention of virion release, inhibition of virus entry, and viral transcription[16]. One example is the MX2 gene, which encodes both MxA and MxB ISG products that have been shown to prevent the uncoating of proviral DNA from HIV-1 capsids and also prevent Herpes Simplex Virus (HSV)-1 DNA from translocating into the nucleus of target cells[17].

1.6 Nuclear Factor-κB

1.6.1 Nuclear Factor-κB Signalling Pathway

NF-κB is a transcription factor that plays many roles in the immune system including the regulation of pro-inflammatory cytokines and chemokines like IFNβ. The NF-κB transcription factor contains dimeric complexes of Rel (c-Rel), Rel A (p65), Relb, NF-κB1 (p50), and NF-κB2 (p52)[18–20]. All members possess a 300 amino acid long N-terminal Rel homology domain that is responsible for dimerization, nuclear translocation, association with IκBs, and DNA binding[18]. In addition, p65, RelB, and c-Rel also contain transactivation domains located on the C terminal

ends[18]. A schematic of NF-κB family members with the location of the Rel homology domain (RHD) and transactivation domain (TAD) is shown in **Figure 1**.

There are two pathways leading to NF-κB activation, 1) the canonical pathway which mediates a cell inflammation and survival response, and 2) the non-canonical pathway which mediates immune cell differentiation and lymphoid organogenesis[21]. In the canonical pathway, NF-κB is triggered by an NF-κB essential modulator (NEMO) dependent IκB Kinase 2(IKK2) [21]. This pathway is activated in the presence of pro-inflammatory signals including cytokines, pathogen-associated molecular patterns (PAMPs), and danger-associated molecular patterns (DAMPs)[21]. The most common dimer in this pathway is p65-p50. NF-κB in its inactive state is bound by IκBα, IκBβ, or IκBε[21]. IκBα has a nuclear export signal which keeps NF-κB at high levels in the cytoplasm[18]. Alternatively, NF-κB -IκBβ complexes are sequestered in the cytoplasm as IκBβ blocks the nuclear localization signals[18]. Upon activation of NF-κB by TLRs, β-Interleukin-1 Receptor (IL-1R), or Tumour necrosis factor receptor (TNFR), IκB is phosphorylated by canonical IKKs, followed by ubiquitination and degradation of IκBs[18,19]. NF-κB can then translocate and sequester into the nucleus and bind to target DNA promoter sites like the IFNβ promoter and activate downstream antiviral signaling **(Figure 2)**.

The distinction between the canonical and non-canonical pathway is such that in the non-canonical pathway, NF-κB activation is mediated through a NEMO independent IKK1 complex[21]. This pathway is mainly activated through survival signals like cellular inhibitor of apoptosis (cIAP1 and cIAP2), TNF receptor-associated factor (TRAF2 and TRAF 3), and NF-κB inducing kinase (NIK)[21]. An increase in the accumulation of NIK triggers phosphorylation of p100 and activation of IKK1[21]. This causes partial degradation of the C-terminus of p100 and inactivation

of the associated IκBδ, leading to the release of both RelB-p50 and RelA-p50 dimers[21]. The phosphorylation of p100 and activation of IKK1 also causes the processing of newly synthesized p100, resulting in nuclear translocation of RelB-p52 dimers[21].

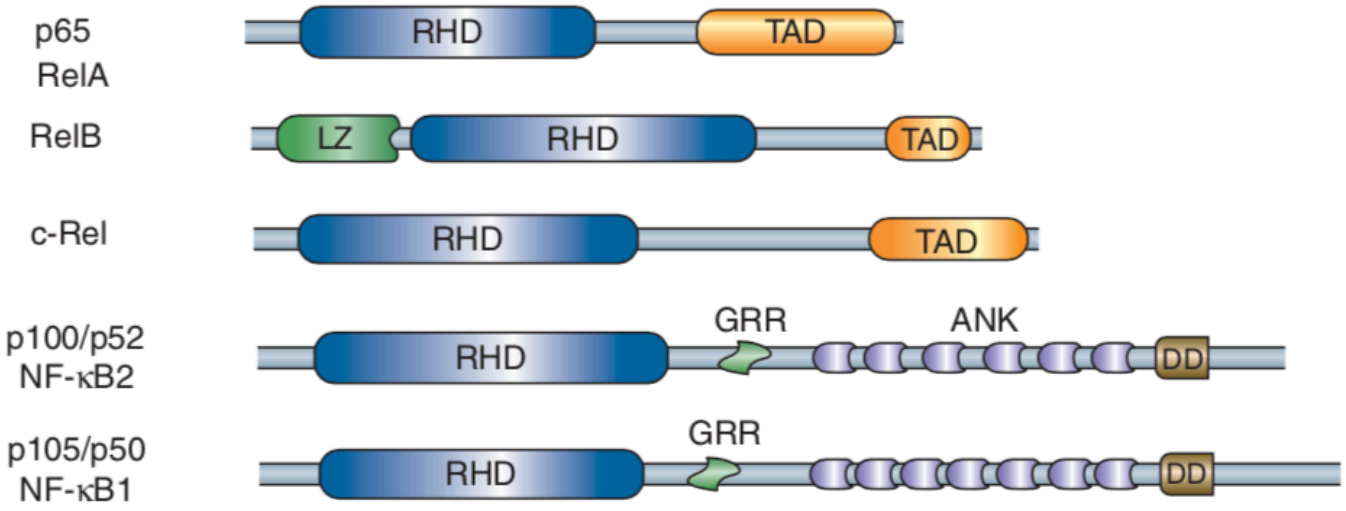
p65
RelA
RHD
TAD
RelB
LZ
RHD
TAD
c-Rel
RHD
TAD
p100/p52
NF-κB2
RHD
GRR
ANK
DD
p105/p50
NF-κB1
RHD
GRR
DD

Figure 1. Schematic view of NF-κB subunits.
NF-*κ*B members all ccontains a Rel Homology domain (RHD) responsible for dimerization, DNA binding, associations with I*κ*Bs, and nuclear translocation. Only some members including p65, RelB and c-Rel possess a transactivation domain (TAD). GRR: glycine rich regions, ANK: ankyrin repeats, DD: death domain. Figure adapted from Oeckinghaus and Ghosh, 2009[22]. © Cold Spring Harbor Laboratory Press

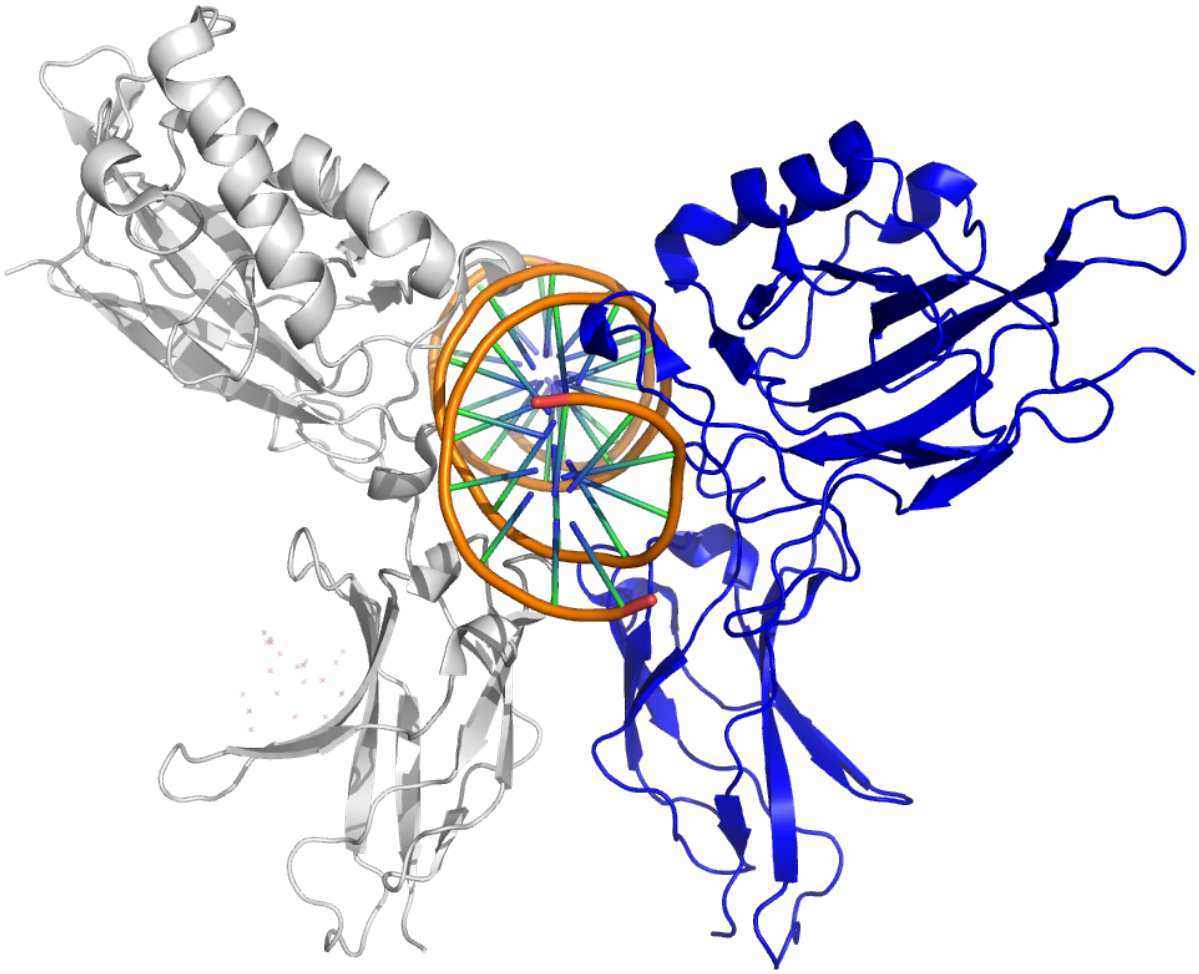

Figure 2. Structure of NF-κB p65/p50 heterodimer bound to PRDII element of IFNβ promoter.
The structure and interaction of p65 (blue) and p50 (Grey) bound to a DNA region in the PRDII element of IFNβ promoter. Image was generated using PyMOL Molecular Graphics system. Crystal structure adapted from Escalante et. al., 2002.

1.6.2 NF-κB in Cancer

Activation of NF-κB helps advance many of the hallmarks of cancer as it promotes transcription of genes involved in cell proliferation, survival, angiogenesis, inflammation, and tumour promotion and metastatsis[18,23]. Chromosomal translocations, deletions, and other mutations that often occur in cancer cells drive the disruption of NF-κB genes or genes controlling the activation of NF-κB, frequently leading to constitutive NF-κB activation[23]. NF-κB can then activate genes that prevent apoptosis and stimulate cell proliferation[23]. In addition, NF-κB has been shown to promote transcription of genes like Vascular Epithelial Growth Factor (VEGF) which can promote tumour angiogenesis[24]. More recently, there is evidence that NF-κB also plays a role in changing tumour metabolism to increase glucose transporter 3 (GLUT3) to allow for higher levels of glycolysis to take place, allowing for increased energy consumption and growth[24].

1.6.3 NF-κB Inhibitors

Due to NF-κB involvement in multiple hallmarks of cancer, many therapeutic attempts have focused on developing strategies to block its activation. In addition, constitutive NF-κB activation has been shown in haematological malignancies like multiple myeloma, and B-cell lymphoma, as well as solid tumours including breast, renal, bladder, and colon cancers[25]. Currently, a limited number of NF-κB inhibitors are being used in the clinic although many compounds with anti-inflammatory and anti-cancer properties have been proven to inhibit NF-κB. There are several classes of compounds that inhibit different steps of the NF-κB pathway, these include upstream of IKK inhibitors, IKK inhibitors, proteasome inhibitors, and NF-κB nuclear translocation or DNA binding inhibitors. A table of NF-κB inhibitors mentioned in this thesis is listed in **Table 1**.

One strategy is to block NF-κB activation upstream of IKK. NIK SM1 is a small molecule inhibitor that targets and inhibits NIK activation leading to decreased activation of NF-κB pathways[26]. Inhibition of NIK using NIK SM1 leads to suppressed immune responses and pro-inflammatory gene expression, improving disease outcome, kidney function, and survival in a systemic lupus erythematosus mouse model[26]. Another example is curcumin, a natural product used for its cytoprotective properties against cancer shown to inhibit NIK/IKK complex and downregulate NF-κB activation[27]. It is thought this inhibition of NIK/IKK is responsible for curcumins ability to inhibit COX2 and attributes to its chemopreventive properties[27].

Another class of NF-κB inhibitors are IKK inhibitors. TPCA-1 is an IKK inhibitor that inhibits downstream NF-κB activation and target genes including TNFα, IL6 and, IL-1β[28]. In addition, TPCA-1 also inhibits STAT3 phosphorylation, DNA binding, and transactivation[29]. TPCA-1 when used for treatment of non-small cell lung carcinomas also showed growth repression *in vivo*[29]. Other IKK inhibitors include wedelolactone and parthenolide[23,30]. Wedelolactone is a natural compound that not only inhibits IKK but has also been shown to downregulate protein kinase Cε triggering apoptosis in prostate cancer cells[31]. Parthenolide is another natural compound derived from the plant feverfew that has anti-inflammatory properties[30]. It specifically interacts with Cys 179 on IKKβ and inhibits NF-κB activation[30]. Another small molecule inhibitor PS-1145 acts as an antagonist to IKK and blocks IκBα degradation[32]. PS-1145 shows anti-cancer properties against multiple myeloma and prostate carcinoma[32,33].

As NF-κB activation requires the ubiquitination and degradation of IκBα, one class of inhibitor targets proteasomes that mediate this process. Bortezomib is a boronic acid dipeptide that can inhibit the 26s proteasome, preventing degradation of IκBα and therefore downstream NF-κB activation[34]. Bortezomib is approved by the FDA for the treatment of multiple myeloma

and mantle cell lymphoma[34]. Another proteasome inhibitor is a small molecule Ro106-9920 which inhibited IκBα degradation and downstream activation of NF-κB[32]. This small molecule was shown to have anti-inflammatory properties in mouse models[35].

Other classes of inhibitors aimed to block the last steps before NF-κB activation, including nuclear translocation and DNA binding. Dehydroxymethyl-epoxyquinomicin (DHMEQ) is derived from the antibiotic epoxyquinomicin C[36]. DHMEQ has both anti-inflammatory and anti-tumour properties and inhibits both canonical and non-canonical NF-κB nuclear translocation[32,36,37]. In addition, DHMEQ was shown to induce apoptosis and cause cell-cycle arrest in human hepatoma cells[36]. Finally, sesquiterpene lactones, which possess anti-inflammatory properties and act through modifying the Cys38 region of p65, located in the DNA-binding loop[38]. This leads to inhibition of NF-κB DNA binding and activation.

In recent years, there have been several clinical trials conducted in an attempt to modulate NF-κB activity for various ailments. One example is a topical treatment for atopic dermatitis using an NF-κB decoy which consists of oligodeoxynucleotides that mimic the NF-κB binding sequence on chromosomal DNA (NCT00125333). Another example was a trial where an NF-κB inhibitor, edasalonexent, was shown to be effective at inhibiting NF-κB p65 dependent inflammatory responses for the treatment of Duchenne Muscular Dystrophy (DMD)[39]. But so far, treatments have been met with limited success due to off-target toxicity.

Due to the many roles of the NF-κB pathway including inflammation, proliferation, cell survival, regulation of immune function, and production of cytokines and chemokines, inhibition could lead to unwanted side effects and toxicities. Also, many of these inhibitors are not specific and can cause off-target effects. In addition, prolonged inhibition of NF-κB pathway could lead to dysregulation of host defenses[40]. Combination therapies with NF-κB inhibitors may prove to be

more effective in order to limit side effects and increase the efficacy of these compounds. There are already some promising examples. Bortezomib has been shown to increase the sensitivity of both chemo and radiotherapy in colorectal cancer. It is thought Bortezomib inhibits NF-κB activation caused by chemo and radiotherapy[34]. TPCA-1, when combined with tyrosine kinase inhibitors like Gefitinib, was able to enhance apoptosis in non-small cell lung cancers[29]. Also, TPCA-1 has shown promising results when combined with oncolytic viruses; inhibiting ISGs and increasing viral infection in malignant peripheral nerve sheath tumour[41].

Class	Name	Target	Mechanism of Action	Reference
Upstream of IKK Inhibitor	NIK SMI1	NF-κB inducing kinase (NIK)	Inhibits NIK and activation of NF-κB non-canonical pathway activation	Brightbill et. al. (25)
	Curcumin	NIK/IKK	Inhibit NIK/IKK complex preventing downstream activation of NF-κB and cyclo-oxygenase 2	Plummer et. al. (26)
IKK Inhibitor	TPCA-1	IκB kinase	Inhibits IKK and subsequent IκBα degradation	Nan et. al. (28)
	Wedelolactone	IκB kinase	Inhibits IKK and subsequent IκBα degradation	Park and Hong (22)
	Parthenolide	IκB kinase	Directly interacts with Cys 179 and inhibits IKKβ	Kwok et. al. (29)
	PS-1145	IκB kinase	Inhibits IKK and subsequent IκBα degradation	Yemelyanov et. al. (32)
Proteasome Inhibitor	Bortezomib	26s Proteasome	Inhibits 26s proteasome preventing degradation of IκBα	Baud and Karin (24)
	Ro106-9920	IκBα	Inhibits ubiquination of IκBα	Swinney et. al. (34)
NF-κB nuclear translocation or DNA binding inhibitor	Dehydoroxymethyl-epoxyquinomicin (DHMEQ)	NF-κB nuclear translocation	Inhibits nuclear translocation of canonical and non-canonical NF-κB dimers	Umezama (36)
	Sesquiterpene lactones	p65	Directly binds p65 and inhibits DNA binding, NF-κB activation, and downstream pro-inflammatory cytokines	García-Piñeres et. al. (37)
	Edasalonexent	p65	Inhibits p65 dependent inflammatory response and downstream pro-inflammatory genes	Donovan et. al. (38)
	Epoxyquinone A monomer	IKKβ and p65	Directly binds both IKKβ and p65 inhibiting downstream signaling of NF-κB activation	Liang et. al. (75)
	Dimethyl Fumarate	p65	Directly binds p65 and inhibits nuclear translocation of p65	Kastrati et. al. (77)

Table 1. Classes of NF-κB Inhibitors.
NF-κB inhibitors block different parts of the pathways. Listed here are different classes of NF-κB inhibitors with examples and their targets and mechanism of action.

1.7 Current Cancer Therapy

Common cancer treatment options presently rely on chemotherapy on its own or in combination with surgery and radiotherapy. Chemotherapy drugs such as paclitaxel target all fast growing cells in the body, whether they are tumour or normal cells, by stabilizing cell microtubules and inhibiting depolymerization of microtubule units and thereby blocking progression of the cell cycle [42,43]. Platinum-based chemotherapeutic agents like cisplatin[44] are being used to treat almost half of all cancer patients. Cisplatin works by crosslinking purine bases in DNA and inhibiting repair mechanisms, thereby causing irreparable DNA damage and cancer cell death[45].

Radiotherapy uses ionizing radiation to deposit energy into tissues it penetrates [46]. This energy can kill cancer cells through mainly two mechanisms: 1) directly, through damage of cellular DNA inhibiting cell proliferation or 2) indirectly, through the production of free radicals that cause DNA damage and cell death[46].

Standard strategies to eradicate cancer are not specific and induce many side effects. Chemotherapy treatments are often administered through short repeated rounds where the highest possible dose of these cytotoxic drugs are administered, and lengthy recovery periods are required for normal cells to recover from the therapy[47]. Furthermore, radiotherapy, like chemotherapy, still presents many challenges in selectively providing ionizing radiation to cancerous cells, although methods like dose fractionation and new technological advances are in place to minimize toxicities[46]. More targeted therapies are required in the quest to find better treatment options for cancer.

Based on the hallmarks of cancer, certain biologics have been developed in an effort to target more specific molecular pathways and characteristics of cancer cells that distinguish them from normal cells, thereby limiting potential harmful off-target effects that treatments like

chemotherapy and radiotherapy have. For example, biological treatments have been used to target epidermal growth factor receptors (EGFR) either with monoclonal antibodies like cetuximab or trastuzumab, which target HER2 receptors present on some breast cancer cells[47]. Other treatments target EGFR using small molecule inhibitors like gefitinib or erlotinib[47].

More recent advances in immune checkpoint blockade have shown some promising results. Most immune checkpoint blockade therapies center around monoclonal antibodies against cytotoxic T lymphocyte-associated antigen 4 (CTLA-4) or programmed cell death protein 1 pathways (PD-1/PD-L1). CTLA-4 and PD-1/PD-L1 play a crucial role in the negative suppression and modulation of T cell activity and by blocking these signals, immune checkpoint blockade therapies attempt to reactivate immune surveillance often suppressed during the cancer immunoediting stage. Thus, using monoclonal antibodies like ipilimumab (anti-CTLA-4) and nivolumab/pembrolizumab (anti-PD-1) can delay or prevent T-cell silencing[48,49]. By blocking these signals, immune checkpoint blockade allows for reactivation of the immune system and better control of the tumour. However, so far monotherapies using immune checkpoint blockade have only been successful in a subset of patients and malignancies.

1.8 Oncolytic Viruses

1.8.1 Development of Oncolytic Viruses

The development of oncolytic viruses (OVs) first started from the observation that tumours were regressing in certain patients who had a viral infection[50]. This led to studies conducted in the 1940s using unmodified viruses that sometimes led to dangerous outcomes, including death[50]. In the 1940s, there were two cases in which patients with Hodgkin's disease who also were infected with viral hepatitis showed improvement in Hodgkins disease prognosis[51]. This led to one of the

first trials involving OVs conducted on patients with Hodgkin's disease using Hepatitis B virus from unpurified human serum and tissue extracts that were administered through parenteral injections[51]. Although some improvement in Hodgkin's disease was noted, the potential dangers of viral hepatitis infection to patients was too high to be deemed a successful therapeutic measure[51].

Natural viruses which are not genetically modified, like Newcastle disease virus (NDV), mumps virus, and reovirus already have tropism for tumour cells[52]. With advancements in molecular techniques, viruses can now be genetically modified to be attenuated and targeted towards certain cell types. Indeed viruses such as adenovirus, vesicular stomatitis virus (VSV), vaccinia virus, and herpes simplex virus can among others be genetically engineered to increase tropism for cancer cells[52]. In addition, humans are not natural hosts to some viruses including VSV and NDV[53,54], which minimizes risks of unwanted infection and increases safety profiles. Whether there is natural or engineered tumour tropism, viruses are attracted to biological characteristics of tumours including their ability to evade immune system detection and destruction, promote uncontrolled cellular metabolism, resistance to apoptosis, and defective innate antiviral responses[8,50]. Oncolytic viruses can kill cancer cells through four main mechanisms: 1) direct virus-mediated cytotoxicity or indirect mechanisms including 2) reactivation of systemic anti-tumour immunity, 3) damage of blood vessels surrounding tumors, and 4) therapeutic effects of transgenes incorporated into genetically engineered viruses[50,55,56].

The first oncolytic virus to receive clinical approval was adenovirus H101 in China in 2005 which was used in combination with chemotherapy for treatment of nasopharyngeal carcinoma[57]. In 2015 the Food and Drug Administration and European Medicines Agency approved talimogene laherparepvec (T-Vec). T-Vec is a genetically modified herpes simplex virus, type 1 that has both γ-34.5 genes deleted to attenuate the virus and prevent neurovirulence[55,58]. Further, two copies of

human granulocyte-macrophage colony-stimulating factor (GM-CSF) were inserted to promote differentiation of antigen-presenting cells (APCs) in infected tumours [55,58]. T-Vec is currently approved for advanced stage melanoma, but there are multiple clinical trials ongoing for T-Vec to be used for other cancers including head and neck cancers and Merkel cell carcinomas, as well as combination therapies of T-Vec with checkpoint inhibitors[58].

1.8.2 Oncolytic Vesicular Stomatitis Virus

Vesicular stomatitis virus (VSV) is an enveloped, bullet shaped, negative-sense RNA virus belonging to the *Rhabdoviridae* family[59]. The two major strains are VSV-Indiana and VSV-New Jersey and both are endemic to parts of Central and South America as well as parts of the United States infecting mostly horses, cattle, and pigs [59]. Most of these infections are non-lethal and appear as fever and blister-like lesions in the oral cavity, feet, and teats[59]. There has been only one case of wildtype VSV (WT VSV) mediated encephalitis in humans[59].

The VSV genome consists of 11,000 nucleotides coding for 5 viral proteins: the nucleocapsid (N), phosphoprotein (P), matrix (M), glycoprotein (G) and large polymerase (L)[59,60]. It infects cells through its glycoprotein (G) which mediates attachment onto ubiquitously expressed low-density lipoprotein receptors (LDLR), followed by endocytosis and internalization into endosomes[60]. Acidification of the endosome causes a conformational change of the G protein, facilitating fusion of the viral envelope to the endosomal membrane and release of the viral genome and proteins in the cytoplasm of the cell[59,60]. The genome, which is protected by the nuclease-resistant N protein, then serves as the template that is transcribed by the VSV polymerase complex consisting of the L and P proteins[59]. The M protein contributes to VSV's pathogenic effects. The M protein binds the nuclear envelope of cells and inhibits the nuclear to cytoplasmic transport of

cell RNA and proteins, and accounts for VSV's ability to block host anti-viral interferon responses[59,60].

Due to the relatively low rate of pre-existing immunity to VSV in the human population, and its ability to rapidly replicate and cause cytotoxicity, it is an attractive platform for oncolytic virotherapy[60]. In order to make WT VSV oncoselective and to improve its safety profile, oncolytic VSV derivatives are often attenuated via genetic modification. One way is a deletion of the 51st methionine of the M protein resulting in VSVΔ51. As the M protein blocks nuclear to cytoplasmic transport of cell RNA and proteins, including antiviral mediators, defects in this protein prevents VSVΔ51 from evading innate antiviral defense mechanisms and only allows replication in IFN defective cells, which is often the case in cancer cells as a consequence of cancer immunoediting[59].

1.9 Combination Therapy with Oncolytic Viruses

1.9.1 Small-Molecule Combination Therapy

Limited clinical efficacy of oncolytic viral therapy has been observed due to tumour heterogeneity and remains a major obstacle in the field [56]. Approximately 30-35% of tumours retain some level of antiviral defense, which severely limits the efficacy of oncolytic viruses like VSVΔ51 that are attenuated in their ability to combat innate antiviral defense mechanisms[61]. Many researchers are now using drug-OV combinations to augment the limitations of OV monotherapy as an alternative to direct genetic insertion of therapeutic transgenes, which could also offer benefits in OV safety profiles.

Currently, many different compounds are being examined that can enhance viral infection of cancer cells in different ways, many of which have been discovered by our group, including vanadium compounds, fumaric and maleic acid esters, and microtubule targeting agents[62–64]. Drug

combinations aim to drive viral efficacy in 4 main ways, by 1) increasing replication/spread of OVs, 2) increasing bystander killing of surrounding cells, 3) achieving systemic immunosuppression, and 4) increasing apoptosis/stress response[65] **(Figure 3)**. These compounds are diverse in structure and function and many are already in use to treat other diseases **(Figure 4)**. Many groups have looked at combining already clinically approved chemotherapeutics, like cyclophosphamide; which is already part of the standard chemotherapeutic regimen used currently to treat lymphomas[66], with OVs. Paclitaxel, another chemotherapeutic used in the treatment of breast, ovarian, and non-small lung cancer has also been shown to enhance the effect of oncolytic Maraba virus in syngeneic murine breast cancer models[64]. Chemotherapeutics have been credited with their ability of synergistic cell killing and apoptosis as well as stimulation of anti-tumour immune responses[65]. There are also other classes of compounds that target different steps in the antiviral signaling pathway. These include compounds like TPCA-1 an IKK inhibitor, which improved *in vitro* spread of oncolytic HSV[41]. Valproic acid, which is already approved in the treatment of epilepsy, a histone deacetylase inhibitor (HDACi) which can dampen expression of interferon stimulated genes and was found to synergize with a wide range of OVs including HSV-1, vaccinia virus, VSV, reovirus, and adenovirus[65].

There are also compounds that have been found to augment killing of infected cells and also induce bystander killing of uninfected cancer cells. Colchicine, a microtubule destabilizer used to treat gouty arthritis showed cancer-selective synergistic killing in both *in vitro* and mouse tumour models when combined with oncolytic rhabdoviruses[65]. In addition, colchicine decreased type I IFN translation and promoted increased viral bystander killing through secretion of virally induced cytokines[65]. Another compound is vanadate, which is a pan-protein tyrosine phosphatase inhibitors, and has been shown to enhance viral titers of multiple RNA viruses in resistant cancer

cell lines[67]. Furthermore, vanadate has also shown to lead to increased virus-induced bystander killing and abscopal effects in mouse bilateral tumour models thereby lead to the eradication of both treated and untreated tumours[67]. In addition, many combination therapies with OVs are being tested in clinical trials, of which a large portion are combinations with chemotherapeutics[65].

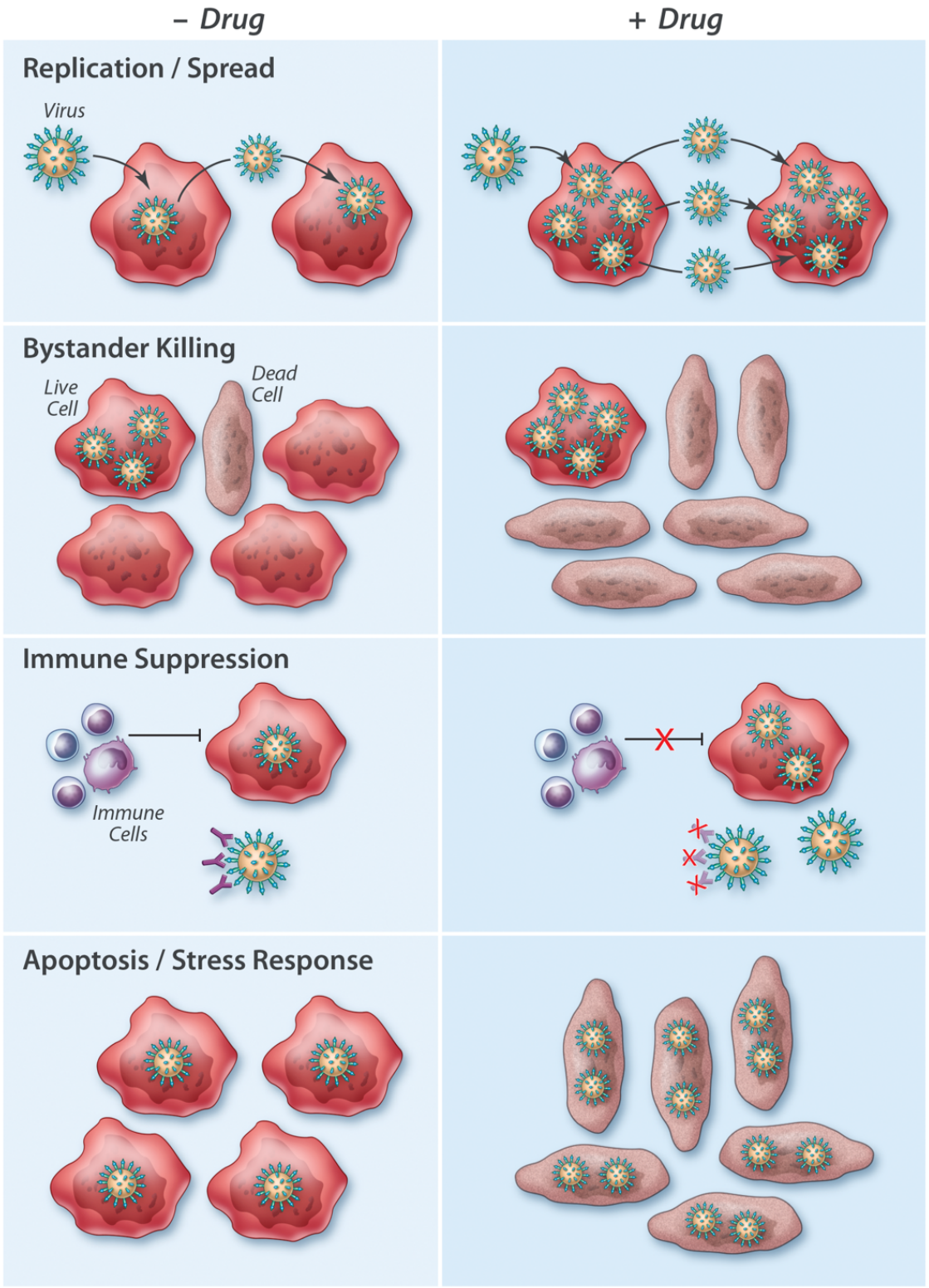
– Drug
+ Drug
Replication / Spread
Virus
Bystander Killing
Live Cell
Dead Cell
Immune Suppression
Immune Cells
Apoptosis / Stress Response

Figure 3. Mechanism of action of compounds combined with OVs.
There are four main mechanisms of action in which small molecules or antibodies can enhance efficacy of oncolytic viruses. 1) increase in viral replication/spread; 2) induction of factors that increase bystander killing, through cytokine release or activation of anti-tumour immunity on uninfected cells; 3) suppression of immune cells and antibody-mediated elimination of viruses; and 4) increased apoptosis and cell stress of infected cells. Figure and caption adapted from Phan et. al., 2018[65].

Chemotherapeutics in combination with OVs

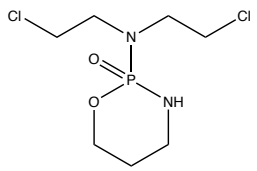

Cyclophosphamide

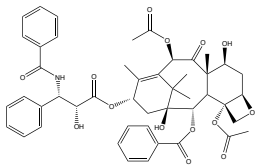

Paclitaxel

Drugs targeting cellular innate immune responses to viruses

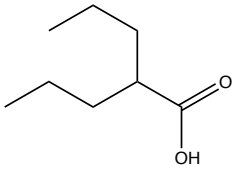

Valproic Acid

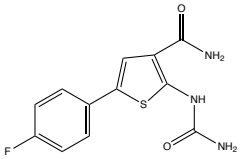

TPCA-1

Drugs that augment killing of infected and induce bystander killing of uninfected cancer cells

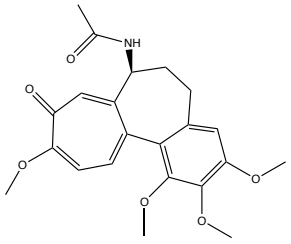

Colchicine

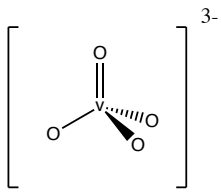

Vanadate

Figure 4. Small molecule enhancers of oncolytic viruses.
These compounds are examples of a broad range of molecular structures and functions from chemotherapeutics, to drugs that target cellular innate immune responses to viruses or drugs that augment killing of infected cells and induce bystander killing of uninfected cancer cells. Figure and caption adapted from Phan et. al., 2018[65].

1.9.2 Viral Sensitizers

Over a decade ago, in a search to find novel small molecule compounds that can enhance oncolytic virus efficacy, our group conducted a high-throughput screen of small molecule compounds. It was believed at the time that some of these small molecule compounds might complement deleted viral genes in oncolytic viruses and allow for more efficacious infection of cancer cells. From this screen, many promising drug candidates that can enhance oncolytic VSVΔ51 were discovered. These compounds were coined "viral sensitizers" for their ability to sensitize cancer cells to OV infection. These compounds included many microtubule destabilizers, like colchicine, described above. Our group has also shown the vanadium based compounds described above are effective viral sensitizing compounds and are effective in CT26wt, 4T1, and DBT *in vivo* tumour models, increasing VSVΔ51 growth and improved survival[67].

1.9.3 VSe1

As its name implies, Viral Sensitizer 1 (VSe1, **Figure 5a**) or 3,4-dichloro-5-phenyl-2,5-dihydrofuran-2-one was the first of several small molecule compounds identified in the high-throughput screen looking for compounds that enhanced oncolytic viral infection of VSVΔ51 in a virus-resistant cancer cell line (4T1)[68]. VSe1 enhanced viral infection in multiple resistant cancer cell lines, showing up to over a 1000-fold increase in titers in the most resistant cancer cell line (786-0)[68]. VSe1 was shown soon after its discovery to transiently inhibit IFNβ transcription and reduce activation of the innate antiviral response. It was hypothesized that this inhibition of IFNβ complements the M protein deletion in VSVΔ51 by blocking cellular antiviral genes and increasing viral infection[69]. Further, testing VSe1 in combination with VSVΔ51 *in vivo* significantly delayed tumour progression without viral spread to normal tissues[68]. While VSe1 is effective, due to its

electrophilic nature and toxicity profile, analogs were developed to try to improve physicochemical and toxicological properties. Using VSe1 as the scaffold, our group aimed to identify other active analogs and examine the structure-activity relationship of these compounds.

1.9.4 VSe1-28

One of the top analogs based on retained viral enhancement activity and improved toxicity and stability profiles synthesized was VSe1-28 (**Figure 5b** (*H*-Pyrrol-2-one,3,4-dichloro-1,5-dihydro-5-hydroxy-1-[2-(4-morpholinyl)ethyl]), which is a pyrrole derivative of VSe1[69]. Compared to VSe1, which has a plasma stability of 0% after three hours, VSe1-28 is much more stable with a plasma stability of 40% remaining after three hours[69]. Furthermore, upon analyzing glutathione (GSH) half-life; a measure of the time it takes for glutathione to form an adduct with the compounds, VSe1-28 demonstrated a half-life of 96 minutes, compared to VSe1 which had a half life of less than 5 minutes[69]. As GSH is conjugated to electrophilic compounds as a way to eliminate them from the human body, a longer GSH half-life suggested VSe1-28 is less electrophilic compared to VSe1 and leading to increased stability. VSe1-28 also retained similar activity and potency (peak potency of VSe1:60μM, VSe1-28: 80μM) compared to VSe1[69]. Notably, VSe1-28 enhanced VSVΔ51 infection in *ex vivo* tumour specimens similarly to VSe1. VSe1-28 showed similar efficacy in inhibiting IFNβ, blocking its antiviral effects[69]. In addition, it showed improved toxicological profiles only showing toxicity at doses higher than 100mg/kg compared to VSe1 which had toxicity starting at 10mg/kg[69]. VSe1-28 was also able to significantly enhance viral replication as well as delay tumour progression and improve survival *in vivo* tumour models[69]. Altogether, this shows that VSe1-28 is a good starting candidate to further pursue clinically for combination therapy with VSVΔ51.

a. VSe1

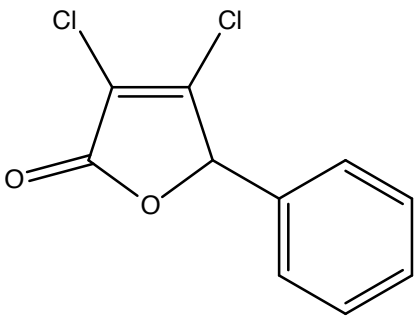

b. VSe1-28

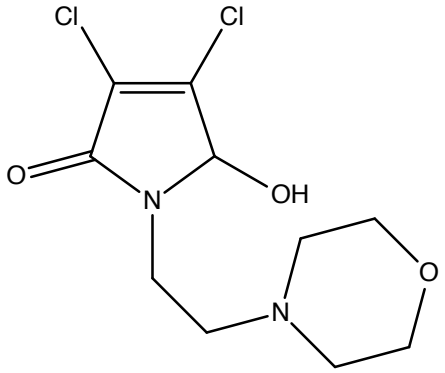

Figure 5. Chemical structure of VSe1 and VSe1-28.

1.10 Deducing the mechanism of action of VSe1 and VSe1-28

VSe1 and VSe1-28 have both been proven to be effective in enhancing oncolytic virus infection both *in vitro* and *in vivo*. But, the specific mechanism of action and molecular targets remain poorly understood. The original hypothesis was based on the small molecules' ability to dampen IFNβ response and decrease antiviral signaling to enhance viral infection, as IFNβ is a cytokine involved in the Type I IFN response that is activated by host innate immune system in response to pathogen infection and tumourgenesis[70]. Our group has recently found that both VSe1 and VSe1-28 significantly decrease mRNA expression of IFNβ as well as ISGs MX2 and IFITM1 with effects observed as early as 8 hours post VSVΔ51 infection and up to 24 hours post-infection in 786-0 cells (Manuscript in preparation-Appendix A). Analysis of nuclear translocation of molecular players involved in the tripartite pathway that activate IFNβ including ATF-2/c-Jun, Interferon Response Factors (IRF) 3 and 7, as well as NF-κB p65/p50, revealed that VSe1 and VSe1-28 both inhibit the translocation of NF-κB p65/p50 into the nucleus following VSVΔ51 infection of 786-0 cells (Manuscript in preparation-Appendix A). The above observations led us to further explore the effects these compounds had on the NF-κB pathway, which so far revealed no effect on upstream effectors including the phosphorylation of p65, dimerization of p65/p50, as well as degradation of IκBα. In addition, looking at NF-κB targeted genes tumour necrosis factor α (TNFα) and IL6[71], showed decreased expression of both genes upon treatment with VSe1 and VSe1-28 and infection of 786-0 with VSVΔ51 as early as 8 hours and up to 24 hours post-infection (Manuscript in preparation-Appendix A).

1.11 GSTP1-1

In our attempts to identify the molecular target of our VSe-1 related compounds, an experiment using ligand-based affinity chromatography was performed. This method aimed to identify non-covalent proteins interacting with an analog of VSe-1 covalently bound to beads. A schematic of the workflow is shown **(Figure 6)**. Using this method, Glutathione S-transferaseπ-1 (GSTP1-1) was identified as a top interacting molecule, identifying the protein in 3/3 runs.

GSTs catalyze the conjugation of GSH to both endogenous and exogenous electrophilic compounds and play a role in the elimination of toxic compounds[72]. GSTs are divided into 6 groups: Alpha, Mu, Omega, Pi, Sigma, Theta, and Zeta[73,74]. GSTP1-1 was found to be the predominant class found in human tumour cell lines and has been increasingly associated with drug resistance in chemotherapy patients[73,75]. GSTs have been shown to interact with members involved in the mitogen-activated protein kinase pathway (MAPK) which is involved in cell survival and death signaling as well as inhibition of c-Jun N-terminal kinase (JNK) through direct interaction[73]. Furthermore, the promoter sites of many GST isoenzymes have been shown to contain binding sites for transcription factors including Jun, AP-1, and NF-κB[74], all of which are key players in antiviral signaling.

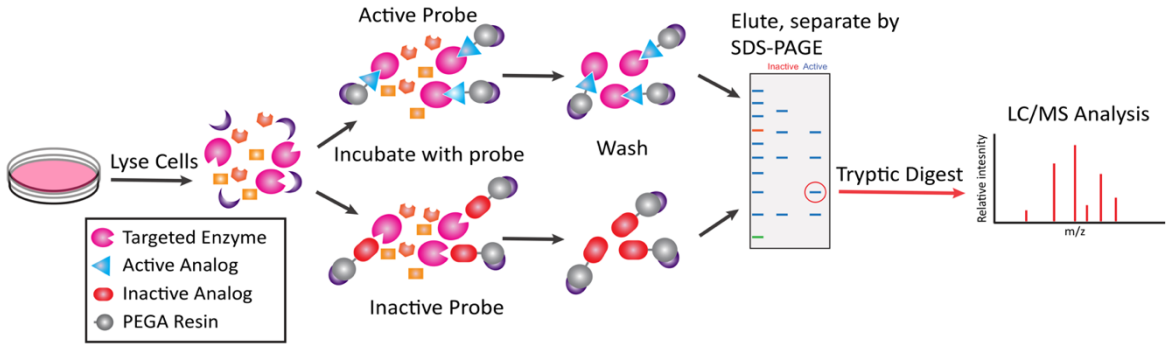
Active Probe
Elute, separate by
SDS-PAGE
Inactive Active
LC/MS Analysis
Lyse Cells
Incubate with probe
Wash
Tryptic Digest
Relative intesnity
m/z
Targeted Enzyme
Active Analog
Inactive Analog
PEGA Resin
Inactive Probe

Figure 6. Schematic view of ligand based-affinity profiling.
Workflow of the steps involved in using ligand based-affinity profiling which identified GSTπ (GSTP1-1) as an interacting protein with an active VSe based probe. Schematic adapted from Krishnan, El-Sayes, and Phan et. al., Manuscript in Preparation-Appendix A.

1.12 Rationale and Hypothesis

Our lab has previously found that VSe1 and VSe1-28 inhibit IFNβ expression and downstream ISGs including MX dynamin-like GTPase 2 (MX2) and Interferon-induced transmembrane protein 1 (IFITM1). Evidence to date suggests that this phenomenon is linked to a compound-induced reduction in the level of NF-κB nuclear accumulation following stimulation either by virus infection or the addition of cytokines like TNF-α, with signaling upstream of NF-κB still seemingly functional. Thus, the next logical step was to perform experiments that could ***identify the molecular target of VSe1 and VSe1-28 and its mechanism of action***.

As GSTP1-1 was identified as an interacting molecule through ligand-based affinity capture chromatography already and is over-expressed in most cancers, this provides a first potential candidate to explore and validate. As an alternative possibility, many drugs and small molecule compounds are known to post-translationally modify their targets. Such targets could not be identified by ligand-based affinity capture chromatography. Indeed, many drugs have been found to affect the nuclear accumulation of NF-κB through covalent modification. These include epoxyquinone A monomer, which is a synthetic derivative of epoxyquinol A, and sesquiterpene lactones which have been shown to directly modify and inhibit the DNA binding domain of the p65 subunit of NF-κB [38,76]. Another compound is Helenalin, which has medicinal properties identified over a century ago, which was shown to modify p65[77]. Of high relevance is dimethyl fumarate (DMF). This fumaric acid ester compound was previously shown by our group to have viral sensitizing properties and like VSe1 and VSe1-28, also inhibits nuclear accumulation of NF-κB [62]. Furthermore, it was recently demonstrated that DMF inhibits nuclear accumulation of NF-κB through covalent modification of a reactive cysteine present in the DNA binding region of p65[78]. Both DMF and Helenalin possess an α,β unsaturated carbonyl moiety that can undergo

hetero Michael addition[79], a moiety which is also present on VSe1 and VSe1-28[77,78]. All this combined provides evidence to hypothesize ***VSe1 and VSe1-28 may follow a similar mechanism through covalent modification of NF-κB p65 and reduce nuclear accumulation.***

In addition, irrespective of the mechanism, we consider that if NF-κB is a key biological target, we should observe its decreased activity by VSe1 and VSe1-28 not only in 786-0 cells but also other cancer cell lines in which VSVΔ51 growth is sensitized by these molecules. This effect should also be observed *in vivo* models where the molecules have been found to be therapeutically effective. In addition, it will be of critical importance for clinical translation to determine whether the impact of these compounds on NF-κB regulation is selective to cancer cells or whether it also occurs in normal cells.

To address these hypotheses, we set out to carry out experiments specifically aiming to:

1. Validate or reject GSTP1-1 as a molecular target in the mechanism of action of VSe1 and VSe1-28.
2. Use activity-based protein profiling to explore the possibility of covalent modification as an alternative mechanism of VSe1 and VSe1-28.
3. Validate the mechanism of action of VSe1 and VSe1-28 in other cancer cell lines and normal cells by analyzing their effects on nuclear accumulation and induction of NF-κB activated genes and interferon stimulated genes.
4. Evaluate the mechanistic impact of VSe1-28 combined with VSVΔ51 in mouse models of cancer.

2 Chapter: Material and Methods

2.1 Drugs, Chemicals, and Cytokines

The synthesis of VSe1, VSe1-28 and DMF probe was carried out by Dr. Christopher Boddy's lab and has been previously described[68,69,78]. The synthesis of the active VSe1-54 probe and inactive VSe1-56 probe was also done by Dr. Christopher Boddy's lab. Dimethyl Fumarate (DMF) was obtained from Sigma-Aldrich (St Louis, MO). TNFα was obtained from R&D systems (Minneapolis, MN).

2.2 Viruses

The virus used in experiments is a recombinant variant of the Indiana serotype of VSV that contains a deletion of the 51st amino acid in the M protein (VSVΔ51). VSVΔ51 constructs expressing green fluorescent protein (GFP) or firefly luciferase (Fluc) which are used in the experiments below are recombinant derivatives of VSVΔ51, and have been described in Stojdl et al[61]. Viruses were produced in Vero cells and purified using an Optiprep gradient as previously described[80] and titered by standard plaque assay as described below.

2.3 Cell Lines

786-0 (human renal carcinoma), Vero (African green monkey kidney), B16F10 (murine melanoma), CT26wt (murine colon carcinoma), 4T1 (murine mammary carcinoma) and 293T (human embryonic kidney) were obtained from the American Type Culture Collection (Manassas, VA). 786-0 and Vero cell lines were maintained in Dulbecco's Modified Eagle's medium (Corning, Manassas, VA) supplemented with 10% 3:1 newborn calf serum:fetal bovine serum (Sigma-Aldrich, St Louis, MO). B16F10 cells were maintained in Minimum Essential Medium Eagle (Corning, Manassas, VA) supplemented with 10% fetal bovine serum (VWR, Mississauga, ON). CT26wt, 4T1, and 293T were maintained in Dulbecco's Modified Eagle's Medium

supplemented with 10% fetal bovine serum (VWR, Mississauga, ON). All cell lines were incubated at 37 °C with 5% CO_2.

2.4 Isolation of Murine Hepatocytes

Primary murine hepatocytes were isolated as previously decribed[81] and provided by Dr. Morgan Fullerton's lab. Briefly, the superior vena cava was clamped and the portal vein was cut from the liver, the liver was perfused through the inferior vena cava with EGTA buffer (140 mM NaCl, 6.7 mM KCl, 10 mM HEPES, and 50 μM EGTA, pH 7.4) at 7 mL/min to a total 25 mL. The perfusion was then switched to a 0.5% Collagenase solution (67 mM NaCl, 6.7 mM KCl, 5 mM CaCl2*2H2O, and 100 mM Hepes, pH 7.6) at 6 mL/min to a total of 25 mL. The liver was then removed and transferred to a dish containing Williams Media E (Wisent Bioproducts, Saint-Jean-Baptiste, Quebec) and liver cells were teased out of the sac and filtered through a 100 μm cell strainer. Cells were centrifuged at 1000 rpm for 5 minutes and resuspended in fresh Williams Media E. Cells were then centrifuged again at 1000 rpm for 5 minutes and resuspended in Williams Media E supplemented with 10% FBS (VWR, Mississauga, ON), 1% Penicillin/Streptomycin (ThermoFisher, Waltham, MA), and 1% L-Glutamine (Thermofisher, Waltham, MA) . Trypan Blue Exclusion was used to determine cell viability. Cells were incubated at 37 °C with 5% CO_2.

2.5 siRNA Transfection

786-0 cells were seeded 6×10^4 cells/well in 12 well plates twenty-four hours prior to transfection. Cells were then transfected with scrambled siRNA control ((ON-TARGETplus Non-targeting Control Pool; # D-001810-10-05; Dharmacon), SMARTpool ON-TARGETplus GSTP1 siRNA (#L-011179-00-0005; Dharmacon), or oligofectamine (Invitrogen, Burlington, ON) alone, following manufacturer's protocols. After forty-eight hours, cell lysates were collected for immunoblot analysis against GSTP1-1 to determine knockdown efficiency. Parallel sets of plates

were either treated with varying concentrations of VSe1 and subsequently infected with VSVΔ51-GFP or with virus alone at MOI 0.01. Supernatants were collected twenty-four and forty-six hour post-infection to be titered by standard plaque assay.

2.6 Luciferase Reporter-Based Viral Titration Assay

This assay has been previously described in detail[68]. Briefly, 786-0 cells were seeded in 96 well plates at 3x10^4 cells/well 24 hours prior to treatment. Cells were then pre-treated for 4 hours with either control (Dimethylsulfoxide (DMSO) or water) or compound at various concentrations and then infected with VSVΔ51 Fluc (MOI 0.005). After forty hours, 25 μL of supernatant from the treated 786-0 cells were transferred onto Vero cells. A standard curve of known amounts of virus starting from 1×10^8 plaque forming units (pfu) to 10 pfu, decreasing by 1 log unit was also added to corresponding wells of Vero cells. Plates were then centrifuged at 430 ×g for 5 minutes and incubated for 5 hours at 37 °C, 5% CO_2. Luciferase expression was measured by the amount of bioluminescence in each well expressed as mean relative light units (mRLU; SynergyMx Microplate Reader, BioTek). The mRLU standard curve was generated by plotting mRLU against known input viral pfu from each standard curve that was added to Vero cell plates. A four-parameter non-linear regression analysis was used to generate a Hill plot from which unknown sample pfu can be interpolated. This represented an estimate of viral titers which are termed "viral expression units (VEU.)" All data transformation was performed using R.

2.7 Cell Viability Assay

Cell viability was measured by incubating cell samples with Rezasurin (Sigma Aldrich, St. Louis, MO) according to the manufacturer's instructions. After 2 hours, fluorescence was measured (530 nm excitation and 590 nm emission) using a fluorescent plate reader (SynergyMx

Microplate Reader, BioTek). Cell viability was calculated by normalizing samples to untreated controls after subtracting background fluorescence from wells with media alone.

2.8 Bradford Assay

To determine protein extract concentration, a Bradford assay was used. BSA standards with concentrations: 100 μg/mL, 200 μg/mL, 400 μg/mL, 600 μg/mL, 800 μg/mL, 900 μg/mL, 2000 μg/mL was used to generate a standard curve. Bio-Rad Protein Assay Dye Reagent Concentrate (Bio-Rad, Mississauga, ON) was used to determine protein concentration on a Vis Spectrophotometer (Thermo Fisher, Waltham, MA).

2.9 Immunoblotting

Cells were lysed for 10 minutes on a rotator at 4 °C with protein extraction buffer (50 mM Hepes, 150 mM NaCl, 10 mM EDTA, 10 mM $Na_4P_2O_7$, 1% NP-40, pH 7.4) containing 0.5 M NaF, 200 mM Na_3VO_4 and protease inhibitor cocktail (Roche, Mississauga, ON). Lysate was collected and centrifuged at 14,000 rpm for 10 minutes. Protein concentration was read using a Bradford Assay. 15-30 μg of lysate were used per sample, prepared in NuPAGE LDS sample buffer (Invitrogen, Burlington, ON) supplemented with 0.5 M dithiothreitol (Sigma Aldrich, St. Louis, MO). Samples were electrophoresed on a 4-12% Bis-Tris precast gradient gel (Invitrogen, Burlington, Ontario) using the Mini Gel Tank system (Invitrogen, Burlington, ON). Gels were transferred onto 0.45 μM nitrocellulose membrane (GE Healthcare, Baie d'Urfe, Quebec) using Mini Blot Module (Invitrogen, Burlington, ON). Membranes were blocked with 5% skim milk or 5% BSA in 0.1% TBS-Tween 20 for 1 hour and then probed overnight with rabbit or mouse antibodies against NF-κB p65 (#8242 Cell Signaling Technology, Danvers, MA), NF-κB p105/p50 (#3035, Cell Signaling Technology, Danvers, MA), β-Actin (#4970, Cell Signaling Technology, Danvers, MA), or α-Tubulin (sc-8035, Santa Cruz Biotechnology, Dallas, Texas). Membranes

were then probed for 1 hour with a rabbit (Cell Signaling Technology, Danvers, MA) or mouse (Cell Signaling Technology, Danvers, MA) antibody conjugated with horseradish-peroxidase. Western bands were visualized using Clarity TM Western ECL blotting solution (Bio-Rad, Mississauga, ON) on a Chemi-Doc MP Imaging System (Bio-Rad, Mississauga, ON).

2.10 Nuclear and Cytoplasmic Protein Extraction

Nuclear and cytoplasmic protein extracts were isolated using NE-PER™ Nuclear and Cytoplasmic Extraction Reagent (Thermo Fisher, Waltham, MA). In brief, cells were harvested using trypsin-EDTA and pelleted at 500 ×g for 5 minutes. Cells were washed once in PBS. 250 µL of ice-cold cytoplasmic extraction reagent I was added to cell pellet, vortexed and incubated on ice for 10 minutes to lyse cells. 11.75 µL of cytoplasmic extraction reagent II was added to the pellet, vortexed and incubated on ice for 1 minute. Cells were then centrifuged at 14000 rpm for 5 minutes and the supernatant containing the cytoplasmic extract was collected. 125 µL of nuclear extraction reagent was then added to the remaining pellet, and incubated on ice for 40 minutes, vortexing the pellet every 10 minutes. Cell extract was centrifuged 14000 rpm for 10 minutes, and the supernatant containing the nuclear extract was collected. Protein concentration for both extracts was determined using Bradford assay.

2.11 Standard Plaque Assay

Methods have been previously described[80]. Briefly, Vero cells are seeded in 12 well plates at $3x10^5$ cells/well the day before so they are 95% confluent at the start of the assay. Serial dilutions of supernatants containing virus are done using serum-free media. 400 µL of diluted supernatants are used to infect Vero cells for 45 minutes while being incubated at 37°C, 5% CO_2. After 45 minute infection, the supernatant is removed off of the Vero cells and a 1:1 volume of 1% agarose:2x DMEM supplemented with 20% FBS is added to each well covering the cells. Cells

are then incubated at 37°C, 5% CO_2 for 24 hours after which they are fixed with 3:1 methanol: acetic acid fixative. After 2h incubation at room temperature, the agarose and fixative are washed off the cells. The cells are then stained with Coomassie blue for 30 minutes on a shaker. Plaques can then be counted at dilutions steps where 15-100 plaques per well are visible and plaque forming units/ml are calculated.

2.12 Activity-Based Protein Profiling

Methods have been previously described[82,83]. Briefly, cells were lysed with cold 1% Triton X-100 in PBS for 10 minutes on a rotator at 4 °C. Cells were then scraped, collected and spun at 14,000 rpm for 10 minutes. Supernatants were collected and protein concentration was determined by Bradford Assay. For fluorescent scanning, rhodamine azide was used. 70 μg of protein was mixed with freshly prepared click chemistry mixture (0.1 mM Rhodamine Azide, 1 mM Tris(2-carboxyethyl)phosphine (TCEP, Sigma Aldrich, St Louis MO), 0.1 mM Tris[1-benzyl-1H-1,2,3-triazol-4-yl)methyl]amine (TBTA, Sigma Aldrich, St Louis, MO), 5 mM $CuSO_4$ (Fisher, Toronto, ON)) and rotated at room temperature for 45 minutes. Samples were then precipitated with 1 mL acetone at -80 °C for 15 minutes. Samples were spun at 6500 rpm for 15 minutes and the supernatant was removed. Pellet was air-dried and then dissolved in 2X SDS gel loading buffer (Bio-rad, Missisauga, ON)) and denatured at 95 °C for 10 minutes. Samples were then loaded on an SDS-PAGE. Gels were imaged on a Bio-Rad Chemi-Doc, using absorbance 501 nM and Emission 525 nM.

For ABPP and western experiments, 1mg of protein was mixed with freshly prepared click chemistry mixture (0.1 mM Biotin Azide (Sigma Aldrich, St Louis, MO), 1 mM TCEP, 0.1 mM TBTA, 5 mM $CuSO_4$) and rotated at room temperature for 2 hours. Acetone was then added to samples and placed at -80 °C for 15 minutes to precipitate proteins. Samples were then centrifuged

at 6500 rpm for 15 minutes. Samples were washed three times with methanol and sonication (30% power) to break up the protein pellet. Proteins were pelleted by centrifuging at 6500 × g between each wash. After washing in methanol, samples were resuspended in 2.5% SDS in PBS and dissolved by sonication and then heated at 60 °C for 5 minutes. Samples were then pelleted at 6500 × g for 4 minutes and the supernatant was transferred to a fresh tube. Samples were topped off to 8mL total volume with PBS and 100 μL of streptavidin-agarose beads were added (Sigma Aldrich, St Louis, MO). Samples containing streptavidin beads were rotated at room temperature for 1.5h to allow biotin to bind to streptavidin beads. Beads were then pelleted at 1400 × g for 2 minutes and washed 3× with 1% SDS in PBS, 3× with 6M Urea, 3× with PBS, pelleting beads between each wash by centrifugation. Beads were eventually resuspended in 2× SDS Page buffer and proteins were removed off the beads by heating samples at 95 °C for 15 minutes. Samples were then loaded on SDS-PAGE gels and transferred onto nitrocellulose to be blotted for antibodies indicated.

2.13 RNA Extraction

Cells were lysed with RLT buffer (Qiagen, Hilden) supplemented with 1% 2-Mercaptoethanol (Life Technologies, Carlsbad, CA). Lysates were then centrifuged using a Qiashredder Spin Column (Qiagen, Hilden) at 14,000 rpm for 1 minute. After centrifugation, flow-through was combined with 70% ethanol (Commercial Alcohols, Brampton, ON) and placed in an RNeasy Mini Kit Spin Column (Qiagen, Hilden, Germany) and centrifuged at 8000 × g for 15 seconds. Column was then washed once with RW1 buffer (Qiagen, Hilden) and twice with RPE Buffer (Qiagen, Hilden). Column was then dried by centrifuging at 14,000 rpm for 1 minute. Samples were eluted off the column by adding 30 μL of RNase free water (Qiagen, Hilden) and

centrifuging at 8000 × g for 1minute. RNA concentrations were read using a Nanodrop Spectrophotometer (Thermo Fisher Scientific, Waltham, MA).

2.14 Quantitative Real Time PCR

cDNA was generated using a RevertAid H Minus First Strand cDNA Synthesis Kit (Thermo Fisher Scientific, Waltham, MA) with 1 μg of RNA. Quantitative Real-Time PCR reactions were performed using Powerup SYBR Green Master Mix (Thermo Fisher Scientific, Waltham, MA) on a 7500 Fast Real-Time PCR System (Applied Biosystems, Foster City, CA) using 20 ng of cDNA per sample. Forward and reverse primers were generated for both human and murine samples for specified genes as shown in Table 1. Samples were normalized to GAPDH and fold change was compared to untreated/uninfected samples using the Pfaffl Method[84]. This method is used to analyze and compare relative expression ratio, normalizes to an endogenous standard and accounts for PCR efficiency (Equation 1)[84].

$$RQ = \frac{(E_{target})^{\Delta Ct\ target(control-sample)}}{(E_{ref})^{\Delta Ct\ ref(control-sample)}}$$

Equation 1. Pfaffl Method.

Model	Gene	Forward Primer (5'→3')	Reverse Primer (5'→3')
Human	IL6	ACCCCCAATAAATATAGGACTGGA	GAAGGCGCTTGTGGAGAAGG
Human	TNFα	GCTGCACTTTGGAGTGATCG	GAGGGTTTGCTACAACATGGG
Human	GAPDH	ACAGTCAGCCGCATCTTCTT	GTTAAAAGCAGCCCTGGTGA
Human	MX2	GAACGTGCAGCGAGCTTGTC	AAGGCTTGTGGGCCTTAGAC
Human	IFITM1	CGTGAAGTCTAGGGACAGG	GGTAGACTGTCACAGAGCCG
Mouse	IL6	TCCTCTCTGCAAGAGACTTCC	GGTCTGTTGGGAGTGGTATCC
Mouse	TNFα	CCTCTTCTCATTCCTGCTTGT	TGGGAACTTCTCATCCCTTTG
Mouse	GAPDH	CCCTTAAGAGGGATGCTGCC	TACGGCCAAATCCGTTCACA
Mouse	MX2	GAATTACCAGGGTGGCTGTAG	CAGGTTGATGGTCTCCTGTTT
Mouse	IFITM1	CAACTAGTGGTGCCAGCCGA	GTGAGGAGCACGTAGTCGGG

Table 2. Primer sequences for quantitative RT-PCR.

2.15 *In vivo* Tumour Models

Six week old female BALB/c mice were obtained from Charles River Laboratory (Senneville, QC). The mice were implanted with subcutaneous tumours by injecting 3 x 10^5 syngeneic CT26wt cells in 100 μL of PBS. Eleven days post-implantation, tumours were treated intratumourally with either VSe1-28 (dissolved in DMSO) or DMSO vehicle control. Four hours later, mice were infected intratumourally with 1 x 10^8 pfu VSVΔ51-Fluc in 25 μL PBS. Tumours were harvested 12 hours later by excising 30 mg of tumour tissue, flash freezing in dry ice and homogenized in RLT buffer using a Tissue Lyser II (Qiagen, Hilden, 25Hz, 4 minutes). RNA was extracted from homogenized tissue as described above. In parallel, IVIS (Perkin Elmer) was used to determine bioluminescent signal intensities to determine the efficiency of VSVΔ51 infection as described below. Quantification of bioluminescent signal intensities was done using Living Image v2.50.1 software. Mice were randomized to the different treatment groups based on tumour size.

2.16 *In vivo* Imaging

Mice were injected intraperitoneally with 200 μL of 10 mg/mL luciferin dissolved in PBS (Corning, Manassas, VA). Mice were then anesthetized using 3% isoflurane and imaged using an *in vivo* imaging system (IVIS; Perkin Elmer, Waltham, MA).

2.17 Statistical Analysis

Results are shown as means +/- standard error. Statistical significance was calculated using either a one way or two-way anova with Dunnett's multiple comparison to mean a P-value equal to or less than 0.05. Graphs and statistics were calculated using GraphPad Prism 6.

3 Chapter: Results

3.1 Identification of GSTP1-1 as an interacting molecule through ligand based affinity chromatography

After identifying GSTP1-1 as an interacting molecule with VSe1 and VSe1-28, we wanted to determine if GSTP1-1 was responsible for the viral sensitizing effects of VSe1 and VSe1-28. Using siRNA against GSTP1-1 to inhibit GSTP1-1 expression, we confirmed knockdown by western blot analysis **(Figure 7c)** at 12.5, 25 and 50 nM concentrations of siRNA. 786-0 cells were transfected with GSTP1-1 siRNA and 48 hours after transfection, cells were infected with VSVΔ51 (MOI 0.01). Supernatant was collected 24 and 46 hours post-infection and titered by standard plaque assay. Knockdown of GSTP1-1 did not lead to the enhancement of viral infection at 24 or 48 hours **(Figure 7a)**. In parallel, after transfecting 786-0 cells with siRNA against GSTP1-1 for 48 hours, cells were also treated with VSe1 and then infected with VSVΔ51 (MOI 0.01). Supernatant was collected at 24 hours post-infection and titered by standard plaque assay revealing that VSe1 was still able to sensitize 786-0 cells to VSVΔ51 infection despite knockdown of GSTP1-1 **(Figure 7b)**. All this suggests that that GSTP1-1, despite being pulled down by ligand affinity chromatography experiments, is not responsible for the viral sensitizing effects of VSe1 and its analogs.

a.

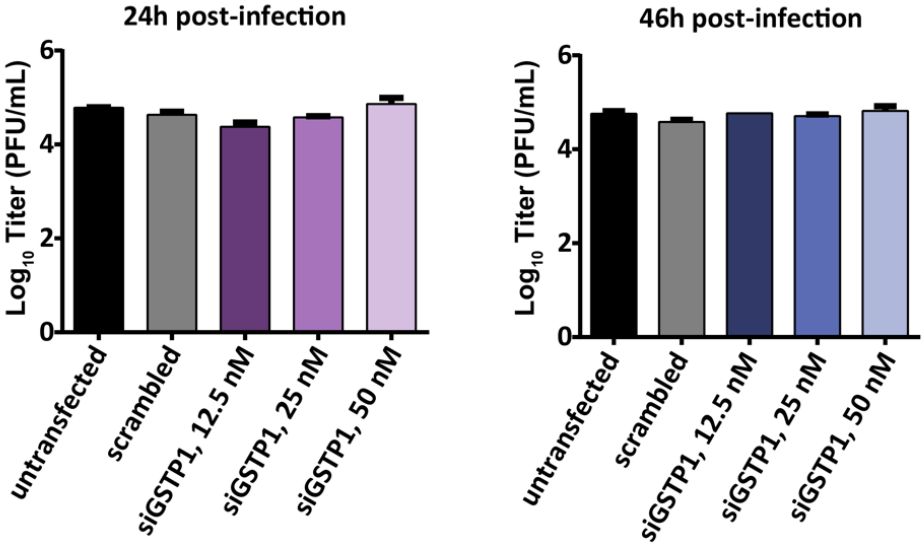
24h post-infection
46h post-infection
Log10 Titer (PFU/mL)
0
2
4
6
untransfected
scrambled
siGSTP1, 12.5 nM
siGSTP1, 25 nM
siGSTP1, 50 nM

b.

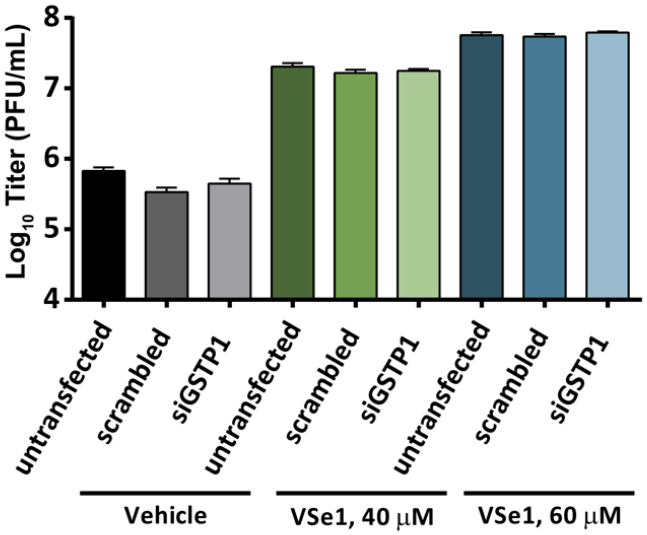
Log10 Titer (PFU/mL)
4
5
6
7
8
untransfected
scrambled
siGSTP1
Vehicle
VSe1, 40 μM
VSe1, 60 μM

c.

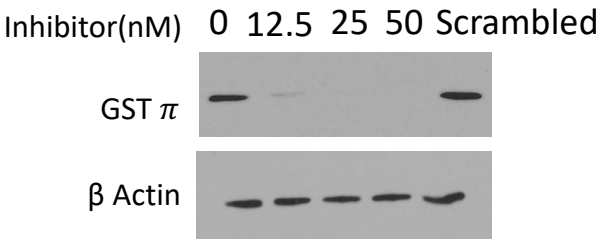
Inhibitor(nM) 0 12.5 25 50 Scrambled
GST π
β Actin

Figure 7. GSTP1-1 fails to abrogate the viral sensitizing effects of VSe1.
(a) 786-0 cells were transfected with vehicle control (0), scrambled siRNA (scrambled) or varying concentration of GSTP1-1 siRNA. 48 hours later, cells were infected with VSVΔ51-GFP (MOI 0.01). Virus output was measured by standard plaque assay at 24 and 46 hours post infection. **(b)** 786-0 cells were transfected with vehicle control, scrambled siRNA or 25 nM GSTP1-1 siRNA. Forty-eight hours post transfection, cells were pre-treated with vehicle control or varying concentration of VSe1 for 4 hours, then infected with VSVΔ51-GFP (MOI 0.01). Virus output was determined by standard plaque assay 24 hours post infection. **(c)** In parallel to **(a)** protein lysate from transfected cells were collected forty-eight hours after transfection and probed for GSTP1-1 and β-actin. Data obtained in **(a)** adapted from Krishnan, El-Sayes, and Phan, Manuscript in Preparation.

3.2 VSe1 and VSe1-28 reduce nuclear accumulation of NF-κB and expression of NF-κB induced ISGs in various cancer cell lines

To further validate NF-κB's involvement in the mechanism of action of VSe-1 and analogs as previously observed in 786-0s, we expanded our evaluation to other cancer cell lines. We chose B16F10 (murine melanoma), CT26wt (murine colon carcinoma), and 4T1 (murine mammary gland cancer), which are three cell lines that can be implanted syngenically in immunocompetent mice and that are relatively resistant to VSVΔ51 infection. Furthermore, we have previously shown VSe1 and VSe1-28 can sensitize these cancer cell lines to VSVΔ51 infection[68,69]. In order to determine the virus sensitizing concentration of VSe1 and VSe1-28 in each cell line, cells were treated with varying concentrations of VSe1 and VSe1-28 and then infected with VSVΔ51-GFP. Viral infection was monitored by GFP pictures 24 hours post-infection **(Figure 8)**, and the most effective concentration was determined by the number of GFP-positive cells. To examine the effect of NF-κB nuclear translocation, B16F10, CT26wt, and 4T1 were pre-treated with VSe1 or VSe1-28 for 2 hours and then treated with TNFα. Nuclear and cytoplasmic protein extracts were collected and analyzed via western blot for NF-κB p65 and p50 nuclear translocation **(Figure 9)**. Both VSe1 and VSe1-28 inhibited TNFα induced nuclear accumulation of NF-κB p65 in all three cell lines, generally by approximately 50%. However, the effects on nuclear accumulation of p50 were not as striking.

We next investigated the ability of VSe1 and VSe1-28 to modulate NF-κB induced genes in B16F10, CT26wt and 4T1 cells following VSVΔ51 infection. RNA was collected from each of the cell lines following pre-treatment with VSe1, VSe1-28, or mock, and infected with or without VSVΔ51 (MOI 1) for 8, 16, and 24 hours. Quantitative RT-PCR was used to analyze gene expression of NF-κB targeted genes TNFα and IL-6 and also ISGs IFITM1 and MX2 **(Figure 10)**.

Markedly, VSe1 and VSe1-28 inhibited TNFα, IL-6, IFITM1, and MX2 in all three cell lines most significantly at 8 hours post-infection. But in B16F10 and 4T1 cells, the effects extend for as long as 24 hours post-infection. Altogether, this suggests that both VSe1 and VSe1-28 can impair NF-κB antiviral response in a variety of different cancer cell lines.

After validating the impact of VSe-1 and VSe1-28 on NF-κB activity in multiple cancer cell lines, we wanted to explore the cancer selectivity of their effects. With that in mind, we treated primary normal murine hepatocytes (obtained from Dr. Morgan Fullerton) with VSe1-28 at varying concentrations for 4 hours and then infected with VSVΔ51. After collecting supernatant 40 hours post-infection and titering the virus output using a previously described luciferase based titering assay[85], it was revealed that VSVΔ51 titers were not increased by VSe1-28 **(Figure 11)**. Consistent with this data, we observed that even the maximum tolerated dose of VSe1-28 in murine hepatocytes was unable to inhibit mRNA expression of NF-κB target genes TNFα and IL6, nor ISGs MX2 and IFTIM1 at both 8 and 16 hours post-infection **(Figure 12)**. Interestingly, when compared to previous cancer cell lines we had tested, B16F10, CT26wt, and 4T1, murine hepatocytes had higher baseline expression of some antiviral genes **(Figure 13)**. Altogether, this data suggests that VSe-1 and VSe1-28 inhibit NF-κB nuclear accumulation and activity in a broad range of cancer cell lines, but do not downregulate this pathway sufficiently to elicit viral sensitization in normal cells.

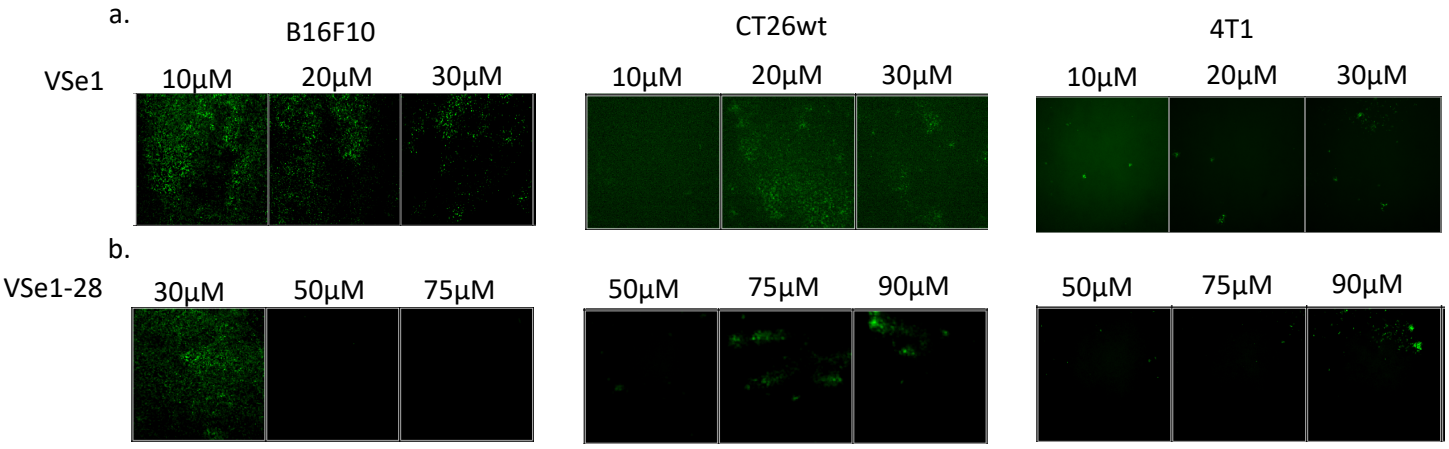
a.
B16F10
CT26wt
4T1
VSe1
10μM
20μM
30μM
10μM
20μM
30μM
10μM
20μM
30μM
b.
VSe1-28
30μM
50μM
75μM
50μM
75μM
90μM
50μM
75μM
90μM

Figure 8. VSe1 and VSe1-28 sensitize various cancer cell lines to VSVΔ51 infection.
B16F10, CT26wt, and 4T1 cell lines were treated with varying concentrations of **(a)** VSe1 or **(b)** VSe1-28. Two hours later, cells were infected with VSVΔ51-GFP (MOI 0.01). GFP pictures were taken twenty-four hours post infection to monitor viral infection.

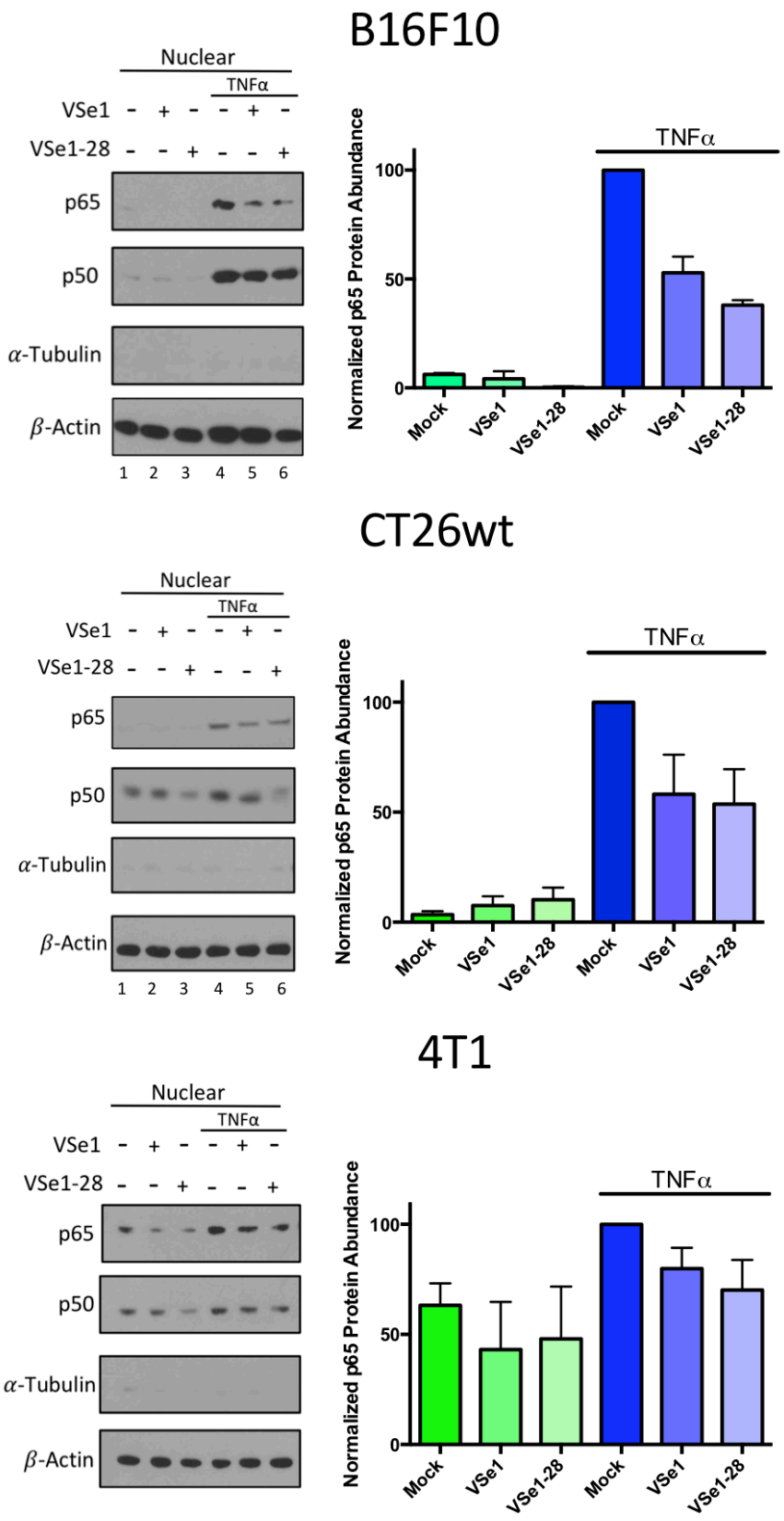
B16F10
Nuclear
TNFα
VSe1 - + - - + -
VSe1-28 - - + - - +
p65
p50
α-Tubulin
β-Actin
1 2 3 4 5 6
Normalized p65 Protein Abundance
100
50
0
TNFα
Mock
VSe1
VSe1-28
Mock
VSe1
VSe1-28
CT26wt
Nuclear
TNFα
VSe1 - + - - + -
VSe1-28 - - + - - +
p65
p50
α-Tubulin
β-Actin
1 2 3 4 5 6
Normalized p65 Protein Abundance
100
50
0
TNFα
Mock
VSe1
VSe1-28
Mock
VSe1
VSe1-28
4T1
Nuclear
TNFα
VSe1 - + - - + -
VSe1-28 - - + - - +
p65
p50
α-Tubulin
β-Actin
Normalized p65 Protein Abundance
100
50
0
TNFα
Mock
VSe1
VSe1-28
Mock
VSe1
VSe1-28

Figure 9. VSe1 and VSe1-28 inhibit nuclear translocation of NF-κB in multiple cancer cell lines.

Western Blot analysis of nuclear extracts of **(a)** B16F10 **(b)** CT26WT **(c)** 4T1 treated with VSe1 (B16F10 and CT26wt: 15 μM, 4T1: 30 μM) and VSe1-28 (B16F10: 40 μM, CT26wt: 60 μM, 4T1: 80 μM) for 2 hours and then treated with TNFα (25 ng/mL) for 30 minutes. NF-κB p65 was quantified using ImageJ and normalized to actin loading control bands.

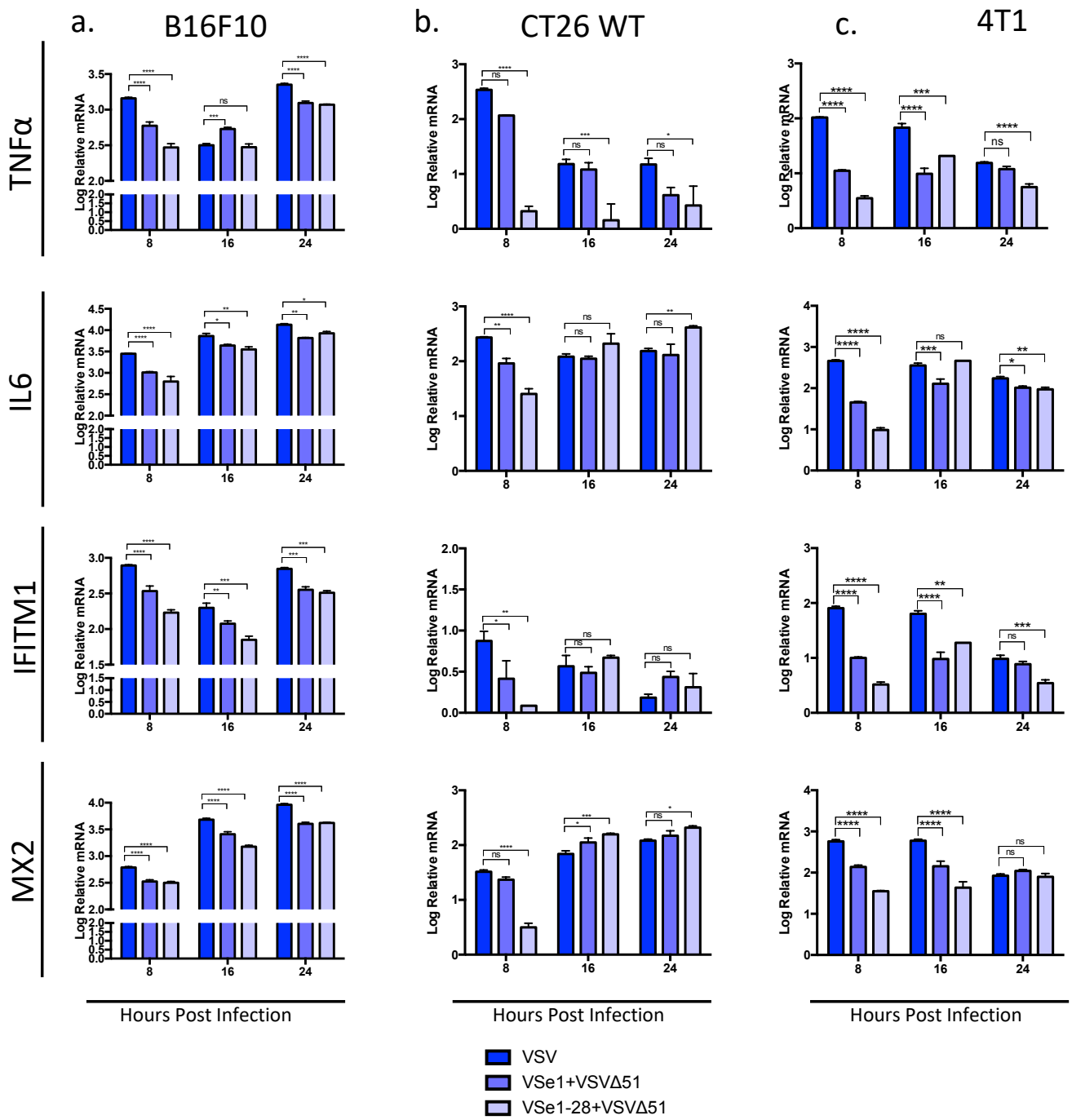
a.
B16F10
b.
CT26 WT
c.
4T1
TNFα
IL6
IFITM1
MX2
Log Relative mRNA
Hours Post Infection
VSV
VSe1+VSVΔ51
VSe1-28+VSVΔ51

Figure 10. VSe1 and VSe1-28 inhibit NF-κB targeted genes and interferon stimulated genes. Quantitative RT-PCR was conducted on RNA collected from **(a)**B16F10 **(b)**CT26WT **(c)**4T1 cells treated with VSe1 (B16F10 and CT26wt: 15 μM, 4T1: 30 μM) and VSe1-28 (B16F10: 40 μM, CT26wt: 60 μM, 4T1: 80 μM) for 2 hours and then infected with VSVΔ51-GFP (MOI 1) for 8, 16 and 24 hours. Gene expression was analyzed for NF-κB targeted genes TNFα and IL6 and ISGs IFITM1 and MX2. ns: $P > 0.05$, *$P<0.05$, **$P<0.01$, ***$P<0.001$ ****$P<0.0001$ (Two-way ANOVA with Dunnett's multiple comparison).

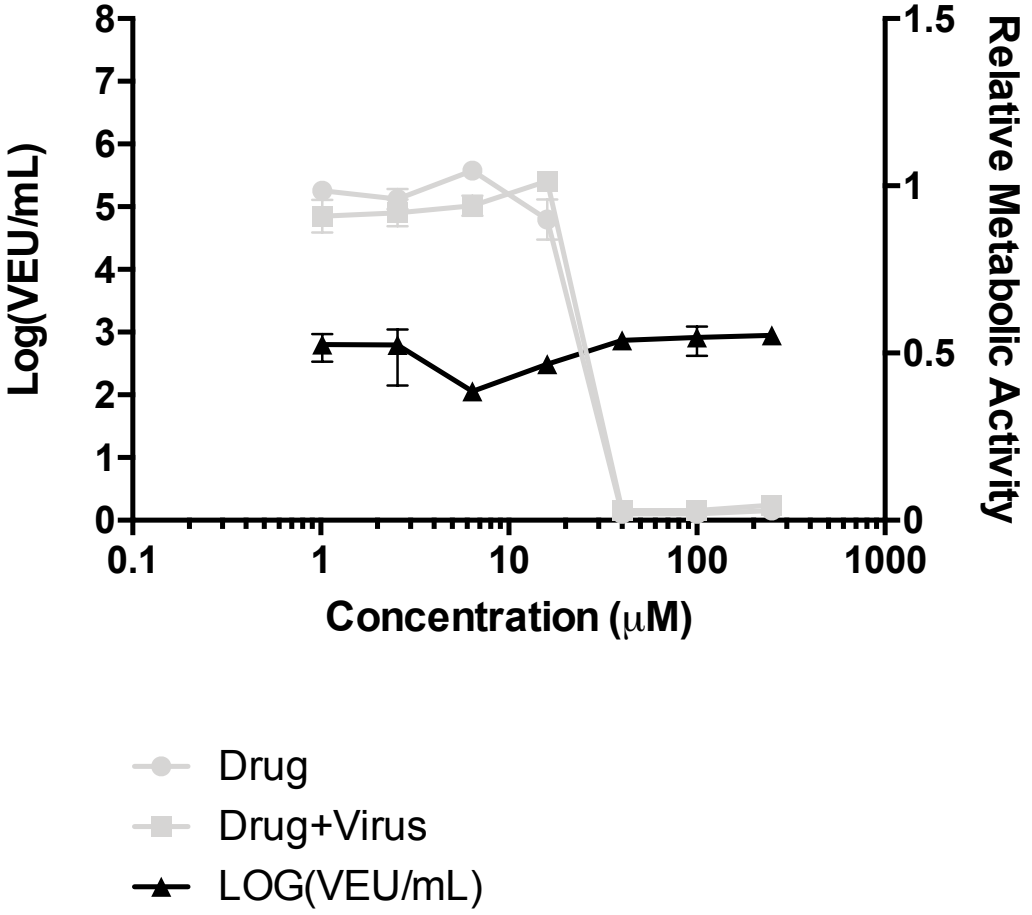
Log(VEU/mL)
Relative Metabolic Activity
Concentration (μM)
0.1
1
10
100
1000
Drug
Drug+Virus
LOG(VEU/mL)

Figure 11. VSe1-28 does not enhance viral efficacy of VSVΔ51-fluc in primary murine hepatocytes.
Primary murine hepatocytes were pre-treated with VSe1-28 at various concentrations for 4 hours and then infected with VSVΔ51-Fluc (MOI 0.005). Supernatants were collected 40 hours later and virus output was determined using a luciferase based titration assay. Relative metabolic activity was determined using resazaurin. Primary hepatocytes were isolated by Dr. Morgan Fullerton and Conor O'Dwyer.

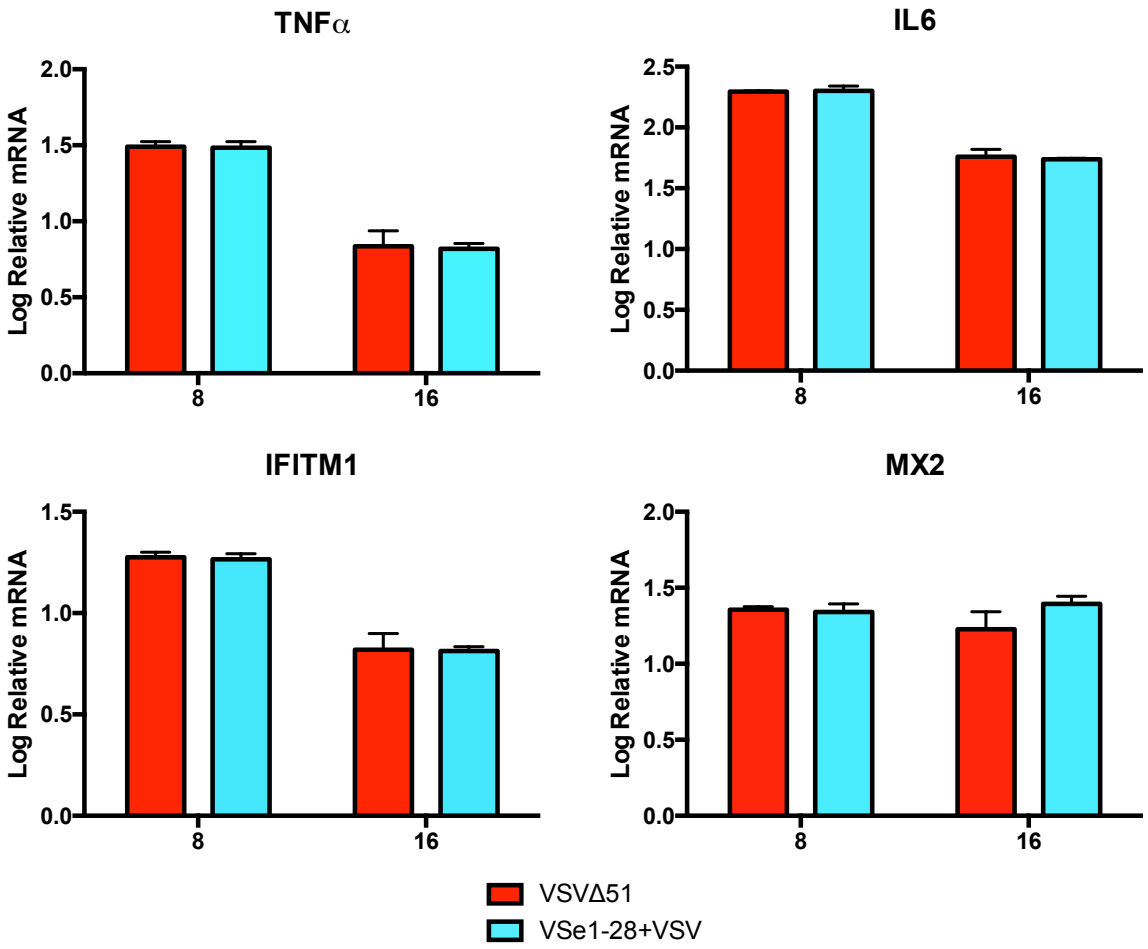
TNFα
IL6
IFITM1
MX2
Log Relative mRNA
2.0
1.5
1.0
0.5
0.0
2.5
8
16
VSVΔ51
VSe1-28+VSV

Figure 12. VSe1-28 does not inhibit expression of NF-κB targeted genes and ISGs in primary murine hepatocytes.
Quantitative RT-PCR was analyzed on RNA collected from primary murine hepatocytes pre-treated with VSe1-28 (10μM) for 2 hours and infected with VSVΔ51-GFP (MOI 1) for 8 and 16 hours. Gene expression was analyzed for NF-κB targeted genes TNFα and IL6 and ISGs MX2 and IFITM1.

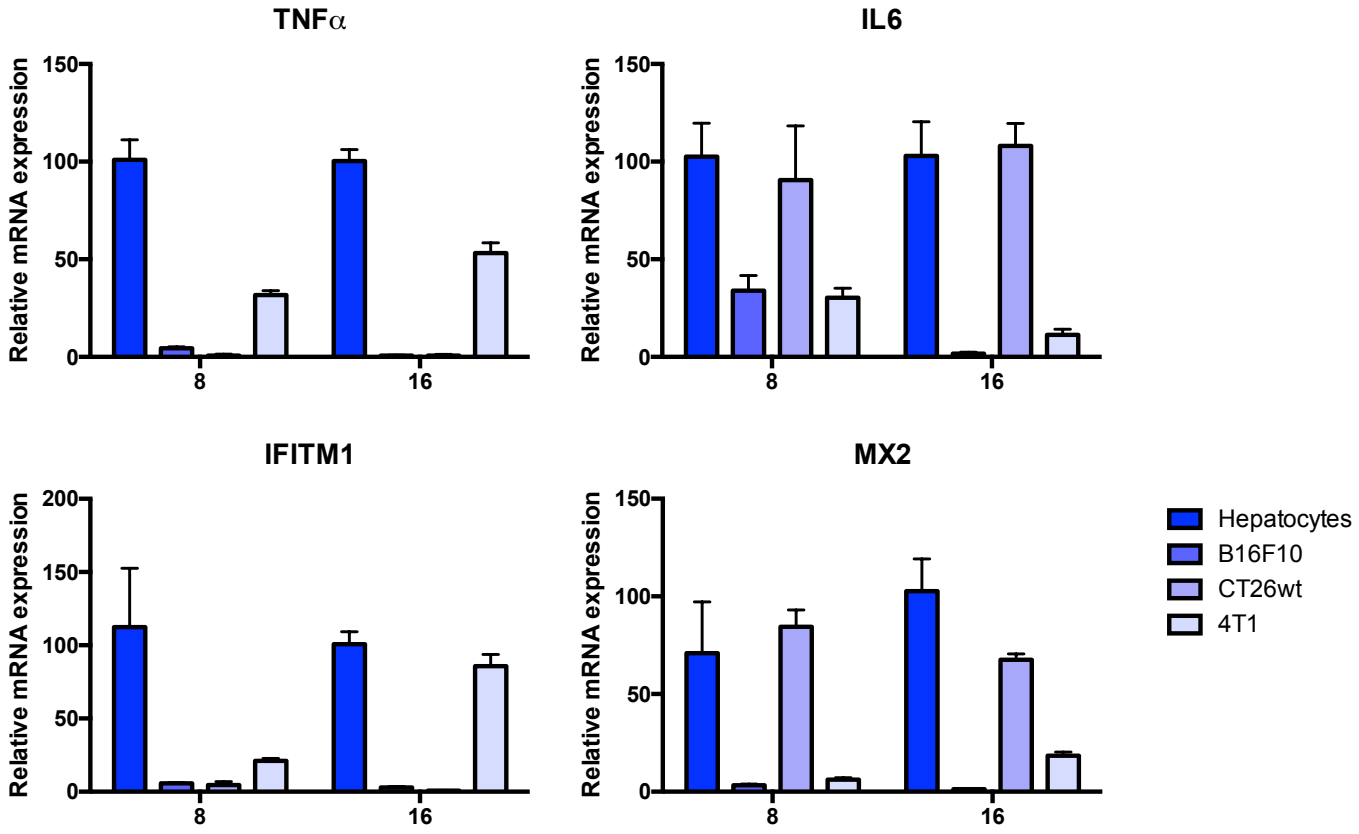
TNFα
IL6
IFITM1
MX2
Relative mRNA expression
150
100
50
0
200
8
16
Hepatocytes
B16F10
CT26wt
4T1

Figure 13. Baseline expression of p65 induced genes higher in primary murine hepatocytes.

Baseline expression of TNFα, IL6, IFITM1, and MX2 of primary murine hepatocytes were compared to B16F10, CT26wt, and 4T1 cancer cell lines. Samples are normalized to GAPDH and expressed as relative mRNA expression compared to hepatocyte mRNA expression.

3.3 Covalent modification of NF-κB p65 identified as molecular target

As an alternative method in identifying the molecular target of VSe1 and its analogs, we used activity-based protein profiling[86] **(Figure 14),** which focuses on covalent interactions of drugs to proteins, aimed to identify the molecular target of VSe1 and its analogs. We designed a panel of probes that had the ability to be linked to biotin and rhodamine azide using click chemistry. This click chemistry method allows for a simplistic way to tag proteins with probes for detection and evaluation[87]. This reaction can be used for the addition of azides to terminal alkynes using copper as the catalyst and is one of the most used click chemistry reaction[87]. This reaction produces an extremely stable bond between the azide and terminal alkyne[87]. Using this reaction, we were able to link protein-bound probe to rhodamine or biotin azide followed by pulldown with streptavidin beads and subsequent detection and evaluation using immunoblotting or fluorescent imaging. Altogether, three probes were synthesized: 1) VSe1-54, which is an active probe of VSe1 and VSe1-28 that retains viral enhancing activity and can be linked to biotin or rhodamine azide **(Figure 15a and b)**, 2) VSe1-56, which is an inactive probe that has the α,β unsaturated carbonyl moiety removed and had no impact on viral titers **(Figure 15a and c)**, and 3) a DMF probe, taking advantage of the fact that DMF has already demonstrated viral sensitizing activity[62] and was shown by another group to covalently modify Cys 38 of p65[78]. The DMF probe was based on the one previously synthesized by Kastrati et al., and we confirmed its viral sensitizing properties **(Figure 15a and d)**.

Using concentrations that potentiated VSVΔ51 infection, 786-0 cells were pre-treated with VSe1-54, VSe1-56 or DMF probe for 2 hours, and then treated with vehicle or TNFα. Whole cell lysates were then collected and a click chemistry reaction performed to link rhodamine azide with VSe1-54, and DMF probes. Rhodamine is a fluorescent dye that has an absorbance of 501 nm and

excitation at 525 nm[88,89]. This allows any protein that has been modified by the two probes to fluoresce when imaged. Lysate was then separated by SDS Page and imaged using a fluorescent gel imager. The DMF probe showed very promiscuous binding to numerous proteins across all size ranges showing strong banding patterns after a 5 second exposure **(Figure 16a)**. VSe1-54 (active probe) also showed binding to multiple proteins across different size ranges, but was weaker, as banding patterns did not appear until 40 second gel exposure **(Figure 16b)**.

Next, we wanted to investigate if covalent modification of our compounds depended on folding states of proteins. The experiment was repeated using whole cell lysates that were heat inactivated at 95 °C for 5 minutes (or unheated), and then treated with VSe1-54 (active probe) or DMF probe. After 1 hour, lysates were incubated with rhodamine azide. In both normal and heat denatured conditions, the DMF probe showed stronger banding patterns of proteins than VSe1-54 **(Figure 17)**. Interestingly, upon heat inactivation of lysate, which causes proteins to denature, the banding pattern of both VSe1-54 (active probe) and DMF probe changed, with some bands, particularly in the 65kDa range, becoming stronger.

To examine if p65 was a molecular target of VSe1 and VSe1-28, we used a competitive activity-based protein profiling approach. As we already know DMF covalently modifies p65[77], we considered that if the target of VSe1 and VSe1-28 is also p65, prior blocking of the binding site with VSe1-28 would reduce DMF probe-bound p65. 786-0 cells were pre-treated with VSe1-28, or VSe1-56 (inactive probe) before being treated with the DMF probe. Whole cell lysate was collected and biotin azide was used to pulldown interacting proteins with the DMF probe. As expected, incubation of DMF probe alone with 786-0 cells resulted in the detection of DMF probe bound p65. But, when cells were pre-treated with increasing concentrations of VSe1-28 (120 μM-500 μM), there was a dose-dependent reduction in DMF bound p65, demonstrating VSe1-28 can

compete with the same binding site(s) as DMF **(Figure 18)**. In contrast, the inactive probe VSe1-56 was unable to inhibit the binding of the DMF probe to p65. Altogether, our data provide evidence that both VSe1 and VSe1-28 covalently modify NF-κB p65, which inhibits nuclear accumulation, leading to dampened IFNβ and ISG expression and increased VSVΔ51 infection.

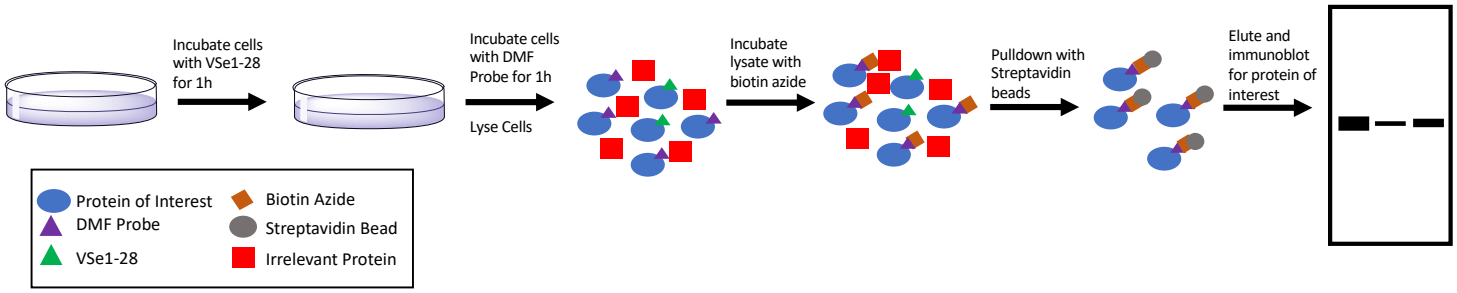
Incubate cells with VSe1-28 for 1h
Incubate cells with DMF Probe for 1h
Lyse Cells
Incubate lysate with biotin azide
Pulldown with Streptavidin beads
Elute and immunoblot for protein of interest
Protein of Interest
DMF Probe
VSe1-28
Biotin Azide
Streptavidin Bead
Irrelevant Protein

Figure 14. Schematic workflow of activity based protein profiling.
Technique was used to identify covalently modified proteins by VSe1-28. VSe based probes were designed and synthesized by Dr. Christopher Boddy's lab to maintain the active α,β unsaturated carbonyl portion of VSe1-28. It also contains an alkyne group to allow addition of biotin azide to be added to the probe using click chemistry so the probe-protein complex can be pulled down and identified.

a.

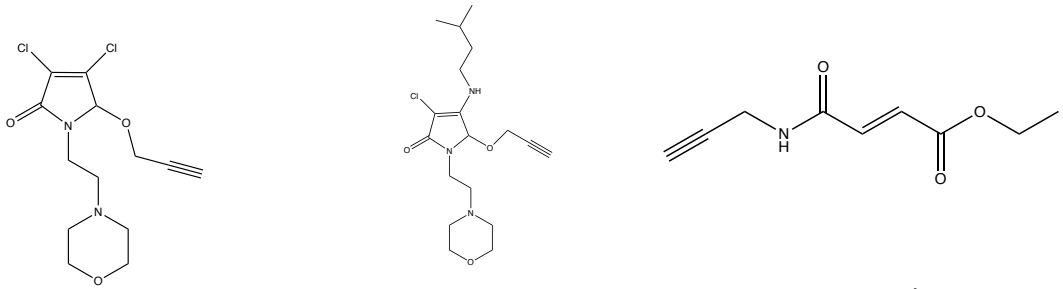
VSe1-54
VSe1-56
DMF Probe

b.

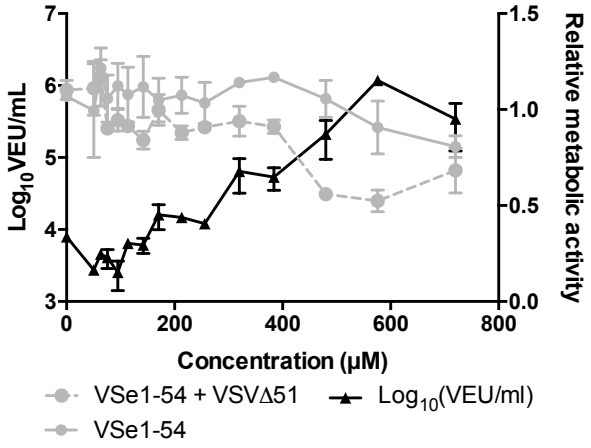
Log10VEU/mL
Relative metabolic activity
Concentration (μM)
VSe1-54 + VSVΔ51
Log10(VEU/ml)
VSe1-54

c.

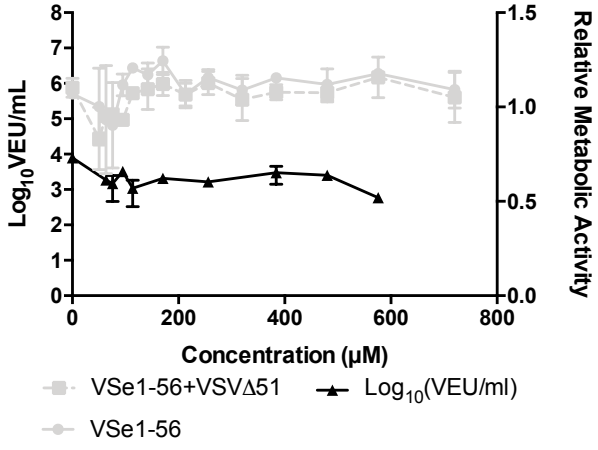
Log10VEU/mL
Relative Metabolic Activity
Concentration (μM)
VSe1-56+VSVΔ51
Log10(VEU/ml)
VSe1-56

d.

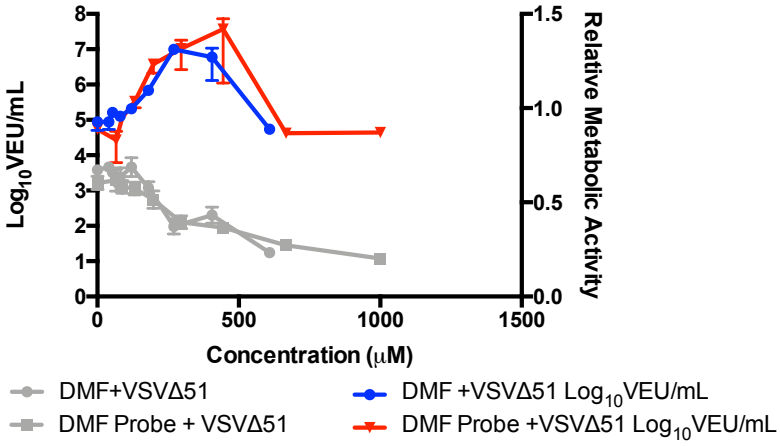
Log10VEU/mL
Relative Metabolic Activity
Concentration (μM)
DMF+VSVΔ51
DMF Probe + VSVΔ51
DMF +VSVΔ51 Log10VEU/mL
DMF Probe +VSVΔ51 Log10VEU/mL

Figure 15. VSe and DMF probes still retain viral enhancement activity.
(a) Chemical structures of VSe1-54 (active probe), VSe1-56 (inactive probe) and DMF probe. 786-0 cells were pretreated for 4 hours with **(b)** VSe1-54 (active probe) **(c)** VSe1-56 (inactive probe) **(d)**DMF and DMF probe and infected with VSVΔ51-Fluc (MOI 0.005). Supernatants were collected 40 hours post infection and titered via a luciferase based method. Viral titers are represented as Log_{10} VEU/mL and graphed on the left Y axis. Cell viability was determined using rezasaurin and represented as relative metabolic activity compared to mock untreated cells and graphed on the right Y axis.

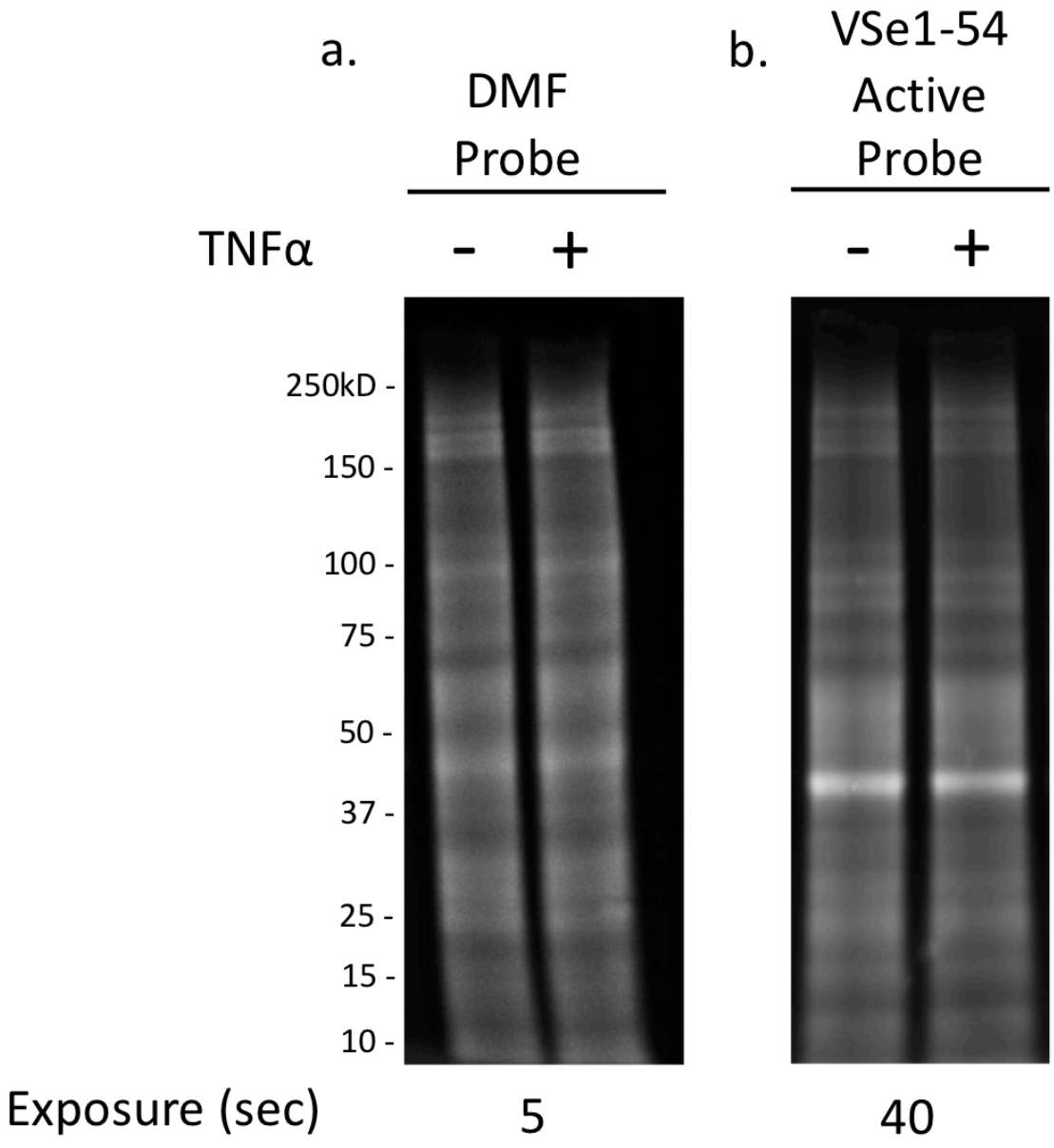
a.
DMF
Probe
b.
VSe1-54
Active
Probe
TNFα
-
+
-
+
250kD -
150 -
100 -
75 -
50 -
37 -
25 -
15 -
10 -
Exposure (sec)
5
40

Figure 16. Comparative Binding of DMF and VSe1-54 active probe.
786-0 cells were treated with VSe1-54 (400μM), or DMF(150μM) probe for 2 hours and then TNFα(25ng/mL) for 30 minutes. Whole cell lysate was collected. Lysate were incubated with rhodamine azide to allow addition of probe-protein complex to bind rhodamine azide. Protein was separated by SDS-PAGE and imaged with Fluorescence Chemi-Doc reader. **(a)** Gel was exposed for 5 seconds **(b)** Gel was exposed for 40 seconds.

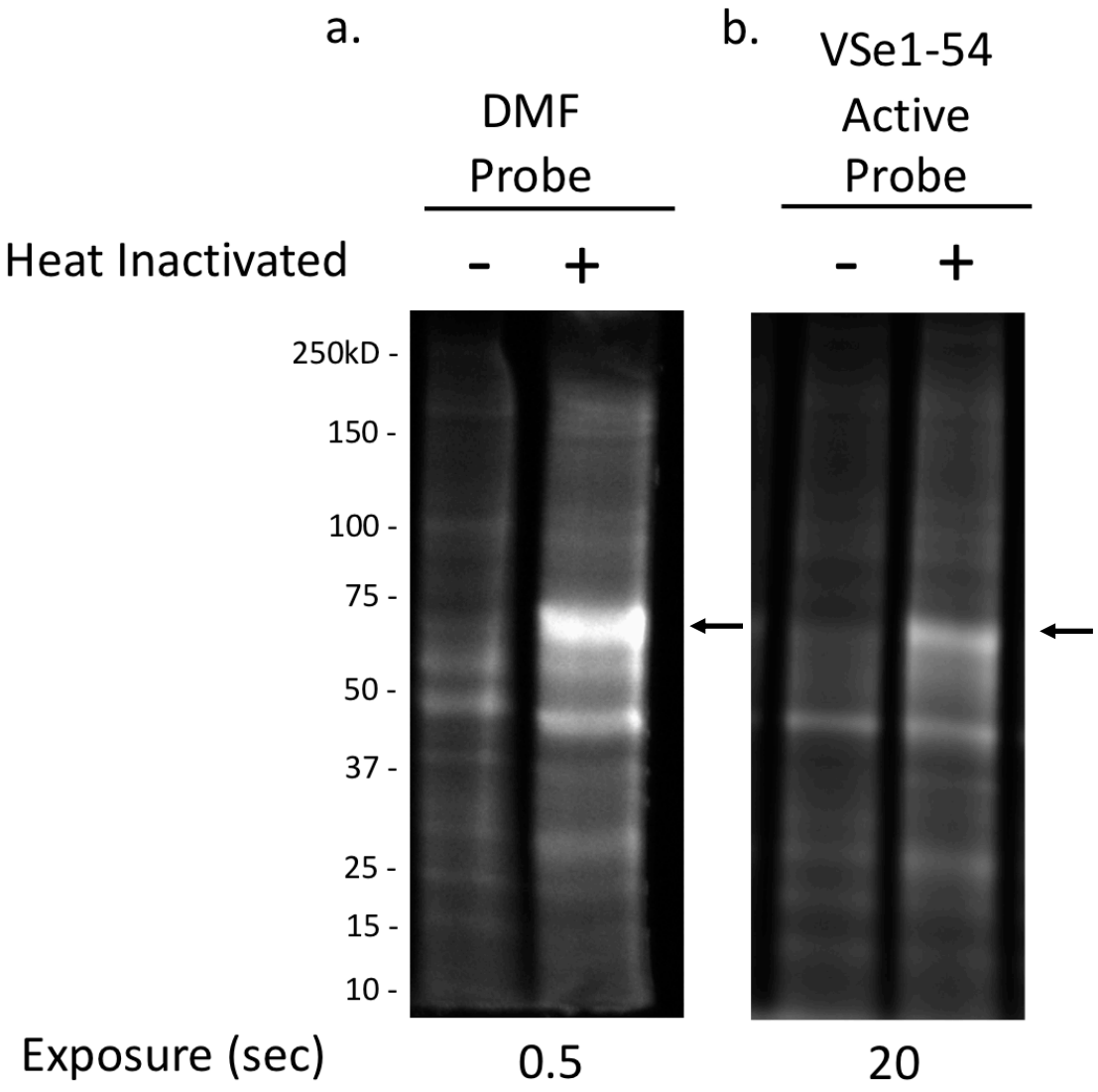
a.
b.
VSe1-54
Active
Probe
DMF
Probe
Heat Inactivated
-
+
-
+
250kD -
150 -
100 -
75 -
50 -
37 -
25 -
15 -
10 -
Exposure (sec)
0.5
20

Figure 17. DMF and VSe-1-54 active probe increase binding to heat inactivated lysate.
Whole cell lysate were collected from 786-0 cells. DMF probe or VSe1-54 was either incubated with whole cell lysate or heat inactivated (95 ºC for 5 minutes) whole cell lysate for 1 hour. Lysate was then incubated with rhodamine azide to allow click-chemistry reaction of rhodamine azide to probes. Proteins were run on SDS-Page and imaged with a Fluorescence gel imager. **(a)** Gel was exposed for 0.5 seconds **(b)** Gel was exposed for 20 seconds. ← indicates a stronger banding pattern in the 65kDa range.

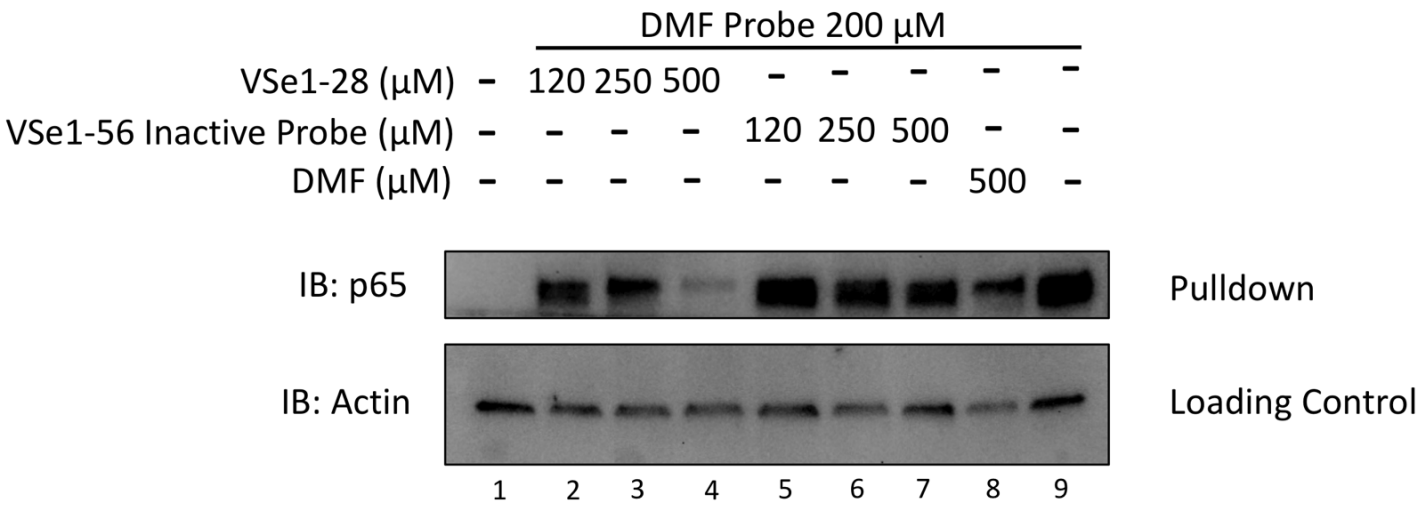
DMF Probe 200 µM
VSe1-28 (µM) - 120 250 500 - - - - -
VSe1-56 Inactive Probe (µM) - - - - 120 250 500 - -
DMF (µM) - - - - - - - 500 -
IB: p65
Pulldown
IB: Actin
Loading Control
1 2 3 4 5 6 7 8 9

Figure 18. VSe1-28 blocks binding of DMF probe to NF-κB p65.
786-0 cells were treated for 1 hour with varying concentrations of VSe1-28, VSe1-56 (Inactive probe), or DMF. Cells were then treated with DMF probe for 1 hour. Whole cell lysate was then collected, biotin azide was incubated with lysate for 1 hour to allow click-chemistry reaction to take place between biotin azide and DMF probe. Probe-protein complex were then pulled down with streptavidin beads and run on a SDS-Page gel and immunoblotted for p65 and β-actin.

3.4 VSe1-28 inhibits NF-κB target genes and interferon stimulated genes in mouse tumours

Our lab has previously shown that VSe1-28 improved therapeutic efficacy in syngeneic CT26wt murine tumour models (Manuscript in Preparation-Appendix A). When VSe1-28 was combined with VSVΔ51-Fluc, it led to a significant delay in tumour progression and extended survival (Manuscript in Preparation-Appendix A). Due to its efficacy already demonstrated in CT26wt tumour models, we attempted to validate the lead analog VSe1-28 and its ability to impact NF-κB target gene transcription in murine tumour models. Balb/c mice were implanted with CT26wt tumours and injected intratumourally with VSe1-28 (40 mg/kg) or vehicle. Four hours later, mice were injected intratumourally with 1×10^8 pfu of VSVΔ51-Fluc. RNA was extracted from tumours 16 hours post-infection, and consistent with our *in vitro* data, we saw that VSe1-28 was able to reduce expression of NF-κB target genes TNFα and IL-6 and ISG IFITM1 **(Figure 19)**. Furthermore, although not significant at this time point, there was a trend of increased VSVΔ51-Fluc luciferase expression in the presence of VSe1-28 **(Figure 20)**. Overall, our data suggest that VSe1-28 can dampen NF-κB mediated transcription of target genes following VSVΔ51 administration, thereby potentiating viral infection of murine tumours.

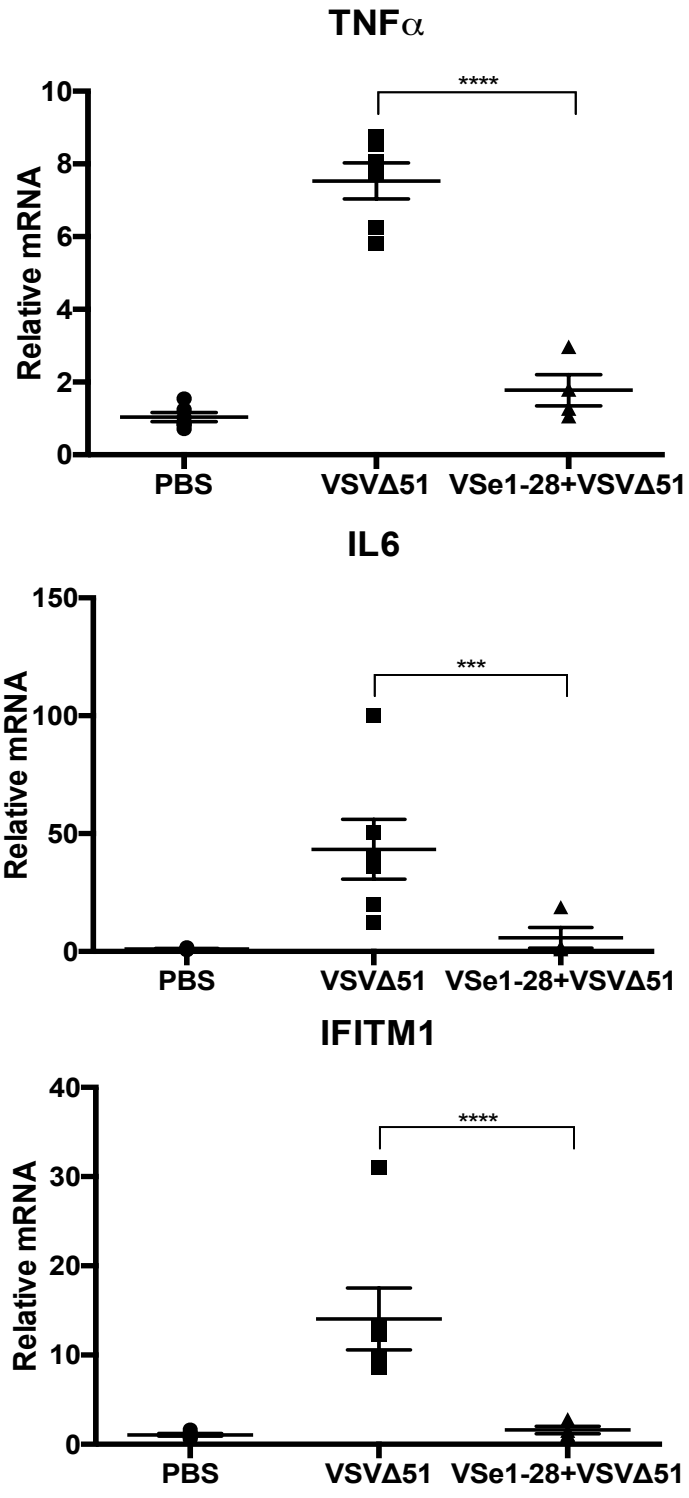
TNFα
Relative mRNA
10
8
6
4
2
0
****
PBS
VSVΔ51
VSe1-28+VSVΔ51
IL6
Relative mRNA
150
100
50
0
***
PBS
VSVΔ51
VSe1-28+VSVΔ51
IFITM1
Relative mRNA
40
30
20
10
0
****
PBS
VSVΔ51
VSe1-28+VSVΔ51

Figure 19. VSe1-28 inhibits NF-κB target gene expression in mouse tumours.
Balb/c mice bearing CT26wt tumours were treated with vehicle (DMSO) or 40 mg/kg VSe1-28 by intratumoural injection. Four hours later, mice were injected with 1×10^8 plaque forming units of VSVΔ51-Fluc. RNA was harvested from tumours 16 hours post infection. Quantitative RT-PCR was used to analyze gene expression of TNFα, IL6 and IFITM1. ***P < 0.001, ****P < 0.0001. (One-way anova with Dunnet's multiple comparison). N=2-3 mice per group.

b. VSVΔ51 a.

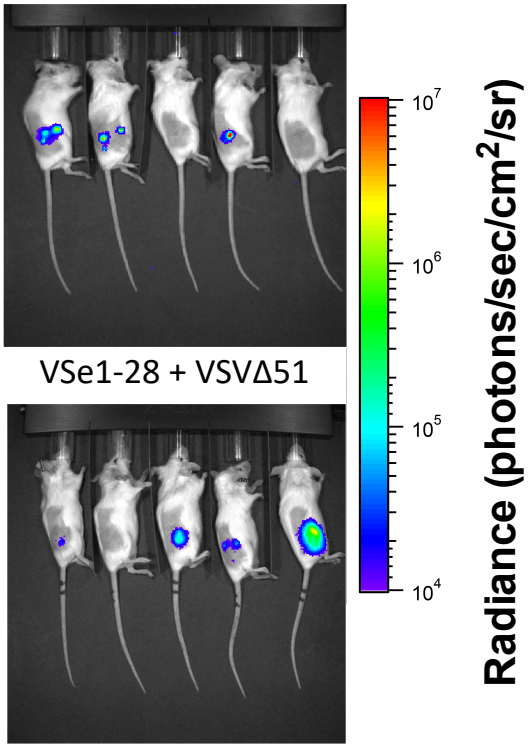
VSe1-28 + VSVΔ51
10^7
10^6
10^5
10^4

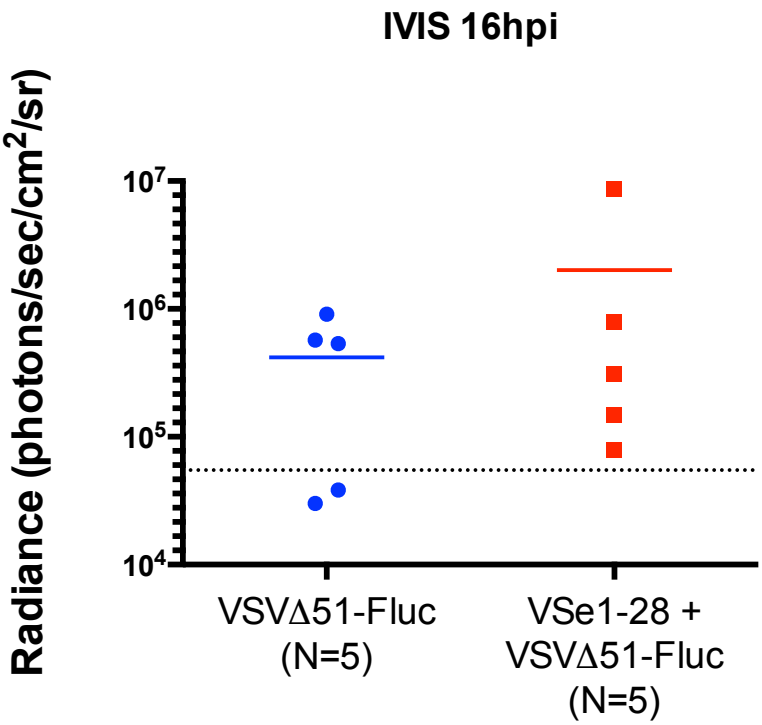
IVIS 16hpi
Radiance (photons/sec/cm²/sr)
10^7
10^6
10^5
10^4
VSVΔ51-Fluc (N=5)
VSe1-28 + VSVΔ51-Fluc (N=5)

Figure 20. VSe1-28 enhance VSVΔ51-Fluc infection in mouse tumour model.
(a) Balb/c mice bearing CT26wt tumours were treated with vehicle or 40 mg/kg of VSe1-28 by intratumoural injection. Four hours later, mice were intratumourally injected with 1×10^8 plaque forming units of VSVΔ51-Fluc. Virus replication was analyzed 16 hours post infection by measuring luminescence using IVIS and **(b)** signal was quantified. N=5 mice per group.

4 Chapter: Discussion

Oncolytic viruses are attenuated to safely target cancer cells, however, this often limits their efficacy. VSVΔ51 which relies on defective IFN pathways in cancer cells to be able to achieve therapeutic benefit can be ineffective in some cases as not all cancers have completely defective antiviral pathways. Many different strategies are being employed to try to enhance the efficacy of oncolytic viruses. Combining VSVΔ51 with small molecule compounds such as VSe1 and VSe1-28 is a particular strategy that our lab has pioneered. But, in trying to enhance the effectiveness of oncolytic viruses, it is important to consider safety and off-target effects that could result. As such, it is important to clearly define the mechanism of action of these compounds and fully understand the mechanism through which they can potentiate oncolytic virus infection of cancer cells.

4.1 GSTP1-1 is not the molecular target of VSe compounds

In a quest to find the molecular target of our compounds, we used ligand-based chromatography techniques. Such techniques often used to study interactions between proteins and ligands were useful in our search for interacting proteins[90]. The top hit from this technique revealed GSTP1-1 as a major interacting molecule (Manuscript in Preparation-Appendix A). GSTP1-1 is responsible for detoxifying both endogenous and exogenous compounds through conjugation with GSH allowing export out of cells[91]. GSTP1-1 has been shown to play an important role in drug detoxification through conjugation with GSH and has been known to attribute to tumour chemoresistance including resistance to cisplatin treatment[91,92]. It has also been shown that GSTP1-1 plays a role in cervical cancer as loss in expression of GSTP1-1 inhibits the proliferation and survival of the cancer cells[93]. It has also been shown in turn that IKK is able to down-regulate

the expression of GSTP1-1 while upregulating other antioxidative and cytoprotective genes[94]. Furthermore, GSTP1-1 has been shown to interact with and modulate the NF-κB pathway. GSTP1-1 associates with IκBα and is hypothesized to prevent the phosphorylation and ubiquitination of IκBα and prevent NF-κB activation[95]. However, it is interesting that our lab has shown no impact on IκBα degradation when cells are treated with VSe1 nor VSe1-28 (Manuscript in Preparation-Appendix A).

However, even though GSTP1-1 was identified as an interacting molecule with the VSe1 analog class of viral sensitizers, knocking down GSTP1-1 expression in 786-0 cells using siRNA and infection with VSVΔ51 showed no enhancement of viral infection **(Figure 7a)**. In addition, knocking down the expression of GSTP1-1, followed by treatment with VSe1 did not prevent robust sensitization to infection **(Figure 7b)**. Altogether, our data imply that GSTP1-1 alone is not likely the main molecular target responsible for VSe1's viral sensitizing activity as knockdown of GSTP1-1 was not able to mimic the viral sensitizing effects seen with VSe1 and after knocking out GSTP1-1, VSe1 was still able to enhance viral infection. Therefore, GSTP1-1 may not play a role in the viral sensitizing effects of VSe1 but may have been identified as an interacting molecule due to VSes electrophilic nature and the role of GSTP1-1 in the detoxification of cells from drug compounds.

4.2 VSe1 and VSe1-28 suppress p65 nuclear-translocation and inhibit target gene expression in various cancer cell lines

To validate the proposed mechanism of action, we needed to examine the reproducibility of the mechanism of action of our compounds across multiple cell lines. In addition to human 786-0 renal carcinoma cells, we have shown that both VSe1 and VSe1-28 decrease nuclear

accumulation of NF-κB p65 in B16F10 (murine melanoma), CT26wt (murine colon carcinoma) and 4T1 (murine breast mammary cancer). These cell lines have all been previously shown to be relatively resistant to VSVΔ51 infection **(Figure 9)**, but pretreating cells with VSe1 or VSe1-28, leads to increased viral titers. It was interesting to note that VSe1 and VSe1-28 consistently decreased nuclear accumulation of p65, but the impact on p50 was more variable across the three cell lines. This suggested that p50 may not be as important in the mechanism of VSe1 and VSe1-28's ability to enhance infection by VSVΔ51.

Analyzing gene expression of NF-κB target genes TNFα and IL-6 as well as interferon stimulated genes (ISGs) IFITM1 and MX2 in B16F10, CT26wt, and 4T1 showed that VSe1 and VSe1-28 inhibit NF-κB mediated genes in these various cancer cell lines. Indeed, dampened RNA upregulation of TNFα, IL-6, IFTIM1, and MX2 was observed as early as 8 hours post-infection **(Figure 10)**. In B16F10 and 4T1 cells, dampened expression of NF-κB controlled genes extends to 16 and 24 hours post-infection **(Figure 10)**. However in CT26wt cells, after the initial reduction around 8h, RNA expression of these genes begins to increase higher than VSVΔ51 infected cells alone at about 16 hours post-infection. This rebound effect is also seen in the other cell lines, but at much later timepoints. The surge in RNA expression of these genes at later timepoints, after the initial dampening due to a reduction in p65 nuclear accumulation, is believed to be due to the increased viral infection of these cells, which in turn will trigger these pathways. In CT26wt cells, this effect seems to be happening much faster than in the other cell lines.

Altogether, seeing both inhibition of nuclear accumulation of NF-κB as well as reduction in RNA expression of TNFα, IL-6 and ISGs IFITM1 and MX2 shows that the mechanism of action of VSe1 and VSe1-28 could be ubiquitous across multiple cancer cell lines.

4.3 VSe1 analogs do not sensitize normal cells to viral infection

We next examined the cancer selectivity of VSe1 and VSe1-28. Treating primary murine hepatocytes with VSe1-28 prior to VSVΔ51 infection led to no increases in infection **(Figure 11)**. Luciferase expression remained at baseline levels at all concentrations of VSe1-28. Our group has also previously shown tumour selectivity in both an *ex vivo* and *in vivo* model[69]. Altogether this provides further evidence that the effect of VSe1 and VSe1-28s exhibits selectivity for cancer cells.

Importantly, we saw no suppression of NF-κB target genes TNFα and IL-6 nor ISGs IFITM1 and MX2 following treatment by VSe1-28 and VSVΔ51 infection of normal murine hepatocytes **(Figure 12)**. VSe1-28 was not able to inhibit the expression of TNFα, IL-6, IFITM1, and MX2, in contrast with what was observed in cancer cell lines. This correlates well with the lack of sensitization to virus VSVΔ51, albeit it remains unclear why this is the case. What was interesting to note was when comparing baseline RNA expression levels of these genes between normal murine hepatocytes and various cancer cell lines including B16F10, CT26wt, and 4T1, we saw higher baseline expression in hepatocytes compared to cancer cell lines in some antiviral genes, markedly TNFα **(Figure 13)**. This could be because in the acute-phase of infection, TNFα and IL-6 are upregulated to mediate the transcriptional activity of key proteins to limit tissue injury and boost host defense systems[96]. In consequence, since VSVΔ51 has an inactive viral M-protein, it loses its ability to inhibit cellular gene expression and limits its ability to infect normal cells with intact antiviral signaling pathways. One possibility is that higher expression of genes like TNFα at baseline limits the ability of VSVΔ51 to infect normal cells altogether, and in consequence, NF-κB nuclear accumulation is not induced, and therefore even though VSe1-28 may still covalently modify p65, there is no effect on target gene expression. Further testing can be done by pre-treating hepatocytes with VSe1-28 and then treating with TNFα to induce NF-κB nuclear accumulation

and expression of target genes. If VSe1-28 does covalently modify p65 in hepatocytes, we should see a decrease in the expression of these target genes.

However, we cannot conclude that TNFα and IL-6 are the only mediators responsible for this and in addition, it remains to be tested whether this is true for all types of normal cells, not just hepatocytes. Further steps would need to be taken, a panel of ISGs should be examined across not only different cancer cell lines but also different normal cell lines to examine exactly which genes may be responsible in preventing normal cells from becoming infected in the presence of viral sensitizers. Also, developing an *in vivo* experiment treating mice with VSe1-28 and subsequently infecting with VSVΔ51 intraperitoneally, and harvesting mouse organs, analyzing viral titer as well as expression of these genes might give us more information on the effects of these compounds in non-cancerous cells.

4.4 NF-κB p65 identified as a molecular target

As GSTP1-1 was not found to be the molecular target responsible for VSe1 and VSe1-28, new approaches were taken to find the correct molecular target. Due to the α, β unsaturated carbonyl moiety present on the chemical structure of both VSe1 and VSe1-28, it was likely that it was able to react covalently with other molecules. In the literature, many compounds were shown to bind NF-κB p65 subunit and decrease nuclear accumulation. We followed up the data by Kastrati et. al who demonstrated that DMF can covalently modify Cys 38 of p65[78]. In addition, our lab has identified DMF as a compound that can potentiate VSVΔ51 infection[62]. Using click-chemistry, we synthesized the DMF probe previously described by Kastrati et. al[78]. In a competition assay, we showed that by treating 786-0 cells with VSe1-28 prior to treating with DMF probe, decreased DMF probe bound to p65 **(Figure 18)**. When treating cells with VSe1-56,

the inactive analog, which does not have an α,β unsaturated carbonyl moiety, we saw no decrease in DMF-bound p65. This provided evidence that VSe1 and VSe1-28 share the same target as DMF as they both compete for p65.

As DMF is currently approved by the FDA to be used for relapsing-remitting multiple sclerosis (MS) and psoriasis[97,98], and VSe1/VSe1-28 and DMF share the same target, it is tempting to speculate that our small molecules could be used as standalone drugs towards treating these diseases. DMF is marketed as Tecifidera for MS and SKilarence and Fumaderm for psoriasis[98,99]. DMF is the most prescribed drug for relapsing-remitting multiple sclerosis in the U.S. [100]. All three are oral formulations and it is thought currently that DMF is a prodrug and is rapidly converted by esterases in the gastrointestinal mucosa to monomethyl fumarate[98,99,101]. DMF seems to act through multiple mechanisms in psoriasis including reacting with glutathione, modulating oxidative stress responses, activation of nuclear factor (erythroid-derived 2)-like (NRF2) stimulating both cytoprotective and anti-inflammatory genes as well as inhibition of NF-κB activity, decreasing cytokine production and modulating the immune response[99]. In MS, DMF also seems to induce an antioxidant and anti-inflammatory response through modulating NRF2 and NF-κB[98,100]. Given that DMF's target is also NF-κB, very similar to VSe1 and VSe1-28, and GSTP1-1, which is involved in the addition of GSH onto compounds and its involvement in oxidative stress, it is interesting to consider VSe1-28s use for treatment of MS and psoriasis. In a direct pull-down assay using active probes for VSe1 as well as one for DMF, we see that the DMF probe binds proteins across a wide range of protein sizes **(Figure 16a)**. But our VSe1-54 probe only shows detectable protein binding after longer exposure **(Figure 16b)**.

Furthermore, in addition to being current therapeutics for MS and psoriasis, NF-κB inhibitors have also been evaluated and tested in cancer therapy, as many cancers exhibit

constitutively active NF-κB pathways, albeit without much success. Much of this is due to off-target effects and resistance[102]. Since the VSe1-28 probe appears less reactive compared to the DMF probe **(Figure 16)**, due to banding signals only appearing after longer exposure times, this could provide evidence that VSe1-28 may have more specific target proteins. Alternatively this could mean that the VSe1-28 probe is comparatively more labile. This could prove beneficial not only as a viral sensitizer and increase the efficacy of oncolytic virotherapy for treatment of cancer, but could be effective when combined with other already existing cancer treatments like chemotherapy or radiotherapy.

Future experiments should be aimed at confirming the interaction between VSe1 and VSe1-28 with p65. As there is a possibility that our VSe1-28 probe is labile when bound to protein, this could be an alternative explanation for the decreased signaling found in the rhodamine azide blots **(Figure 16)**, new probes are being synthesized that contains an alkyne bond that is more stable and less likely to break apart during click-chemistry reactions. The alkyne on VSe1-54 (active probe) and VSe1-56 (inactive probe) is attached to an oxygen that is apart of a N,O acetal which is unstable. As both the nitrogen and oxygen are bonded to the same carbon atom, the oxygen that the alkyne is bonded to can be easily eliminated resulting in the inability of biotin azide or rhodamine azide to be linked to our probes. A more stable probe can be used to examine if VSe1-28 directly modifies p65. Efforts are also being made to identify the direct site of binding to p65. As other molecules have shown binding to the Cys 38 region of p65, this is where our efforts are currently being concentrated. Also, we can treat purified recombinant p65 *in silico* that has a mutated cysteine 38 with VSe1-28, and if this is the site of binding, we should see no covalent modification of p65 using mass spectrometry. Upon examining the crystal structure of p65 **(Figure 2)**, it is noted that Cys 38 is located in close proximity to DNA, and it is therefore possible that

covalent modification of this cysteine could disrupt DNA binding. All this should confirm that VSe1 and VSe1-28 are acting by blocking NF-κB nuclear accumulation through binding of p65 resulting in decreased antiviral signaling allowing for sensitization to viral infection. However, from our data, p65 may not be the only target of VSe1 and VSe1-28 **(Figure 16)**, therefore a broader investigation using mass spectrometry can be used to further uncover other potential targets. Comparing these hits to targets of other drugs like DMF could also lead us to investigate the effectiveness of VSe1 and VSe1-28 for the treatments for other diseases other than cancer.

4.5 VSe1-28 decrease expression of NF-κB target genes in mouse tumour models

As our group has previously shown, VSe1-28 is much more stable in aqueous media, has higher plasma stability, and dose escalation studies *in vivo* have revealed much better tolerability profiles compared to VSe1, therefore, VSe1-28 is much better suited for animal and eventually human testing. Previous data from our lab has indicated increased survival and tumour regression in mice bearing CT26wt tumours treated with VSe1-28 followed by VSVΔ51 (Manuscript in preparation-Appendix A). With that in mind, we wanted to examine if VSe1-28 followed the same mechanism as we have demonstrated *in vitro*.

RNA expression analysis of tumour tissue revealed that VSe1-28 pre-treatment, followed by VSVΔ51 administration, significantly inhibited expression of NF-κB target genes TNFα and IL-6 as well as ISG IFITM1 at 16 hours post-infection **(Figure 19)**. This suggests that our compounds act in murine models through NF-κB mediated inhibition of antiviral signaling pathways, very similar to what we have already seen *in vitro* in various cancer cell lines, including CT26wt. This provides important evidence into the translation of this combination therapy into a clinical setting. We have shown that VSe1-28 in combination with VSV can inhibit anti-viral

signaling in tumours and potentiates the oncolytic effect of VSVΔ51. Future work will be needed to further confirm the effects in mouse models. For example, quantifying the impact of VSe1-28 on nuclear accumulation of NF-κB p65 in tumours using immunohistochemistry. Furthermore, as safety will be an important criterion for clinical translation, the effects of VSe1-28 on organs and surrounding tissue should be analyzed.

5 Chapter: Conclusion

Oncolytic virotherapy is a new and improving avenue of cancer therapeutics. But due to tumour heterogeneity, efficacy is severely limited. Through the administration of VSes in combination with oncolytic viruses, our group has already shown increased efficacy. In this study, we have deduced the mechanism of action and molecular target of how VSe1 and VSe1-28 work. We were able to uncover that these compounds are acting through direct modification of NF-κB p65, a key player in antiviral signaling, decreasing its nuclear accumulation. This results in a decrease in NF-κB target gene expression including expression of IFNβ which ultimately increases the efficacy of oncolytic viruses to infect cancer cells. Furthermore, we confirmed the oncoselectivity of our compounds for cancer cell lines over normal cell lines. Following up on past results done by our group proving that VSe1-28 was able to slow tumour progression and increase survival in mouse tumour models, we show that VSe1-28 decreases expression of NF-κB target genes and ISGs *in vivo.* Although further work will be needed to validate VSes effects in mouse tumour models and its ability to enhance oncolytic viral therapy, this study has laid the groundwork to the mechanism of action of VSe1 and VSe1-28. This provides valuable information into both the mechanism of action and safety of these compounds for future development and clinical translation.

Appendices

Appendix A : Draft: Viral sensitizers suppress innate immunity to sensitize cancer cells to oncolytic virotherapy: Manuscript In Preparation

A.1 Manuscript in Preparation Text

Viral sensitizers suppress innate immunity to sensitize cancer cells to oncolytic virotherapy

Ramya Krishnan[1,2]*, Nader El Sayes[1,2]*, Michael Phan[1,2], Johanne Mathieu[1,2], Mohammed Selman[1,2], Andrew Macklin[3], Mark Dornan[4], Jesse Brown[4], Andre Paquette[4], Boaz Wong[2], Anna Jirovec[1,2], Geneviève F. Desrochers[4], Hilary Groom[7], David Patten[2], Colin Davis[1,2], Frances Lai[5], Brian Lichty[5], Mary-Ellen Harper[2], Rozanne Arulanandam[1], John C. Bell[1,2], Tommy Alain[2,6], David Josephy[7], John P. Pezacki[4], Jeffrey C. Smith[3], Christopher N. Boddy[4], Jean-Simon Diallo[1,2].

1. Center for Innovative Cancer Research, Ottawa Hospital Research Institute
2. Department of Biochemistry, Microbiology and Immunology, Faculty of Medicine, University of Ottawa
3. Department of Chemistry and Institute of Biochemistry, Carleton University
4. Department of Chemistry and Biomedical Sciences, University of Ottawa
5. McMaster Immunology Research Centre, Department of Pathology and Molecular Medicine, McMaster University,
6. Children's Hospital of Eastern Ontario Research Institute
7. Department of Molecular and Cellular Biology, Summerlee Science Complex, University of Guelph

*Equal contribution

Abstract

Oncolytic viruses (OVs) are often attenuated to increase their safety profile, however this can lead to reduced efficacy in heterogeneous malignancies and result in resistance to OV therapy. Our group has previously discovered a novel class of furan and pyrrole-based small molecule viral sensitizers (VSes) that can sensitize resistant tumours to OV infection leading to reduced tumour burden and prolonged survival *in vivo*. In this study, we dissected the effect of these VSes on the cellular innate antiviral response in order to identify the principal molecular target responsible for their viral-sensitizing properties. We found that treatment with the VSes inhibits nuclear translocation of NF-κB via covalent modification of the p65 subunit and dampens transcriptional expression and downstream secretion of IFN-β, increasing viral replication and spread preferentially in cancer cells. This study identifies NF-κB as a key target for viral sensitization to improve OV infection of resistant tumours and opens a path to clinical translation of novel VSe compounds.

Introduction

Cancer cells have evolved to resist apoptosis, fuel cell growth via altered cellular energy metabolism, and avoid detection and destruction by the immune system. Altogether, this makes tumours ideal microenvironments for viral replication, rendering them uniquely vulnerable to viral infection and lysis[1,2]. Oncolytic viruses (OVs) are anti-cancer bio-therapeutic agents that target tumours by exploiting multiple cancer-specific defects. Through engineering or experimental selection, OV tropism for cancerous tissues over normal tissues can be further enhanced compared to wild-type viruses. OVs are multi-mechanistic and destroy tumours by inducing direct lysis of cancer cells, expresing therapeutic transgenes, causing vascular shutdown of tumour-associated blood vessels, and generating an anti-tumour immune response[2,3]. Interest in the development of OVs as targeted cancer therapeutics has skyrocketed over the past few years owing to the recent approval of the HSV-1-based Talimogene laherparepvec or T-VEC[4,5] and the realization that OVs mechanistically complement immune checkpoint blockade (PMID 24598590).

Vesiculoviruses (rhabdoviridae) were some of the earliest OV candidates tested pre-clinically and have emerged as promising OV platforms due to their ability to rapidly induce cell death and generate a strong anti-tumour immune response (PMID 23052398). Furthermore, unlike many other platforms based on human pathogens or vaccines, pre-existing immunity in the human population is rare (PMID 23052398). Oncolytic variants of vesicular stomatitis virus (VSV), as well as the closely related Maraba virus, are now undergoing phase I/II clinical evaluation in a number of malignancies as a monotherapy or in combination with immune checkpoint blockade (NCT02285816, NCT02879760, NCT03618953, NCT03773744). Cancer cells with defective type I IFN signalling pathways have been shown to be particularly vulnerable to rhabdovirus infection, a property that has been exploited to generate IFN-sensitive and thereby tumour selective variants such as VSVΔ51[6]. However, approximately 30-35% of cancer cell lines are fully IFN-responsive and block viral spread and oncolysis[7–11]. Tumour resistance to OV infection is a well-known contributor to the heterogeneous clinical response to OVs, which is not mechanistically addressed through combination with immune checkpoint blockade[12–17]. This highlights a need for novel

strategies to improve the infection of resistant tumours by IFN-sensitive OVs such as, but not limited to, oncolytic rhabdoviruses.

Our group has previously described a novel class of OV-sensitizing small molecules derived from the synthetic furan VSe1, which was identified by phenotypic high-throughput screening[18]. VSe1 and its pharmacologically-improved pyrrole analogs (e.g. VSe1-28) enhance the oncolytic effects of multiple OVs, including those based on HSV-1, Maraba, and VSV[19]. VSe1 and its analogs have been previously shown to sensitize resistant tumours to infection by OVs *in vitro* and *in vivo* by inhibiting the production of interferon-β (IFNβ), as well as dampening the expression of interferon-stimulated genes (ISGs) and ultimately blocking the antiviral effects of exogenous type-I IFN treatment [19,20]. While the compounds have a broad impact on the type I IFN response, the exact molecular target remains unknown, limiting their potential for clinical translation as adjuvant-enhancers of OV therapy. In the current study, we set out to determine the molecular mechanism of action consistent with the robust activity of both furan and pyrrole VSe1 derivatives on both type I IFN secretion and response.

Results

VSe1 analogs inhibit nuclear translocation of NF-κB, increase VSVΔ51 growth in cancer cells

We have previously reported the viral sensitizing activity of VSe1 (3,4-dichloro-5-phenyl-2,5-dihydrofuran-2-one) (PMID 20389287) and its pyrrole analogs and lead derivative VSe1-28 (3,4-dichloro-5-hydroxy-1-(2-morpholinoethyl)-1*H*-pyrrol-2(5*H*)-one) (PMID 27226390); structures shown in Figure 1a. Single and multi-step growth curves in VSVΔ51-resistant human renal carcinoma cells (786-0 cells), where cells are infected at high or low multiplicity of infection (MOI) respectively revealed that these compounds increase both virus burst size (production per cell) and spread of VSVΔ51 as early as 8h post infection (Figure 1b). This is consistent with prior studies demonstrating that both VSe1 and VSe1-28 impair the production of antiviral IFNβ following infection with VSVΔ51, as well as reduce ISG expression in cancer cells (PMID 20389287) [19]. We further investigated the kinetics of this interference by quantitative RT-PCR at multiple times post-infection with a high MOI (MOI = 1). As shown in Figure 1c, VSe1 and VSe1-

28 each significantly inhibit the mRNA expression of IFNβ as early as 8 hours and for up to 24 hours post-infection, which parallels the enhancement of viral titers seen in Figure 1b.

It has been previously shown that the IFNβ promoter requires a tripartite signal from NF-κB, IRF3/7, and c-jun/ATF2 for maximal activation[21]. Based on this, we next investigated the effect of VSe1 and VSe1-28 on the phosphorylation and nuclear translocation of NF-κB (p65 and p50 subunits), IRF3, c-jun and ATF2. 786-0 cells were pre-treated with VSe1 and VSe1-28 then infected with VSVΔ51 at MOI 1. Whole cell lysates or nuclear/cytoplasmic fractions were collected 8 hours post-infection and probed by Western blot. While IRF3, and c-jun nuclear translocation were unaffected by VSe1 (Figures 1d, lane 5 vs 4, and S1, lane 3 vs 2) or VSe1-28 (Figures 1d, lane 6 vs 4, and S1, lane 4 vs 2), the nuclear translocation of NF-κB (both p65 and p50 subunits) was substantially decreased by VSe1 (Fig. 1d, lane 5 vs 4) and VSe1-28 (Figure 1d, lane 6 vs 4). In the classical/canonical pathway of NF-κB signalling, NF-κB p50 and p65 subunits are initially sequestered by IκBα. Upon signalling through TLRs or the TNFR superfamily, phosphorylation of IκBα by the IKK complex leads to its ubiquitination and degradation, thereby freeing p50-p65 homo or heterodimers. NF-κB subunits can then be post-translationally modified through phosphorylation prior to nuclear translocation. We investigated the effects of VSe1 and VSe1-28 on NF-κB signalling upstream of nuclear translocation, and found that virus-induced dimerization of p65 and p50 was not affected, as assessed by CoIP (Figure S2). To assess the effect of VSe1 and VSe1-28 on canonical NF-κB signalling more specifically, TNF-α was used to induce NF-κB signalling through the TNFR superfamily. Western blots of nuclear/cytoplasmic extracts confirmed that both compounds inhibited TNF-α-induced nuclear translocation of NF-κB p65 as early as 30 minutes post-stimulation with TNF-α (Figure S3, lanes 5 and 6 vs 4). Interestingly, TNFα-induced phosphorylation of p65, as well as IκBα degradation, were not inhibited by VSe1 or VSe1-28 (Figure 1e, lanes 5 and 6 vs 4), suggesting that upstream signals from the IKK complex are not impacted by these small molecules [22]. We next investigated the effect of VSe1 and VSe1-28 on NF-κB transcriptional activity by measuring the expression of TNF-α and IL-6, two target genes of NF-κB [23–26]. Consistent with NF-κB inhibition, VSVΔ51 infection-induced expression of TNF-α and IL-6 was inhibited by both compounds as early as 8h and for up to 24 hours post infection (Figure 1f). Furthermore, significantly less TNF-α was secreted into the supernatant of VSVΔ51-infected cells treated with VSe1 and VSe1-28 at these time points as shown by ELISA

(Figure 1g). Finally, using a 3xκB reporter in 293T cells, we observed inhibition of TNF-α induced NF-κB transcriptional activity by VSe1 in a dose-dependent manner (Figure S4). Additionally, as we have previously shown (PMID 29367345), we observed that the compound TPCA-1 (2-[(aminocarbonyl)amino]-5 -(4-fluorophenyl)-3- thiophenecarboxamide), which inhibits NF-κB by targeting the IKK complex (PMID 26331681), was able to sensitize 786-0 cells to VSVΔ51 infection (~4log increase) and subsequent addition of VSe1 or VSe1-28 was not able to significantly increase viral titers any further (Figure S5). Altogether, these data suggest that VSe1 and VSe1-28 consistently inhibit the nuclear translocation of NF-κB and its transcriptional activity, which coincides with the suppression of virus-induced production of IFNβ and TNF-α, and enhancement of VSVΔ51 growth in these cells.

VSe1 analogs inhibit NF-κB and increase VSVΔ51 growth preferentially in cancer cells

We have previously shown that VSe1 and several pyrrole-based analogs can sensitize murine cancer cell lines, including virus-resistant B16-F10 (melanoma), CT26wt (colon carcinoma) and 4T1 (breast carcinoma) to infection with OVs. In contrast, these compounds have little impact on OV growth in normal cells and tissues (PMID 27226390, 20389287). We therefore investigated the scope and tumour selectivity of NF-κB inhibition in cancerous and normal murine cell lines. B16F10, CT26wt and 4T1 cells were pre-treated with virus sensitizing concentrations of VSe1 and VSe1-28 then treated with TNF-α. Western blotting from nuclear (Figure 2a)/cytoplasmic (Figure S6) protein extracts shows that VSe-1 and VSe1-28 inhibits TNFα-induced nuclear translocation of NF-κB (p65), generally by 50% (Figure 2a). The impact of these compounds on nuclear translocation of the p50 subunit of NF-κB was not as striking as their effect on p65 (Figure 2a). We next sought to investigate whether VSe1 and VSe1-28 could modulate mRNA expression of NF-κB-induced genes in these cell lines following VSVΔ51 infection at high MOI. Figure 2b shows that both VSe1 and VSe1-28 inhibit mRNA expression of TNFα and IL6 most significantly at 8 hours post infection. In addition, VSe1 and VSe1-28 could inhibit mRNA expression of the interferon-stimulated genes (ISGs) MX2 and IFITM1 as early as 8 hours post-infection (Figure 2b). The effect of VSe1-28 on these target genes was generally more pronounced than that of VSe1 in all 3 cell lines (Figure 2b). Taken together these data suggest that VSe1 and

VSe1-28 can impair NF-κB-mediated antiviral responses in a variety of different cancer cell lines and that this mechanism is likely driven by their impact on p65 nuclear translocation.

To further understand the tumour selectivity of VSe1 and VSe1-28, we isolated normal murine primary hepatocytes and plated them in tissue culture dishes. Primary hepatocytes were pretreated for 4h with a range of concentrations of VSe1-28 followed by infection with VSVΔ51-Fluc (MOI 0.005) or mock infection. Metabolic activity and high-throughput viral quantification assays revealed that VSVΔ51 titers were not increased by the compound in these cells in contrast with cancer cells (Figure 2c, 1b). Consistent with a lack of viral sensitization, the maximum non-toxic dose of VSe1-28 did not inhibit mRNA expression of NF-κB target genes TNFα and IL6, or interferon stimulated genes MX2 and IFITM1 (Figure 2d). Interestingly, compared to cancer cell lines (Figure 2b), we observed higher baseline expression of some antiviral genes (Figure S7) in cultured normal mouse hepatocytes, which could explain their resistance to VSVΔ51 infection. Altogether this data suggests that NF-κB is activated following VSVΔ51 infection preferentially in cancer cell lines, and that VSe1 and VSe1-28 impinge on NF-κB activation by inhibiting p65 nuclear translocation independently of upstream signaling.

Role of glutathione homeostasis in viral sensitization by VSe1 analogs

While the inhibition of NF-κB by VSe1 and VSe1-28 explained their capacity to block both response to and production of IFNβ, the molecular mechanisms linking the treatment of cells with VSe1/VSe1-28 to NF-κB inhibition remained unclear. We therefore set out to use ligand affinity capture techniques along with LC-MS/MS to identify proteins interacting with VSe1 and its structural analogs. To this end, VSe1-27, an active analog of VSe1 (Figure S8) was linked to amino PEGA resins and incubated with lysates from 786-0 cells. An inactive analog (VSe1-57) was also used as a negative control (Figure S8). Bound proteins were eluted and separated by gel electrophoresis (Figure S9). Visible bands were purified and sequenced via LC-MS/MS. These experiments consistently identified glutathione S-transferase-pi (GSTP1) as interacting specifically with VSe1-27 (Figure 3a), although other proteins of similar molecular weight such as peroxiredoxin were also identified in some attempts (Table S1) .

GSTs play a key role in glutathione (GSH) metabolism and the maintenance of cellular redox homeostasis and are best known for their role in detoxification of reactive electrophiles and xenobiotics through conjugation to GSH[28,29]. GSTs can further modulate cell signaling pathways

by directly interacting with transcription factors in the absence of physical or chemical stress. Notably GSTs have been shown to impact NF-κB signaling by either inducing S-glutathionylation of its inhibitor IκBα in unstimulated cells or indirectly through the metabolism of lipid oxidation products (PMID 27058114, 27840321). In light of the interaction between VSe1-27 and GSTP1, we wondered whether VSe1 and its analogs could affect NF-κB indirectly by impacting the enzymatic activity of GSTs. GST enzymatic assays (as described in Groom *et al*[30]) revealed that VSe1 inhibits multiple GST isoforms including GSTP1-1 (IC_{50} of 2.67 μM), GSTA4-4 (IC_{50} of 46.6 μM) and GSTM1-1 (IC_{50} of 1.74 μM), as determined using dialysis (Figures 3b and S10). VSe1-28, also inhibited GSTP1-1, albeit much less potently than VSe1 and only when co-incubated with the enzyme for a longer period of time (Figure 3c).We next used siRNA-mediated knock-down of *GSTP1* in 786-0 cells to definitively assess the impact of GSTP1 on VSVΔ51 spread. Although the knock-down was successful (Figure 3d), inhibition of GSTP1 through this method did not increase viral titers (Figure 3e). Furthermore, when siGSTP1-transfected cells were treated with VSe1, enhancement of VSVΔ51 titers was still observed, and was not significantly different from the enhancement observed in untransfected samples and samples transfected with scrambled control siRNA (Figure 3f).

These observations argued against a role for GSTs and GSTP1 in mediating the viral sensitizing effects of VSe1 and analogs. Given that VSe1 and VSe1-28 can directly react with free GSH[19], it remained possible that their viral sensitizing effects are mediated through an imbalance in glutathione homeostasis. We thus evaluated the kinetic effects of VSe1 and VSe1-28 on cellular GSH levels. This revealed that the compounds significantly decreased free GSH levels after 1 hour of treatment while oxidized GSH (GSSG) levels remained stable (Figure S11). However, GSH depletion was ultimately short-lived and was followed by recovery and accumulation of GSH above control levels by 12 hours post-treatment (Figure S11). We next attempted to deplete GSH by culturing 786-0 cells in buthionine sulfoximine (BSO); a potent inhibitor of γ-glutamylcysteine synthase, which is the rate-limiting step in glutathionine biosynthesis (PMID: 19061505), for at least 3 days. Upon verifying by HPLC that intracellular GSH was depleted (Figure S12) cells were pre-treated with VSe1 or VSe1-28 (or mock) followed by infection with VSVΔ51. Viral titration assays revealed that BSO-mediated GSH depletion , led to a modest increase in viral titer on its own (Figure S13). However, arguing against a role of GSH in mediating the viral sensitizing effects of VSe1 and analogs, culturing cells in BSO led to an increase in potency rather than an

abrogation of the effects of VSe1 and VSe1-28 (Figure S14). BSO-mediated GSH depletion was verified and maintained even after treatment with the compounds (Figure S15). Altogether this suggests that while GSH depletion alone may have a moderate impact on VSVΔ51 infection, it does not fully explain the virus sensitizing effects of VSe1 and VSe1-28. Furthermore, we failed to detect glutathionylation of the p65 subunit of NF-κB upon treatment of 786-0 cells with our compounds (Figure S16). Altogether, our data suggests that the viral enhancement effects of VSe1 and its pyrrole derivative may not be mediated through their impact on GSTP1 or GSH depletion.

VSe1 and VSe1-28 inhibition of NF-κB involves covalent modification of p65

As an alternative to inhibitor affinity capture which is designed to identify high affinity by non-covalent binders, we next turned to activity based protein profiling to investigate potentially covalently modified molecular targets of VSe1 and VSe1-28. It has been well-established that the oxidation and/or subsequent covalent modification of specific cysteine residues of subunits p65 and p50 inhibit nuclear translocation and transcriptional activity (PMID 26683377, 12213807, 15356172). In fact, Cys38 in p65 (located at its DNA-binding interface (PMID 9450761) has been shown to be covalently modified by compounds such as dimethyl fumarate (DMF PMID 26683377, 15356172), a compound we have also recently shown to have viral sensitizing properties (PMID 29367345) and that contains an α, β-unsaturated carbonyl moiety, similar to VSe1 and analogs. To specifically investigate a potential covalent interaction with p65, we applied a click chemistry approach using a biotin-azide-linked probe followed by pull-down with streptavidin beads then immunoblotting (Figure 4a). We took advantage of the fact that DMF has been previously shown to covalently modify Cys38 of p65 in order to perform binding competition assays with VSe1 and VSe1-28. To this end, we synthesized a DMF probe similar to the construct previously validated by Kastrati et. al. (Figure S17), which we further demonstrated to have viral enhancement properties similar to unmodified DMF(Figure 4b). To examine if p65 was a molecular target of VSe1 and VSe1-28, cells were mock treated or pretreated with either VSe1-28, or an inactive VSe1 analog (Figure 4c) that had no impact on viral titers (Figure S18), prior to incubation with the DMF probe. As expected, incubation of mock-treated 786-0 cells with the DMF probe resulted in the detection of DMF-bound p65. When cells were pretreated with increasing amounts of VSe1-28 (120-500μM) we observed a dose-dependent reduction in the ability of the DMF probe to bind and pull down p65, demonstrating that VSe1-28 can compete for

the same site (Figure 4d, lanes 2 - 4 vs. lane 9). In contrast, incubation of 786-0 with the inactive compound at the highest concentration (500μM) did not impact DMF binding to p65 (Figure 4d). Altogether, our data suggests that both VSe1 and VSe1-28, like DMF, covalently modifies NF-κB (p65), which inhibits its nuclear translocation. Following VSVΔ51 infection in cancer cells, this leads to dampened IFNβ and ISG expression, and increased viral growth.

VSe1-28 can suppress the expression of p65-induced genes in murine models of cancer leading to increased therapeutic efficacy in combination with VSVΔ51

We next attempted to validate whether the lead analog VSe1-28 could impact p65-mediated transcription in murine models of cancer and the therapeutic efficacy of VSVΔ51 . Balb/c mice bearing subcutaneous CT26. WT tumours were treated intratumourally with either vehicle or 40 mg/kg of VSe1-28. Four hours later, mice were treated intratumourally with VSVΔ51-Fluc or PBS. Tumours were excised 16h following VSVΔ51 treatment and RNA was extracted and assessed for the expression of IFITM1 and NF-κB target genes IL6 and TNFα by qPCR. Consistent with our *in vitro* data, we found that treatment with VSe1-28 reduced the expression of these genes (Figure 5a), enhanced expression of viral M-protein (Figure S19) and VSVΔ51-Fluc associated luminescence specifically in the tumour (Figure S20).

To expand on our previous studies carried out in human xenograft models, we further evaluated the therapeutic efficacy of VSe1-28 in the syngeneic CT26.WT and B16-F10 murine tumour models where mice were treated as described above. VSe1-28 treatment combined with VSVΔ51-Fluc led to a significant delay in tumour progression and improved survival over vehicle ($p=0.0012$) in the CT26.WT model (Figure 5b-c). When administered in a similar manner in the B16-F10 melanoma model, the combination of VSe1-28 and VSVΔ51 also delayed tumour progression and significantly extended survival compared to vehicle ($p=0.0002$), VSe1-28 ($p=0.0003$) and virus alone ($p=0.0002$, Figure 5d-e)). Overall our data demonstrate that VSe1-28 treatment can inhibit NF-κB-mediated transcription of target genes, thereby enhancing the infection of tumours with VSVΔ51, and leading to improved therapeutic outcomes in murine models of cancer.

Discussion

In this study, we demonstrate for the first time that the viral sensitizing effect of VSe1 and its novel pyrrole derivatives occurs through the inhibition of nuclear translocation of NF-κB,

specifically through covalent association with its p65 subunit. We have previously demonstrated that VSe1 and its analogs are able to enhance the replication and cytopathic effect of VSVΔ51, Maraba MG1 and HSV-1 in cancer cells (PMID 27226390). Notably, these oncolytic viruses induce type I IFNs and are susceptible to type I IFN antiviral signaling (PMID 10644380, 14585354, 20551913, 19073732, 9603331, 24743339). Previously published data with VSe1 suggests that it dampens the type I IFN response induced by viral infection (PMID 20389287, 27226390). In the current study we provide evidence that in cancer cells, VSe1 and its analogs inhibit the nuclear translocation of NF-κB, leading to decreased expression of its target genes *IFNB*, *TNFA* and *IL6* (Figure C, F, and G). We demonstrate that the compounds are likely acting downstream of IKK-mediated IκBα phosphorylation and subsequent degradation, as IκBα and p65 phosphorylation still occurs upon TNFα treatment even in the presence of VSe1 or VSe1-28 (Figure 1d-e). Furthermore, while the IKK inhibitor TPCA-1 can sensitize 786-0 cells to VSVΔ51, co-treatment with VSe1 or VSe1-28 does not enhance infection any further (Figure S5). Thus, it is conceivable that the action of VSe1 and VSe1-28 are also downstream of TPCA-1's targets, namely IKKs.

Further, as it is critical for clinical translation and efficacy, we examined our compounds effects in different cancer cell lines including B16F10 (murine melanoma), CT26.WT (colon carcinoma) and 4T1 (murine mammary gland carcinoma) showed much the same results. In all three cell lines we saw inhibition of nuclear translocation of the p65 subunit of NF-κB (Figure 2a) and decrease expression of target genes TNFa, IL6, MX2 and IFITM1 (Figure 2b) as early as 8 hours post infection. What is interesting was the inhibition of nuclear translocation of p50 seen in 786-0s was less consistent in these cancer cell lines, signifying that p65 might play a more important role in our compounds ability to potentiate oncolytic viral infection.

Most notably, our data highlights the remarkable selectivity of our compounds for cancer cells over normal cells (Figure 2c) or tissue, demonstrated *ex vivo* and *in vivo* (PMID 27226390). We reveal that suppression of NF-κB target genes and downstream ISGs is not observed following treatment of normal murine hepatocytes with VSe1-28 followed by infection with VSVΔ51 (Figure 2d). The inactivation of the viral M-protein's ability to inhibit cellular gene expression in VSVΔ51 renders it susceptible to antiviral innate responses generated in normal cells. This is in line with our observations that normal hepatocytes demonstrated a higher baseline expression of some antiviral genes (*TNFα and IFITM1*) compared to cancer cell lines. This suggests expression

of these genes abrogates VSVΔ51's ability to infect normal cells, and consequently NF-κB nuclear translocation would not be triggered and VSe1-28 cannot exert its effects. It would be interesting to pinpoint the exact antiviral gene responsible for the inability of VSVΔ51 to infect these cells. Overall these data support the oncoselectivity and safety of this combination approach.

We first explored affinity-based chromatography to identify direct targets of our compounds, which we could potentially link to their impact on NF-κB nuclear translocation. Results directed us towards GSTs and GSH as possible candidates, and indeed GSTs have previously shown to impact NF-κB signaling by either inducing S-gluathionylation of IκBα (PMID 27058114) in unstimulated cells or indirectly through the metabolism of lipid oxidation products (PMID 27840321). Despite discovering that VSe1 and VSe1-28 are novel inhibitors of GSTP1, the fact that knockdown of *GSTP1* by siRNA transfection could not increase viral titers and VSe1 supplementation could still exert viral sensitization in these cells indicated that the mechanism of action of VSe1 cannot be attributed to GSTP1 inhibition alone. Indeed while there is some degree of redundancy between the conjugating activities of GSTs (PMID 15822171), it would be interesting to knock down multiple GSTs at once and examine the impact on VSVΔ51 growth. However the affinity of VSe1 and analogs for GSTP1 specifically appeared the strongest based on our pulldown results. Furthermore, while depletion of cellular GSH by BSO could significantly increase viral titers, the magnitude of this effect was small in comparison to VSe1 and VSe1-28, and interestingly, the potency of VSe1 and VSe1-28 improved in the absence of GSH. Hence, the observed link between these compounds and GSTs may simple be due to an electrophile detoxifying process.

Given that our group has already identified DMF as a compound with the ability to potentiate VSVΔ51 infection (PMID: 29367345), and Kastrati et. al., had demonstrated that DMF was acting through covalent modification of p65 (PMID: 26683377), we turned to investigate if VSe1 and VSe1-28 had similar mechanism. Compounds with a α,β unsaturated carbonyl, like DMF, VSe1, and VSe1-28 can act as Michael acceptors and covalently react with nucleophilic residues on proteins, such as cysteines and lysines. In addition, multiple other compounds including quinones and santonin derived compounds have been shown to covalently modify NF-κB (PMID: 28103680, 11500489, 16360644, 26683377, 11971029, 26004161, 25443417).

Using click-chemistry, we used a previously described DMF probe to examine the ability

of our compounds to bind to NF-κB (PMID 26683377). Our observations show that VSe1-28 decreased the binding of the DMF probe to the p65 subunit of NF-κB. Treating cells with an inactive VSe1-28 analog without the α,β, unsaturated carbonyl moiety (which had no viral sensitizing effects (Figure 4d)), led to no inhibition of the DMF probe binding to p65. This strongly suggests that VSe1 and VSe1-28 act through the same mechanism as DMF, covalently modifying the p65 subunit of NF-κB and inhibiting its nuclear translocation and ultimately leading to enhanced viral growth. We have previously demonstrated that pyrrole derivatives such as VSe1-28 possess an improved safety profile compared to VSe1 as demonstrated by selective replication in *ex vivo* tumour tissues and superior *in vivo* tolerability in dose escalation studies (PMID 27226390). Along with their enhanced plasma stability (PMID 27226390), these advantages over VSe1 and furan derivatives make the pyrrole analogs much better suited for *in vivo* use. As we demonstrate here, VSe1-28 administered in combination with VSVΔ51 provides a clear significant survival (Figure 5c and e) advantage in murine models of cancer and qPCR results suggest that this may be indeed mediated through the impact of our compounds on NFκB-mediated inhibition of antiviral signaling pathways based on a significant reduction by qPCR of IL6, TNFα and IFITM1 (Figure 5a)

Given that a number of cancers exhibit constitutive NF-κB signaling (PMID: 26179906, 24116146, 25187272) and the fact that our compounds target NF-κB subunits and impede downstream responses with inherent tumour selectivity when administered in combination with oncolytic viruses provides a key opportunity for clinical translation. Further, it is interesting that VSe1-28 shares a common target with dimethyl fumarate, which is currently being used to treat relapsing-remitting multiple sclerosis (MS) and psoriasis, by targeting NF-κB signalling. It would be interesting to see VSe1-28 effect in the treatment of both of these diseases. Ultimately, the knowledge gained from this study contributes to the growing repertoire of understanding the mechanism of combination therapy strategies to enhance OV therapy and overcome heterogeneity

in clinical responses.

Materials and Methods

Drugs, chemicals and cytokines

The synthesis of VSe1 and its analogs (VSe1-2, VSe1-6, VSe1-10, VSe1-25, VSe1-27, VSe1-28, VSe1-29, VSe1-40, VSe1-57, CP02040, negative probe, and VSe1-10-GSH adduct)) has been previously described [19]. DMF was obtained from Sigma-Aldrich (St Louis, MO). The synthesis of DMF probe has been previously described (citation). Buthionine sulfoximine (BSO), oxidized glutathione (GSSG), N-aceylcysteine (NAC), cinnamaldehye and ML385 were obtained from Sigma-Aldrich (St Louis, MO). H_2O_2 was obtained from Fisher Scientific (Fair Lawn, NJ). Ezatiostat hydrochloride was obtained from ApexBio (Houston, TX). TPCA-1 was obtained from Abcam. IFNβ was obtained from PBL Interferon Source (Piscataway, NJ). TNF was obtained from R&D systems (Minneapolis, MN).

Cell lines

786-0 (human renal carcinoma), Vero (monkey kidney), B16F10 (murine skin melanoma), CT26wt (murine colon carcinoma), 4T1 (murine mammary carcinoma) and 293T (human embryonic kidney) were obtained from the American Type Culture Collection (Manassas,VA) and maintained in Dulbecco's Modified Eagle's medium (Corning, Manassas, VA) supplemented with 10% fetal bovine serum or 10% 3:1 newborn calf serum:fetal bovine serum (Sigma-Aldrich, St Louis, MO) and buffered with 30 mM Hepes (Thermo Fisher Scientific, Waltham, MA). Primary murine hepatocytes were isolated as previously described in Fullerton et. al. (PMID: 19625253). All cell lines were incubated at 37 °C with 5% CO_2 in a humidified incubator.

Viruses

A recombinant variant of the Indiana serotype of VSV harbouring a deletion of the 51st methionine in the M protein (VSVΔ51) was used throughout this study. VSVΔ51 expressing green fluorescent protein (GFP) or firefly luciferase (FLuc) are recombinant derivatives of VSVΔ51 that have been

previously described in Stojdl *et al* [6]. Viruses were propagated on Vero cells and purified on Optiprep gradient, and titered on Vero cells as previously described [55].

Luciferase-based viral titration assay

This assay has previously been described in detail [19]. Briefly, supernatants from samples infected with VSVΔ51-FLuc were added Vero cells seeded in white-bottom 96 well plates (Corning, Kennebunk, ME, USA). At the same time, known amounts of virus (starting at $1x10^8$ plaque forming units (pfu) and decreasing by 1 log unit to 10 pfu) were added to adjacent columns on the plate to generate a standard curve. Plates were centrifuged at 430xg for 5 minutes and then incubated for 5 hours at 37°C. Luciferase expression was then measured and bioluminescence was expressed in mean relative light units (mRLU; SynergyMx Microplate Reader, BioTek). To generate the standard curve, mRLU was plotted against known input pfu. Four-parameter non-linear regression analysis generated a Hill plot from which unknown input pfu (estimate of viral titer) was interpolated. Data transformation was conducted in R. These estimated titers are termed "viral expression units" (VEU).

Immunoblotting

Cells were lysed for 10 minutes on ice in protein extraction buffer (50mM Hepes, 150mM NaCl, 10mM EDTA, 10mM $Na_4P_2O_7$, 1% NP-40 pH 7.4) supplemented with 1M NaF, 200mM Na_3VO_4 and protease inhibitor cocktail (Roche, Mississauga, Ontario, Canada). Lysates were centrifuged at 16,000 g for 10 minutes at 4°C. NE-PER™ nuclear and cytoplasmic extraction reagents (Pierce Biotechnology, Rockford, IL) were used as per the manufacturer's protocol for separation of nuclear and cytoplasmic fractions. Following protein determination by Bradford assay (Protein Assay Solution, BioRad, Mississauga, Ontario) 20-50 μg of protein extracts were prepared in NuPAGE LDS sample buffer (Invitrogen, Burlington, Ontario) supplemented with dithiothreitol. Lysates were electrophoresed on a 4-12% precast gradient gel (Invitrogen, Burlington, Ontario) using the XCell *SureLock*® Mini-cell (Invitrogen, Burlington, Ontario) and transferred onto a nitrocellulose membrane (GE Healthcare, Baie d'Urfe, Quebec). The membranes were blocked with 5% BSA or 5% nonfat dry milk in 0.1% TBS-Tween-20 and probed with rabbit or mouse antibodies against NF-κB p65 (#8242 Cell Signalling Technology, Danvers, MA), phospho-NF-κB p65 (Ser536, #3033, Cell Signalling Technology, Danvers, MA), NF-κB p105/p50 (#3035, Cell Signalling Technology, Danvers, MA), IRF-3 (#11904, Cell Signalling Technology, Danvers,

MA), phospho-IRF-3 (Ser396, #4947, Cell Signalling Technology, Danvers, MA), c-jun (#9165, Cell Signalling Technology, Danvers, MA), phospho-c-jun (Ser63, #9261, Cell Signalling Technology, Danvers, MA), ATF2 (#9226, Cell Signalling Technology, Danvers, MA), phospho-ATF2 (Thr71, #9221, Cell Signalling Technology, Danvers, MA), IκBα (#4814, Cell Signalling Technology, Danvers, MA), β-Actin (#4970, Cell Signalling Technology, Danvers, MA), α-Tubulin (sc-8035, Santa Cruz Biotechnology, Dallas, Texas) or glutathione (ab19534, Abcam, Toronto, ON). The membranes were then probed with horseradish-peroxidase conjugated rabbit (Jackson Immunoresearch Labs, West Grove, PA) or mouse (Cell Signalling Technology, Danvers, MA) secondary antibodies. Bands were visualized using Clarity™ Western ECL blotting substrates (Bio-Rad, Mississauga, Ontario).

Immunoprecipitation

Cells were lysed as described above and 250 µL of lysates were pre-cleared with protein G Dynabeads (Invitrogen, Burlington, ON) for 30 minutes at room temperature. Lysates were then incubated with fresh beads and rabbit anti-NF-κB p65 antibody for 1 hour at room temperature (1:250 ratio for antibody to lysate). Beads were pelleted, washed three times with protein extraction buffer and bound proteins were eluted with 100 mM glycine pH 2.8. Eluate was diluted in NuPAGE LDS sample buffer with DTT and immunoblotting was performed as described above.

Quantitative real-time PCR

RNA extraction was performed using RNeasy® Mini Kit (Qiagen, Valencia, CA) according to the manufacturer's protocol. 1 µg of purified RNA was reverse transcribed using RevertAid H Minus First Strand cDNA Synthesis Kit (Thermo Fisher Scientific, Waltham, MA). Real-time PCR reactions were performed with QuantiTect® SYBR® Green PCR Kit (Qiagen, Valencia, CA) on a 7500 Fast Real-Time PCR system (Applied Biosystems, Foster City, CA) with 20ng of cDNA. Relative mRNA expression is normalized to GAPDH and fold induction was calculated relative to the untreated/uninfected controls using the Pfaffl method [56].

Model	Gene	Forward Primer (5'→3')	Reverse Primer (5'→3')
Human	IL6	ACCCCCAATAAATATAGGACTGGA	GAAGGCGCTTGTGGAGAAGG
Human	TNFα	GCTGCACTTTGGAGTGATCG	GAGGGTTTGCTACAACATGGG
Human	IFNβ	CATTACCTGAAGGCCAAGGA	CAGCATCTGCTGGTTGAAGA
Human	GAPDH	ACAGTCAGCCGCATCTTCTT	GTTAAAAGCAGCCCTGGTGA
Human	HMOX1	ACTGCGTTCCTGCTCAACAT	GGGGCAGAATCTTGCACTTT
Human	OSGIN	GTTCCCCTGACCCTCCTAGT	GGCCGTTACCCACAATGATG
Human	MX2	GAACGTGCAGCGAGCTTGTC	AAGGCTTGTGGGCCTTAGAC
Human	IFITM1	CGTGAAGTCTAGGGACAGG	GGTAGACTGTCACAGAGCCG
Mouse	IL6	TCCTCTCTGCAAGAGACTTCC	GGTCTGTTGGGAGTGGTATCC
Mouse	TNFα	CCTCTTCTCATTCCTGCTTGT	TGGGAACTTCTCATCCCTTTG
Mouse	GAPDH	CCCTTAAGAGGGATGCTGCC	TACGGCCAAATCCGTTCACA
Mouse	MX2	GAATTACCAGGGTGGCTGTAG	CAGGTTGATGGTCTCCTGTTT
Mouse	IFITM1	CAACTAGTGGTGCCAGCCGA	GTGAGGAGCACGTAGTCGGG

ELISA

TNF-α ELISA was done using the Human TNF-alpha Quantikine ELISA Kit (R&D Systems, Minneapolis, MN) with supernatants from treated cells according to the manufacturer's protocol.

Ligand-based affinity chromatography

Active and inactive probes were independently conjugated to Amino PEGA resin (dimethyl acrylamide and mono-2-acrylamidoprop-1-yl[2-aminoprop-1-yl] polyethylene glycol cross-linked with bis 2-acrylamidoprop-1-yl polyethyleneglycol; Novabiochem). Confluent 15 cm plates of 786-0s were mock-infected or infected with VSV51-GFP (MOI 0.005). Twenty-four hours later, cells were then lysed on ice (in 50 mM Tris-HCl pH 7.4, 150 mM NaCl, 0.5% Triton-X, 10% glycerol, 5 mM EDTA, 1 M NaF, 200 mM Na_3VO_4 and protease inhibitor cocktail). Three mock-infected plates were pooled, 6 infected plates were pooled and both lysates were incubated with

resin-bound active or inactive probe overnight at 4°C. The following day, resins were washed in lysis buffer, eluted by boiling in Laemmli buffer and resolved by SDS-PAGE on 4-12% precast gradient gels (Invitrogen, Burlington, Ontario). Proteins were stained with a 0.25% Coomassie Blue R-250 solution (in a 50% methanol, 10% acetic acid solution) and de-stained overnight in a 45% methanol, 10% acetic acid solution. Visible bands were cut out and sent for liquid chromatography-mass spectrometry (LC-MS) analysis.

GST assay

GST activity was assayed as described in Groom et al [30], with 1-chloro-2,4-dinitrobenzene (CDNB) and by monitoring the formation of the dinitrophenyl-GSH adduct. Enzyme assays performed in 100 mM potassium phosphate buffer. Recombinant human GST purified from *Escherichia coli* (a kind gift from Dr. Bengt Mannervik, Uppsala University, Sweden) was incubated with inhibitor and GSH for the indicated length of time. The reaction was initiated by the addition of 1-chloro-2,4-dinitrobenzene (CDNB) . The final concentration of non-aqueous compents in the reaction mixture was ≤2%. Formation of the reaction product (GSH-CDNB adduct; S-((2,4)-dinitrobenzene)glutathione) was monitored at 340 with an Evolution™ 60S UV-Visible Spectrophotometer (Thermo Scientific) in quartz cuvettes. The initial rate of the reaction (V_0) was calculated using the following equation:

$$V_o = Absorption/(\varepsilon \times l)$$

where l (path length of cuvette) is 1 cm and ε for the GSH-CDNB adduct is 9.6 $mM^{-1}cm^{-1}$. IC50 values were measured by fitting the four-parameter logistic function [57] to each data set, using Sigma-Plot™ software.

Reversibility of GST inhibition

Reversibility of inhibition was tested by removing the inhibitor (VSe1) by dialysis. GST P1-1 (25 ug) was incubated with VSe1 (0.5 mM), and GSH (1 mM) in 100 mM potassium phosphate buffer, pH 6.5. Control incubations lacked VSe1. Dialysis was carried out for 3 hours at 4°C in 100 mM

potassium phosphate buffer. Enzyme activity was subsequently measured as described above, with 1 mM GSH and 0.5 mM CDNB.

siRNA Transfections

786-0 cells were seeded in 12-well plates at $6x10^4$ cells/well. Twenty-four hours later, cells were transfected with scrambled siRNA control (ON-TARGETplus Non-targeting Control Pool; # D-001810-10-05; Dharmacon), or SMARTpool ON-TARGETplus GSTP1 siRNA (#L-011179-00-0005; Dharmacon) or oligofectamine (#12252011, Invitrogen) alone, according to the manufacturers' protocols. Forty-eight hours later, cell lysates were collected for immunoblot analysis with anti-GSTP1 (#LS-C154708; LifeSpan Biosciences, Inc.). Parallel sets of plates were either treated with VSe1 and subsequently infected or virus alone with VSV51-GFP at MOI 0.01. Supernatants were collected 24 and 46 hours post-infection and titered by plaque assay.

GSH and GSSG determinations by High Performance Liquid Chromatography

GSH, GSSG and their ratio was calculated with an Agilent HPLC system [58]. 786-0 cells were grown in 60mm tissue culture plates with the indicated treatments. Cells were then washed twice with ice cold PBS and lysed on ice for 20 minutes in 125mM sucrose, 1.5mM EDTA, 5mM Tris, 0.1% TFA and 0.5% MPA in mobile phase (10% HPLC grade methanol, 0.09% TFA – 0.2 micron filtered). Lysates were cleared by centrifugation for 20 min at 14,000 g at 4°C. Each sample was run in duplicate on a Pursuit5 C18 column (150 × 4.6 mm, 5 μm; Agilent Technologies, Santa Clara, CA) with a 1 mL/min flow rate. GSH and GSSG were detected with an Agilent UV-Vis wavelength detector at 215 nm. Retention times were determined by injecting standard solutions prepared in the same buffer. Absolute amounts of GSH and GSSG were obtained by integrating the area under each peak using Agilent ChemStation software. Quantities in nanomoles were obtained by interpolating from GSH and GSSG standard curves. A parallel set of treated 786-0 plates were trypsinized so that GSH and GSSG levels could be calculated on a per cell basis.

Ratiometric detection of GSH and GSSG levels with cyto-Grx1-roGFP2

293T cells were seeded in poly-D-lysine coated 96-well plates at a denstiy of $1.25x10^4$ cells/well. 24 hours later, cells were transfected with cyto-Grx1-roGFP2 (a kind gift from Dr. Brett Finlay, University of British Columbia, Canada) or a GFP plasmid (pEGFP-C3, Clonetech, Mountain View, CA, USA, Cat. PT3052-5) using Genejuice®, according to the manufacturer's protocol

(EMD Millipore,). 48 hours later, cells were excited at 408 and 488 nm and the ratios of the emissions in the green channel (530 nM) were calculated. Cells were then treated with H_2O_2, VSe1 or VSe1-28 and fluorescent readings were made after the indicated timepoints. After the last reading, cells were treated with 5 mM of DTT and fluorescence readings were taken after 2 minutes.

In Situ Affinity Based Protein Profiling

In order to confirm the molecular target of our VSes, in situ labelling of protein targets followed by pull-down and immunoblotting were carried out as described below. 786-0 cells were grown to 95% confluency in 10cm plates as described above. Medium was removed and cells were treated with 5ml of DMEM containing DMF(concentration) or VSe1-28 (concentration) for 1h. As shown in figure 4a, DMF-probe (200µM final concentration) was then added to the medium for 1h. Final DMSO concentration on cells did not exceed 0.05%. Medium was removed and cells were washed with ice cold PBS. Cells were lysed with 1% Triton X-100 in PBS for 10minutes placed on a rotator at 4C. Cells were then scraped, and spun at 14,000 rpm for 10 minutes. Supernatant was collected and protein concentration was determined by Bradford assay as described above. For pulldown of targets, biotin azide was attached to probes through click chemistry. 1mg of protein lysates per sample was mixed with freshly prepared click-chemistry mixture (0.1mM Biotin Azide (Sigma Aldrich, St Louis, MO) in DMSO, 1mM Tris(2-carboxyethyl)phosphine (TCEP, Sigma Aldrich, St. Louis, MO), 0.1mM Tris[1-benzyl-1H-1,2,3-triazol-4-yl)methyl]amine (TBTA, Sigma Aldrich, St. Louis, MO), 5mM CuSO4 (Fisher, Toronto, Ontario)) and incubated for 2 hours on a rotator at room temperature. To precipitate proteins, acetone was added to protein lysates and incubated at -80C for 15 minutes. Protein was then pelleted and washed with methanol. Samples were resuspended in PBS and streptavidin-agarose beads (Sigma Aldrich, St. Louis, MO) for 90 minutes on a rotator at room temp. Beads were then pelleted and washed 3x in 1% SDS, 3x in fresh 6M urea, and 3x PBS. Protein was eluted off streptavidin beads by resuspending in 2x SDS-Page and heating at 95C for 15 minutes. Samples were then electrophoresised, transferred and immunoblotted as described above.

Statistics

The results shown in this study are presented as means ± standard error. For all experiments statistical significance (using indicated statistical tests) was considered to mean a P value less than

or equal to 0.05. Graphs and statistics were computed using GraphPad Prism 6 and Microsoft Excel.

Acknowledgements

JSD is supported by the Canadian Institute for Health Research (CIHR). JSD, TA, JCB, BL are supported by the Terry Fox Foundation (grant no. TFF 122868). JSD, JCB hold a grant from The Lotte & John Hecht Memorial Foundation Innovation Grant of the Canadian Cancer Society (grant no. 2012-701460; grant no. 703014). CNB, JSD, AND JCS were supported by a Collborative Health Research Project grant from CIHR and NSERC. RK is a recipient of the Ontario Graduate Scholarship. MS received a doctoral fellowship from CIHR. Primary murine hepatocytes were isolated by Conor Dwyer and gifted to us by Dr. Morgan Fullerton.

Contributions

JSD, NES, RK participated in the conception and design of the study. All authors participated in the acquisition, analysis and/or the interpretation of data. RK, NES and JSD drafted the manuscript. JSD, C.N.B, and J.C.S supervised the study. All the authors have read and approved the final manuscript. We have no conflict of interest to declare.

Figure legends

Figure 1. VSe1 and VSe1-28 inhibit virus-induced NF-κB nuclear translocation. (**a**) Chemical structures of VSe1 and VSe1-28. (**b**) 786-0 cells were pre-treated with VSe1 (64 μM) or VSe1-28 (90 μM) for 8 hours and then infected with VSVΔ51-Fluc at MOI 3 (single-step growth curve) or MOI 0.01 (multi-step growth curve). For the single-step growth curve, virus inoculum was replaced with media after 1 hour. Supernatants were collected and frozen at the indicated times and virus titer was determined using a previously described luciferase-based titration assay [31] (**c**) 786-0 cells were treated with VSe1 (60 μM) and VSe1-28 (80 μM) then infected with VSVΔ51-GFP (MOI 1). RNA was extracted 8, 16 and 24 hours post-infection and quantitative RT-PCR was used to measure relative levels of IFNβ mRNA. Values were normalized to GAPDH and are relative to untreated control for each timepoint. (**d**) 786-0 cells were treated as in **c** then infected with VSVΔ51-GFP (MOI 1). Nuclear and cytoplasmic extracts were collected 8 hours post-infection and were probed with the indicated antibodies. (**e**) 786-0 cells were treated as in **c** then treated with TNFα (50ng/μL). Nuclear and cytoplasmic extracts were collected 30 minutes later

and were probed with the indicated antibodies. (**f**) RNA from **c** was used to measure relative levels of TNFα and IL-6 mRNA. Values were normalized to GAPDH and are relative to untreated control for each timepoint. (**g**) Supernatants from **c** were collected and levels of secreted TNFα were measured by ELISA. Error bars represent s.e. from biological triplicates and statistical significance was calculated using two-way ANOVA with Dunnett's multiple comparison (*** $P < 0.001$, ** $P < 0.01$, ns = $P > 0.05$). Values from **c** and **f** were log transformed before analyzing statistical significance.

Figure 2. Inhibition of virus-induced NF-κB nuclear translocation of VSe1 and VSe1-28 in various normal and cancer cell lines. (a) B16F10 cells were treated with VSe1 (15μM) and VSe1-28(40μM). CT26wt cells were treated with VSe1 (15μM) and VSe1-28 (60μM). 4T1 cells were treated with VSe1 (30μM) and VSe1-28 (80uμM). Cells were then treated with TNFα (25ng/μl). Nuclear and cytoplasmic extracts were collected 30 minutes later and were probed with the indicated antibodies. (b) Cells were treated as described in (a) with VSe1 and VSe1-28 and then infected with VSVΔ51-GFP (MOI 1). RNA was collected 8, 16, and 24 hours post infection and quantitative RT-PCR was used to measure relative levels of TNFα, Il6, MX2 and IFITM1 RNA. Values were normalized to GAPDH and are relative to untreated control for each timepoint. **(c)** Primary murine hepatocytes were treated with VSe1-28 and infected with VSVΔ51-Fluc (MOI 0.01). Supernatants were collected 40 hours post-infection virus output was determined using a previously described luciferase-based titration assay. Viral titers are shown on the right hand y-axis. On the left hand y-axis shows relative metabolic activity of the hepatocytes after treatment with VSe1-28 and infection. **(d)** Primary murine hepatocytes were treated with 10μM VSe1-28 and infected with VSVΔ51-GFP (MOI 1). RNA was collected 8 and 16 hours post-infection and quantitative RT-PCR was used to measure relative levels of TNFa, IL6, MX2 and IFITM1 RNA. Values were normalized to GAPDH and are relative to untreated control for each timepoint.

Figure 3. VSe1 and VSe1-28 inhibit GST-π enzymatic activity. (**a**) Schematic workflow of ligand-based affinity chromatography. Active and inactive analogs of VSe1 were linked to amino PEGA resins and incubated with lysates from 786-0 cells. Lysates were separated by gel electrophoresis and visualized by coomassie blue. Visualized bands were cut out and sent for sequencing via LC-MS/MS. (**b**) GST P1-1 (5 μg) was incubated with VSe1 and GSH, 1 mM, at

37°C for 5 min, in 100 mM potassium phosphate buffer, pH 6.5. CDNB (dissolved in ethanol) was added to initiate the reaction (final concentration, 0.5 mM), and product formation was monitored at 340 nm. Final concentrations of DMSO and ethanol were 1% each. Data points represent the mean ± s.e. of three independent experiments. IC50 values were determined by curve-fitting, as described in Materials and Methods. (**c**) GSTP1-1 (1 μg) was pre-incubated with vehicle (DMSO), VSe1, VSe1-28, and GSH, 1 mM, for 5 min or 120 min at 37 °C. CDNB was added to initiate the reaction (final concentration, 0.5 mM), and product formation was monitored at 340 nm. Final concentration of DMSO was 2%. Bars represent the mean ± standard error of three or four biological replicates. Statistical significance was calculated using two-way ANOVA with Dunnett's multiple comparisons test (**** $P < 0.0001$, *** $P < 0.001$, ** $P < 0.01$, * $P < 0.05$, ns = $P > 0.05$). **(d)** 786-0 cells were transfected with vehicle control ("0"), scrambled siRNA control ("scrambled"; final concentration 25nM) or various amounts of *GSTP1* siRNA (GSTP1) such that final concentrations of siRNA was 12.5nM, 25nM, or 50nM. Forty-eight hours later, samples were lysed, and triplicate protein lysates were pooled, separated by SDS-PAGE and probed for GSTP1 and β-acting by immunoblotting. **(e)** In parallel to (d), transfected 786-0 cells and controls were infected with VSVΔ51-GFP at MOI 0.01. Supernatants were collected 24 and 46 hours post-infection and titered by plaque assay. **(f)** 786-0 cells were transfected with vehicle control ("untransfected"), scrambled siRNA ("scrambled") or siRNA against *GSTP1* ("siGSTP1") such that the final concentration of siRNA was 25nM. 48 hours post-transfection cells were treated with vehicle control or VSe1, and then infected 4 hours later with VSVΔ51-GFP at MOI 0.01. Supernatants were collected 24 hours post-infection and titered by plaque assay.

Figure 4. Using affinity based protein profiling shows VSe1-28 covalently modifying NF-κB. **(a)** Schematic workflow of affinity based protein profiling using a previously described DMF probe and VSe1-28. **(b)**786-0 cells were treated with inactive VSe1-28 probe or DMF probe and infected with VSVd51 Fluc (MOI 0.005). Supernatants were collected 40 hours post-infection and virus output was determined using a previously described luciferase-based titration assay. Viral output is shown as Log VEU/ml on the right y-axis. Relative cell metabolic activity measured by Alamarblue is shown on the left y-axis. **(c)** Structure of DMF probe **(d)** 786-0 cells treated with various concentrations of VSe1-28, inactive VSe1-28 or DMF for 1h and then treated with DMF Probe (200μM) for 1h. Whole cell lysate was collected and biotin azide was linked using click-

chemistry. Pulldown was done using streptavidin beads and eluent was probed with indicated antibodies.

Figure 5. VSe1-28 inhibit p65-induced genes in murine cancer models and increase therapeutic efficacy in combination with VSVΔ51. (A) Balb/C mice bearing CT26wt cells treated with vehicle or 40mg/kg of VSe1-28 by intratumoural injection and four hours later treated with $1x10^8$ plaque-forming units of VSVΔ51-FLuc. Tumours were harvested 16 hours post infection for RNA. Quantitative RT-PCR was used to analyze gene expression of TNFα, IL6 and IFITM1. ***P < 0.001, ****P < 0.0001. **(B)** Balb/c mice bearing CT26.WT cells were treated with vehicle (DMSO) or 40 mg/kg of VSe1-28 by intratumoural injection. Four hours later, mice were treated with 1×10^8 plaque-forming units of VSVΔ51-FLuc. Treatments (compound and virus, or respective vehicles) were re-administered on day 2 and 4 post-initial treatment. Tumour volumes were monitored every day and averages of relative tumour volumes (relative to volume on day 1 of treatment) for each treatment group are shown. Tumour volume curves are terminated when the first mouse in each group reaches endpoint (based on tumour size). Error bars correspond to standard error. Differences between average relative tumour volumes of the VSe1-28 + VSVΔ51-Fluc group were compared to the 3 other treatment groups. Statistical significance was calculated by two-way ANOVA with Dunnett's multiple comparison test (for VSe1-28 + VSVΔ51 versus VSVΔ51 alone, * P < 0.05, ** P < 0.01). **(C)** Survival was monitored over time. Log –rank tests indicate that treatment with VSe1-28 and virus significantly improved survival compared to vehicle alone (p = 0.0012), but not VSe1-28 alone (p = 0.0934) or virus alone (0.1032). **(D)** C57/B6 mice bearing subcutaneous B16-F10 tumours were treated with vehicle (DMSO) or 40 mg/kg of VSe1-28 by intratumoural injection. Four hours later, mice were treated with $1x10^8$ plaque-forming units of VSVΔ51-FLuc. Tumour volumes were monitored daily and average tumour volumes for each treatment group are shown. Tumour volume curves are terminated when the first mouse in each group reaches endpoint (based on tumour size). Error bars represent standard error. Differences between average volumes of the VSe1-28 + VSVΔ51-Fluc group were compared to the 3 other treatment groups. Statistical significance was calculated by two-way ANOVA with Dunnett's multiple comparison test (for VSe1-28 + VSVΔ51 vs. VSVΔ51 alone, * P < 0.05, **** P < 0.0001). **(E)** Survival was monitored over time. Log –rank tests indicate that treatment with

VSe1-28 and virus significantly improved survival compared to vehicle control ($p = 0.0001$), VSe1-28 alone ($p = 0.0003$) or virus alone ($p = 0.0002$).

Figure S1. Effect of VSe1 and VSe1-28 on phosphorylation of p65, c-jun, IRF3 and ATF2. 786-0 cells were treated with VSe1 (60 μM) and VSe1-29 (80 μM) then infected with VSVΔ51-GFP (MOI 1). Whole cell lysates were collected 8 hours post-infection and were probed with the indicated antibodies.

Figure S2. Effect of VSe1 and VSe1-28 on dimerization of p65 with p50. NF-**κ**B p65 was immunoprecipitated using whole cell lysates from 786-0 cells treated with VSe1 or VSe1-28 for 2 hours and then infected with VSVΔ51-GFP (MOI 1) for 8 hours. Proteins were separated by SDS-PAGE and probed for NF-**κ**B p50

Figure S3. Effect of VSe1 and VSe1-28 on TNFα-induced nuclear translocation of NF-κB. 786-0 cells were treated with VSe1 (60 μM) or VSe1-28 (80 μM) then treated with TNFα (25 ng/mL). Nuclear and cytoplasmic extracts were collected 30 minutes later and were probed with the indicated antibodies.

Figure S4.

Figure S5. TPCA-1 sensitizes 786-0 cells to oncolytic viral infection. (A) 786-0 cells were pre-treated with TPCA-1, (B) 3 different concentration of VSe1 and TPCA-1, (C) 3 different concentrations of VSe1-28 and TPCA-1, then infected with VSVΔ51-Fluc (MOI 0.005). (B) Supernatants were collected 40 hours later and virus output was determined using a previously described luciferase-based titration assay [31].

Figure S6. Nuclear/Cytoplasmic Fractionation of various cancer cell lines treated with VSe1 and VSe1-28. (A) B16F10 cells were treated with VSe1 (15μM) and VSe1-28(40μM). (B) CT26wt cells were treated with VSe1 (15μM) and VSe1-28 (60μM). (C) 4T1 cells were treated with VSe1 (30μM) and VSe1-28 (80uμM). Cells were then treated with TNFα (25ng/μl). Nuclear

and cytoplasmic extracts were collected 30 minutes later and were probed with the indicated antibodies.

Figure S7. Baseline expression of p65 induced genes higher in primary murine hepatocytes.

Baseline expression of TNFa, IL6, IFITM1, MX2 of primary murine hepatocytes were compared to B16F10, CT26wt, and 4T1 cancer cell lines. Samples are normalized to GAPDH and expressed as relative mRNA expression compared to hepatocyte mRNA expression.

Figure S8. Chemical structures and activity of active and inactive VSe1 analog probes. 786-0 cells were pre-treated with the VSe1 analogs used to make the active (VSe1-27) and inactive probes. After a 4 hour pretreatment, cells were infected with VSVΔ51-Fluc (MOI 0.005). Supernatants were collected 40 hours later and virus output was determined using a previously described luciferase-based titration assay [31].

Figure S9. Coomassie-stained gel after SDS-PAGE separation of eluted proteins from affinity capture experiments. (i) Lysate incubated with with inactive probe. (ii) Lysate incubated with active probe. Bands shown around 25 kDa was identified to be GSTP1-1.

Figure S10. Reversibility of enzyme inhibition by VSe1. GSTP1-1 enzymatic activity was tested pre- and post-dialysis, with and without VSe1.

Figure S11. VSe1 and VSe1-28 deplete cellular GSH levels. 786-0 cells were treated with VSe1 or VSe1-28 for 1, 4, and 12 hours before whole cell lysates were collected. Cellular GSH and GSSG levels were measured by HPLC-UV detection. Error bars represent s.e. from biological duplicates and technical duplicates. Statistical significance was calculated using two-way ANOVA with Dunnett's multiple comparison (*** $P < 0.001$, * $P < 0.05$).

Figure S12. Verification of depletion of intracellular GSH with BSO. 786-0 cells were cultured in 2mM BSO for 3 days prior to collecting whole cell lysates. Cellular GSH and GSSG levels were measured by HPLC-UV detection. Error bars represent standard error from biological duplicates and technical duplicates. Statistical significance was calculated using a 2-way ANOVA with with Holm-Sidak multiple comparisons test (****$P < 0.001$, * $P < 0.05$, ns = $P > 0.05$).

Figure S13. Depletion of GSH with BSO leads to increase in viral titers. 786-0 cells were cultured in 2mM BSO for 3 days and then infected with VSVΔ51-Fluc (MOI 0.05). Supernatants

were collected 40 hours later and virus output was determined using a previously described luciferase-based titration assay [31]. Statistical significance was calculated using unpaired t-test.

Figure S14. Treating cells with BSO does not abrogate effects of VSe1 nor VSe1-28. 786-0 cells were cultured in DMEM or DMEM supplemented with BSO 2mM for 10 days. Cells were then treated with VSe1 or VSe1-28 for 4 hours and then infected with VSVΔ51-Fluc (MOI 0.005). Supernatants were collected 40 hours later and virus output was determined using a previously described luciferase-based titration assay [31].

Figure S15. GSH and GSSG levels after BSO and VSe1-28 treatment. 786-0 cells were cultured in 2mM BSO for 24 hours and then treated with VSe1-28 for 1, 4, 12, or 24 hours prior to collecting whole cell lysates. Cellular GSH and GSSG levels were measured by HPLC-UV detection. Error bars represent s.e. from biological duplicates and technical duplicates.

Figure S16. Effect of VSe1 and VSe1-28 on the glutathionylation of NF-κB subunit p65. 786-0 cells were treated with VSe1 or VSe1-28 for 12 hours before collecting whole cell lysates. P65 was precipitated from the lysates using an anti-NF-κB p65 antibody and its glutathionylation status was assessed by western blot. As a positive control, lysates were treated with 50mM GSSG for 30 minutes to induce protein glutathionylation.

Figure S17. Chemical Structure of DMF probe (PMID: 26683377).

Figure S18. Inactive VSe1-28 analog does not enhance VSVΔ51 activity. 786-0 cells were treated with various concentrations of inactive VSe1-28 analog (VSe1-56) for 4 hours and then infected with VSVΔ51-Fluc (MOI 0.005). Supernatants were collected 40 hours post infection and virus output was determined using a previously decribed luciferased-based titration assay (left y-axis). Cell viability was determined using rezasaurin (right y-axis).

Figure S19. VSVM gene expression in murine cancer models. Balb/c mice bearing CT26wt tumours were treated with 40mg/kg VSe1-28 intratumourally for 4 hours and then infected with 1e8 pfu/ml of VSVΔ51-Fluc intratumourally. Tumours were collected 16 hours post infection and harvested for RNA. Real-time quantitative PCR was used to analyze gene expression of VSVM.

Figure S20. Luciferase expression of murine cancer models treated with VSe1-28 in combination with VSVΔ51. Balb/c mice bearing CT26wt tumours were treated with 40mg/kg VSe1-28 intratumourally for 4 hours and then infected with 1e8 pfu/ml of VSVΔ51-Fluc

intratumourally. 16 hours post infection, virus replication was analyzed by measuring luminescence using IVIS and signal was quantified.

References for Draft Paper

1. Russell, SJ, Peng, K-W and Bell, JC (2012). Oncolytic virotherapy. *Nat. Biotechnol.* **30**: 658–670.
2. Ilkow, CS, Swift, SL, Bell, JC and Diallo, J-S (2014). From scourge to cure: tumour-selective viral pathogenesis as a new strategy against cancer. *PLoS Pathog.* **10**: e1003836.
3. Keller, BA and Bell, JC (2016). Oncolytic viruses—immunotherapeutics on the rise. *J. Mol. Med.* **94**: 979–991.
4. Patel, MR and Kratzke, RA (2013). Oncolytic virus therapy for cancer: the first wave of translational clinical trials. *Transl. Res.* **161**: 355–364.
5. Grigg, C, Blake, Z, Gartrell, R, Sacher, A, Taback, B and Saenger, Y (2016). Talimogene laherparepvec (T-Vec) for the treatment of melanoma and other cancers. *Semin. Oncol.* **43**: 638–646.
6. Stojdl, DF, Lichty, BD, tenOever, BR, Paterson, JM, Power, AT, Knowles, S, *et al.* (2003). VSV strains with defects in their ability to shutdown innate immunity are potent systemic anti-cancer agents. *Cancer Cell* **4**: 263–275.
7. Stojdl, DF, Lichty, BD, tenOever, BR, Paterson, JM, Power, AT, Knowles, S, *et al.* (2003). VSV strains with defects in their ability to shutdown innate immunity are potent systemic anti-cancer agents. *Cancer Cell* **4**: 263–275.
8. Saloura, V, Wang, L-CS, Fridlender, ZG, Sun, J, Cheng, G, Kapoor, V, *et al.* (2010). Evaluation of an attenuated vesicular stomatitis virus vector expressing interferon-beta for use in malignant pleural mesothelioma: heterogeneity in interferon responsiveness defines potential efficacy. *Hum. Gene Ther.* **21**: 51–64.
9. Liu, Y-P, Suksanpaisan, L, Steele, MB, Russell, SJ and Peng, K-W (2013). Induction of antiviral genes by the tumor microenvironment confers resistance to virotherapy. *Sci. Rep.* **3**: 2375.
10. Berchtold, S, Lampe, J, Weiland, T, Smirnow, I, Schleicher, S, Handgretinger, R, *et al.* (2013). Innate immune defense defines susceptibility of sarcoma cells to measles vaccine virus-based oncolysis. *J. Virol.* **87**: 3484–3501.
11. Liikanen, I, Monsurrò, V, Ahtiainen, L, Raki, M, Hakkarainen, T, Diaconu, I, *et al.* (2011). Induction of interferon pathways mediates in vivo resistance to oncolytic adenovirus. *Mol. Ther.* **19**: 1858–1866.
12. Puzanov, I, Milhem, MM, Minor, D, Hamid, O, Li, A, Chen, L, *et al.* (2016). Talimogene Laherparepvec in Combination With Ipilimumab in Previously Untreated, Unresectable Stage IIIB-IV Melanoma. *J. Clin. Oncol.* **34**: 2619–2626.
13. Shen, W, Patnaik, MM, Ruiz, A, Russell, SJ and Peng, K-W (2016). Immunovirotherapy with vesicular stomatitis virus and PD-L1 blockade enhances therapeutic outcome in murine acute myeloid leukemia. *Blood* **127**: 1449–1458.
14. Zamarin, D, Holmgaard, RB, Subudhi, SK, Park, JS, Mansour, M, Palese, P, *et al.* (2014). Localized oncolytic virotherapy overcomes systemic tumor resistance to immune checkpoint blockade immunotherapy. *Sci. Transl. Med.* **6**: 226ra32.
15. Ribas, A, Dummer, R, Puzanov, I, VanderWalde, A, Andtbacka, RHI, Michielin, O, *et al.* (2017). Oncolytic Virotherapy Promotes Intratumoral T Cell Infiltration and Improves Anti-PD-1 Immunotherapy. *Cell* **170**: 1109–1119.e10.
16. Durham, NM, Mulgrew, K, McGlinchey, K, Monks, NR, Ji, H, Herbst, R, *et al.* (2017).

Oncolytic VSV Primes Differential Responses to Immuno-oncology Therapy. *Mol. Ther.* **25**: 1917–1932.
17. Samson, A, Scott, KJ, Taggart, D, West, EJ, Wilson, E, Nuovo, GJ, *et al.* (2018). Intravenous delivery of oncolytic reovirus to brain tumor patients immunologically primes for subsequent checkpoint blockade. *Sci. Transl. Med.* **10**.
18. Diallo, J-S, Le Boeuf, F, Lai, F, Cox, J, Vaha-Koskela, M, Abdelbary, H, *et al.* (2010). A high-throughput pharmacoviral approach identifies novel oncolytic virus sensitizers. *Mol. Ther.* **18**: 1123–1129.
19. Dornan, MH, Krishnan, R, Macklin, AM, Selman, M, El Sayes, N, Son, HH, *et al.* (2016). First-in-class small molecule potentiators of cancer virotherapy. *Sci. Rep.* **6**: 26786.
20. Diallo, J-S, Le Boeuf, F, Lai, F, Cox, J, Vaha-Koskela, M, Abdelbary, H, *et al.* (2010). A high-throughput pharmacoviral approach identifies novel oncolytic virus sensitizers. *Mol. Ther.* **18**: 1123–1129.
21. Panne, D, Maniatis, T and Harrison, SC (2007). An atomic model of the interferon-beta enhanceosome. *Cell* **129**: 1111–1123.
22. Perkins, ND (2007). Integrating cell-signalling pathways with NF-kappaB and IKK function. *Nat. Rev. Mol. Cell Biol.* **8**: 49–62.
23. Collart, MA, Baeuerle, P and Vassalli, P (1990). Regulation of tumor necrosis factor alpha transcription in macrophages: involvement of four kappa B-like motifs and of constitutive and inducible forms of NF-kappa B. *Mol. Cell. Biol.* **10**: 1498–1506.
24. Son, Y-H, Jeong, Y-T, Lee, K-A, Choi, K-H, Kim, S-M, Rhim, B-Y, *et al.* (2008). Roles of MAPK and NF-kappaB in interleukin-6 induction by lipopolysaccharide in vascular smooth muscle cells. *J. Cardiovasc. Pharmacol.* **51**: 71–77.
25. Libermann, TA and Baltimore, D (1990). Activation of interleukin-6 gene expression through the NF-kappa B transcription factor. *Mol. Cell. Biol.* **10**: 2327–2334.
26. Shakhov, AN, Kuprash, DV, Azizov, MM, Jongeneel, CV and Nedospasov, SA (1990). Structural analysis of the rabbit TNF locus, containing the genes encoding TNF-beta (lymphotoxin) and TNF-alpha (tumor necrosis factor). *Gene* **95**: 215–221.
27. Pfeffer, LM (2011). The role of nuclear factor κB in the interferon response. *J. Interferon Cytokine Res.* **31**: 553–559.
28. Sheehan, D, Meade, G, Foley, VM and Dowd, CA (2001). Structure, function and evolution of glutathione transferases: implications for classification of non-mammalian members of an ancient enzyme superfamily. *Biochem. J* **360**: 1–16.
29. Armstrong, RN (1997). Structure, catalytic mechanism, and evolution of the glutathione transferases. *Chem. Res. Toxicol.* **10**: 2–18.
30. Groom, H, Lee, M, Patil, P and Josephy, PD (2014). Inhibition of human glutathione transferases by dinitronaphthalene derivatives. *Arch. Biochem. Biophys.* **555-556**: 71–76.
31. Garcia, V, Krishnan, R, Davis, C, Batenchuk, C, Le Boeuf, F, Abdelbary, H, *et al.* (2014). High-throughput titration of luciferase-expressing recombinant viruses. *J. Vis. Exp.*: 51890.
32. Liao, B-C, Hsieh, C-W, Lin, Y-C and Wung, B-S (2010). The glutaredoxin/glutathione system modulates NF-kappaB activity by glutathionylation of p65 in cinnamaldehyde-treated endothelial cells. *Toxicol. Sci.* **116**: 151–163.
33. Markovic, J, Mora, NJ, Broseta, AM, Gimeno, A, de-la-Concepción, N, Viña, J, *et al.* (2009). The depletion of nuclear glutathione impairs cell proliferation in 3t3 fibroblasts. *PLoS One* **4**: e6413.
34. Gutscher, M, Pauleau, A-L, Marty, L, Brach, T, Wabnitz, GH, Samstag, Y, *et al.* (2008).

Real-time imaging of the intracellular glutathione redox potential. *Nat. Methods* **5**: 553–559.
35. Gorrini, C, Harris, IS and Mak, TW (2013). Modulation of oxidative stress as an anticancer strategy. *Nat. Rev. Drug Discov.* **12**: 931–947.
36. Brennan, MS, Matos, MF, Richter, KE, Li, B and Scannevin, RH (2017). The NRF2 transcriptional target, OSGIN1, contributes to monomethyl fumarate-mediated cytoprotection in human astrocytes. *Sci. Rep.* **7**: 42054.
37. Singh, A, Venkannagari, S, Oh, KH, Zhang, Y-Q, Rohde, JM, Liu, L, *et al.* (2016). Small Molecule Inhibitor of NRF2 Selectively Intervenes Therapeutic Resistance in KEAP1-Deficient NSCLC Tumors. *ACS Chem. Biol.* **11**: 3214–3225.
38. Nishi, T, Shimizu, N, Hiramoto, M, Sato, I, Yamaguchi, Y, Hasegawa, M, *et al.* (2002). Spatial redox regulation of a critical cysteine residue of NF-kappa B in vivo. *J. Biol. Chem.* **277**: 44548–44556.
39. Kabe, Y, Ando, K, Hirao, S, Yoshida, M and Handa, H (2005). Redox regulation of NF-kappaB activation: distinct redox regulation between the cytoplasm and the nucleus. *Antioxid. Redox Signal.* **7**: 395–403.
40. García-Piñeres, AJ, Castro, V, Mora, G, Schmidt, TJ, Strunck, E, Pahl, HL, *et al.* (2001). Cysteine 38 in p65/NF-kappaB plays a crucial role in DNA binding inhibition by sesquiterpene lactones. *J. Biol. Chem.* **276**: 39713–39720.
41. Di Bona, D, Cippitelli, M, Fionda, C, Cammà, C, Licata, A, Santoni, A, *et al.* (2006). Oxidative stress inhibits IFN-alpha-induced antiviral gene expression by blocking the JAK-STAT pathway. *J. Hepatol.* **45**: 271–279.
42. Gonzalez-Dosal, R, Horan, KA, Rahbek, SH, Ichijo, H, Chen, ZJ, Mieyal, JJ, *et al.* (2011). HSV infection induces production of ROS, which potentiate signaling from pattern recognition receptors: role for S-glutathionylation of TRAF3 and 6. *PLoS Pathog.* **7**: e1002250.
42. Eden, E., Navon, R., Steinfeld, I., Lipson, D. & Yakhini, Z. GOrilla: a tool for discovery and visualization of enriched GO terms in ranked gene lists. *BMC Bioinformatics* **10,** 48 (2009).
43. Bottero, V, Chakraborty, S and Chandran, B (2013). Reactive oxygen species are induced by Kaposi's sarcoma-associated herpesvirus early during primary infection of endothelial cells to promote virus entry. *J. Virol.* **87**: 1733–1749.
44. Paracha, UZ, Fatima, K, Alqahtani, M, Chaudhary, A, Abuzenadah, A, Damanhouri, G, *et al.* (2013). Oxidative stress and hepatitis C virus. *Virol. J.* **10**: 251.
45. Lin, X, Wang, R, Zou, W, Sun, X, Liu, X, Zhao, L, *et al.* (2016). The Influenza Virus H5N1 Infection Can Induce ROS Production for Viral Replication and Host Cell Death in A549 Cells Modulated by Human Cu/Zn Superoxide Dismutase (SOD1) Overexpression. *Viruses* **8**.
46. Zhu, L, Yuan, C, Zhang, D, Ma, Y, Ding, X and Zhu, G (2016). BHV-1 induced oxidative stress contributes to mitochondrial dysfunction in MDBK cells. *Vet. Res.* **47**: 47.
47. Bartee, E, Mohamed, MR, Lopez, MC, Baker, HV and McFadden, G (2009). The addition of tumor necrosis factor plus beta interferon induces a novel synergistic antiviral state against poxviruses in primary human fibroblasts. *J. Virol.* **83**: 498–511.
48. Zhang, J, Grek, C, Ye, Z-W, Manevich, Y, Tew, KD and Townsend, DM (2014). Pleiotropic functions of glutathione S-transferase P. *Adv. Cancer Res.* **122**: 143–175.
49. Singh, S (2015). Cytoprotective and regulatory functions of glutathione S-transferases in

cancer cell proliferation and cell death. *Cancer Chemother. Pharmacol.* **75**: 1–15.
50. Reuter, S, Gupta, SC, Chaturvedi, MM and Aggarwal, BB (2010). Oxidative stress, inflammation, and cancer: how are they linked? *Free Radic. Biol. Med.* **49**: 1603–1616.
51. Mahadevan, D and Sutton, GR (2015). Ezatiostat hydrochloride for the treatment of myelodysplastic syndromes. *Expert Opin. Investig. Drugs* **24**: 725–733.
52. Gilmore, TD and Herscovitch, M (2006). Inhibitors of NF-kappaB signaling: 785 and counting. *Oncogene* **25**: 6887–6899.
53. Du, Z, Whitt, MA, Baumann, J, Garner, JM, Morton, CL, Davidoff, AM, *et al.* (2012). Inhibition of type I interferon-mediated antiviral action in human glioma cells by the IKK inhibitors BMS-345541 and TPCA-1. *J. Interferon Cytokine Res.* **32**: 368–377.
54. Cataldi, M, Shah, NR, Felt, SA and Grdzelishvili, VZ (2015). Breaking resistance of pancreatic cancer cells to an attenuated vesicular stomatitis virus through a novel activity of IKK inhibitor TPCA-1. *Virology* **485**: 340–354.
55. Diallo, J-S, Vähä-Koskela, M, Le Boeuf, F and Bell, J (2012). Propagation, purification, and in vivo testing of oncolytic vesicular stomatitis virus strains. *Methods Mol. Biol.* **797**: 127–140.
56. Pfaffl, MW (2001). A new mathematical model for relative quantification in real-time RT-PCR. *Nucleic Acids Res.* **29**: e45.
57. Healy, MJ (1972). Statistical analysis of radioimmunoassay data. *Biochem. J* **130**: 207–210.
58. Mailloux, RJ, Xuan, JY, McBride, S, Maharsy, W, Thorn, S, Holterman, CE, *et al.* (2014). Glutaredoxin-2 is required to control oxidative phosphorylation in cardiac muscle by mediating deglutathionylation reactions. *J. Biol. Chem.* **289**: 14812–14828.
59. Eden, E, Navon, R, Steinfeld, I, Lipson, D and Yakhini, Z (2009). GOrilla: a tool for discovery and visualization of enriched GO terms in ranked gene lists. *BMC Bioinformatics* **10**: 48.

A.2 Manuscript In Preparation Figures

Figure 1.

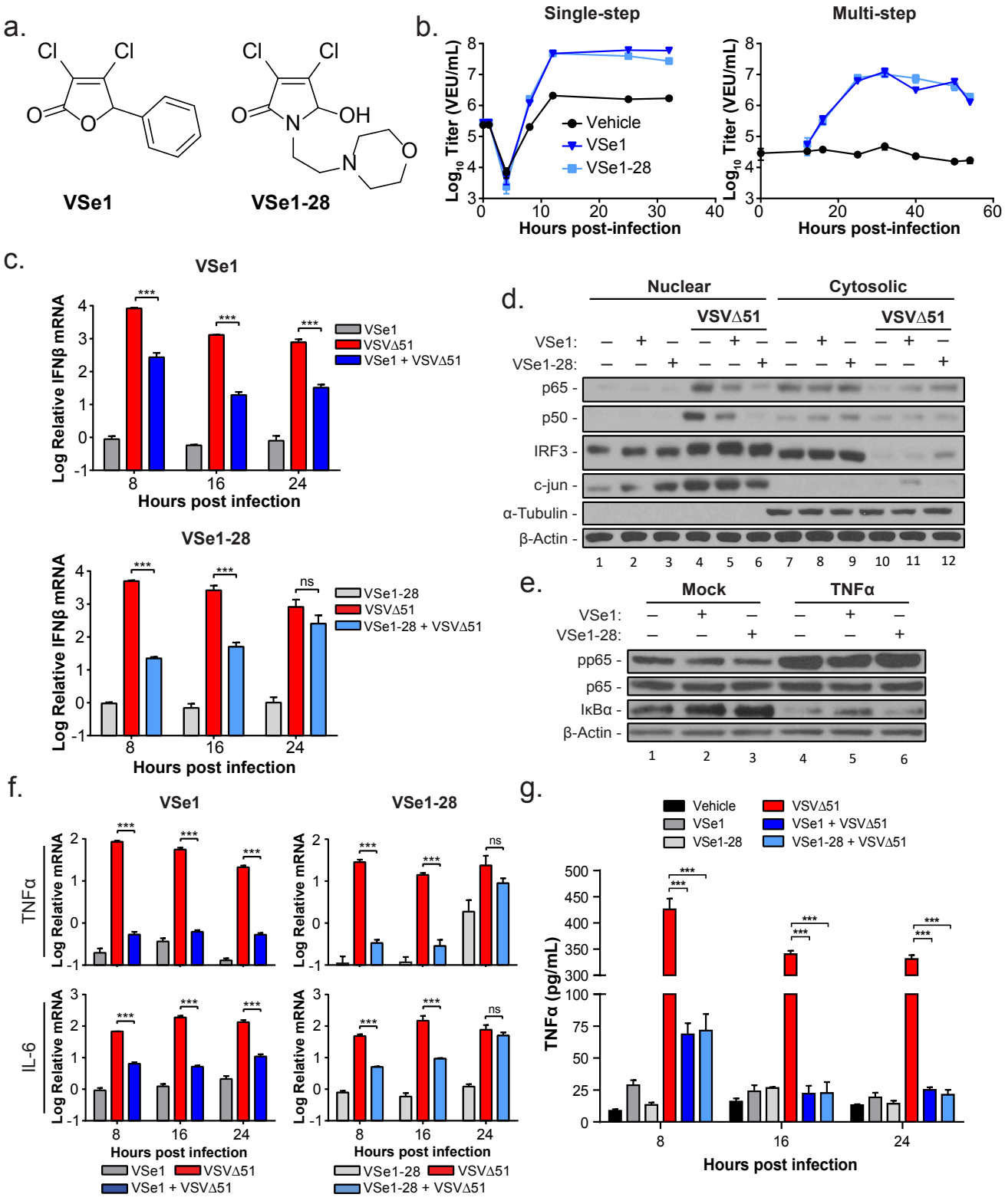

Figure 2

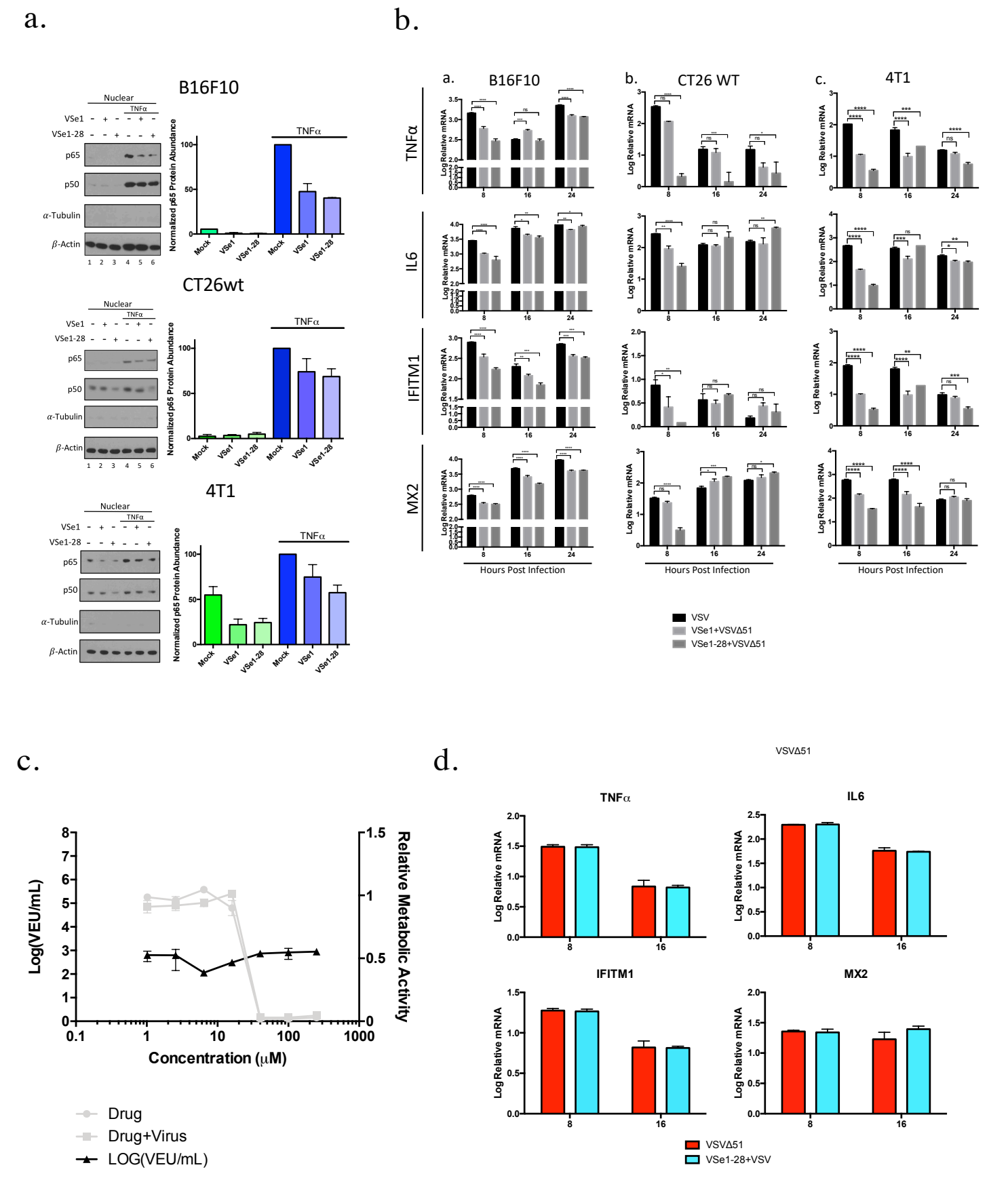
a.
b.
B16F10
CT26wt
4T1
Nuclear
TNFα
VSe1
VSe1-28
p65
p50
α-Tubulin
β-Actin
Normalized p65 Protein Abundance
Mock
VSe1
VSe1-28
a. B16F10
b. CT26 WT
c. 4T1
TNFα
IL9
IFITM1
MX2
Log Relative mRNA
Hours Post Infection
VSV
VSe1+VSVΔ51
VSe1-28+VSVΔ51
c.
d.
Log(VEU/mL)
Relative Metabolic Activity
Concentration (μM)
Drug
Drug+Virus
LOG(VEU/mL)
VSVΔ51
IL6
VSe1-28+VSV

Figure 3

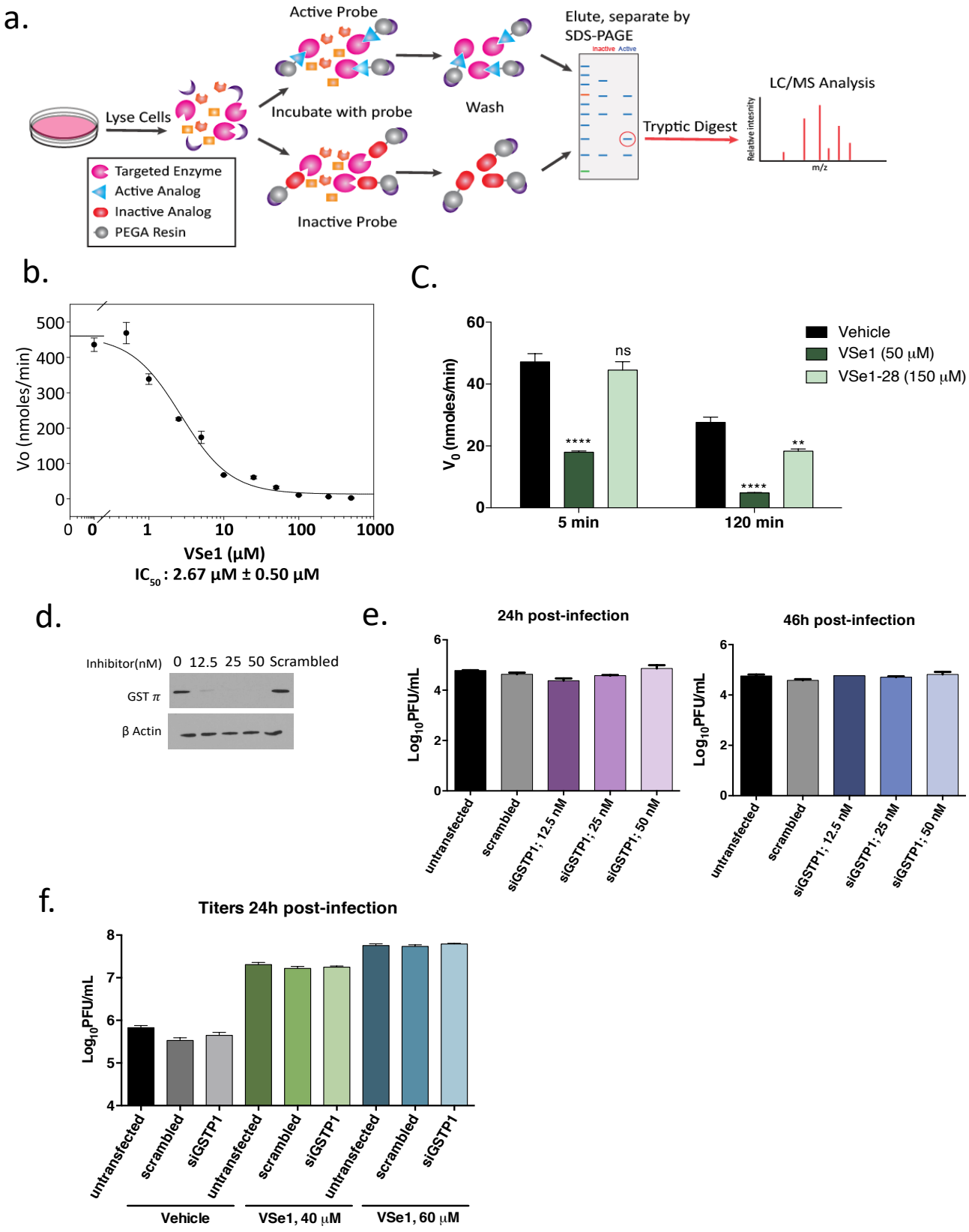
a.
Active Probe
Elute, separate by SDS-PAGE
Inactive Active
LC/MS Analysis
Lyse Cells
Incubate with probe
Wash
Tryptic Digest
Relative intensity
m/z
Targeted Enzyme
Active Analog
Inactive Analog
PEGA Resin
Inactive Probe
b.
Vo (nmoles/min)
VSe1 (μM)
IC50 : 2.67 μM ± 0.50 μM
C.
V0 (nmoles/min)
Vehicle
VSe1 (50 μM)
VSe1-28 (150 μM)
ns
****
**
5 min
120 min
d.
Inhibitor(nM) 0 12.5 25 50 Scrambled
GST π
β Actin
e.
24h post-infection
46h post-infection
Log10PFU/mL
untransfected
scrambled
siGSTP1; 12.5 nM
siGSTP1; 25 nM
siGSTP1; 50 nM
f.
Titers 24h post-infection
Log10PFU/mL
untransfected
scrambled
siGSTP1
Vehicle
VSe1, 40 μM
VSe1, 60 μM

Figure 4

a.

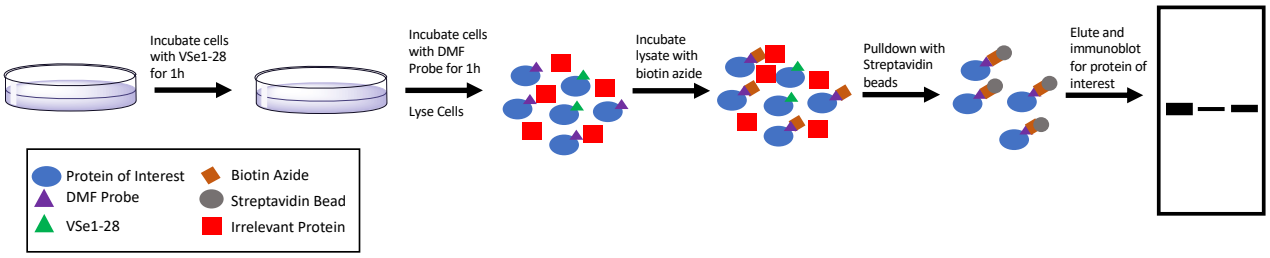

b.

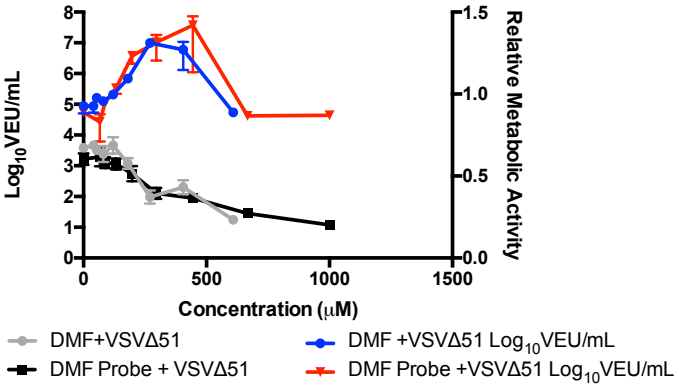

c.

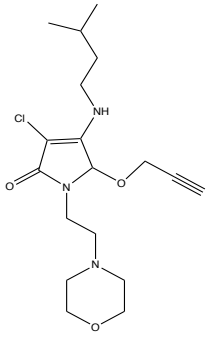

d.

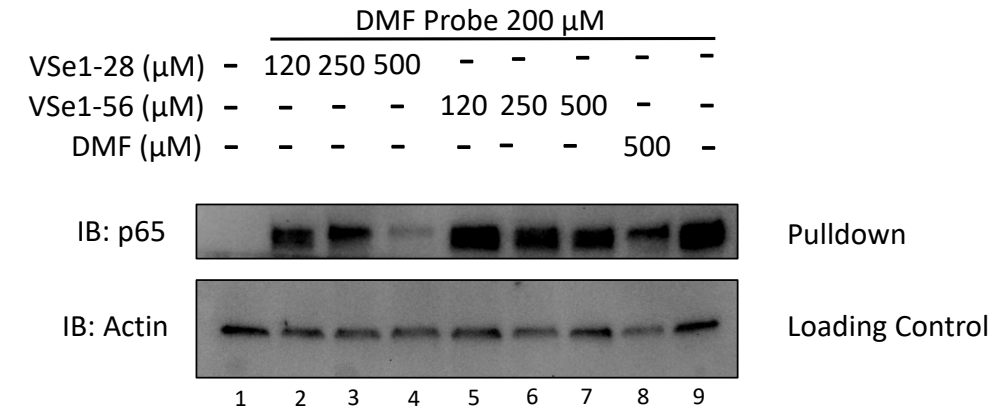

Figure 5.

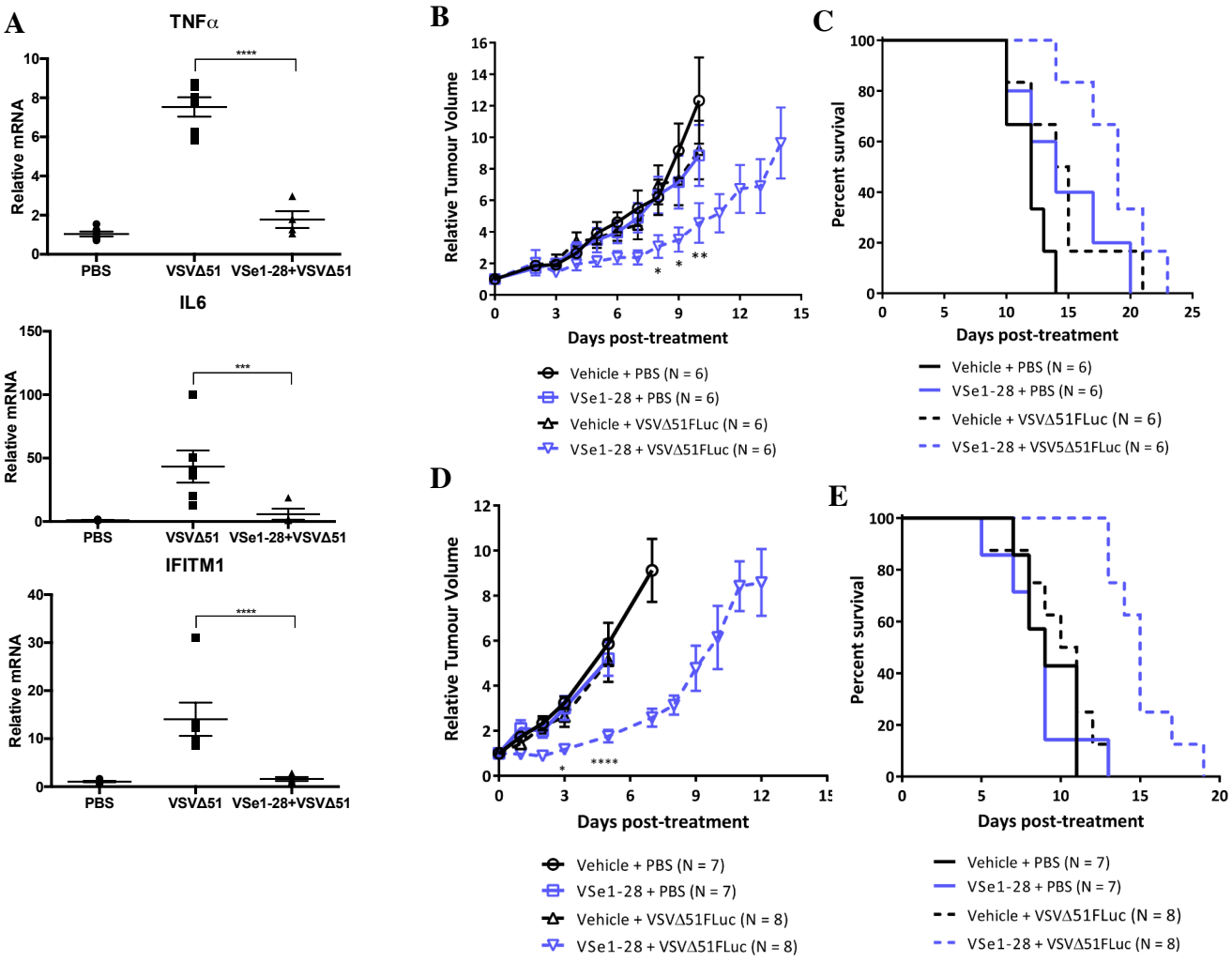
A
TNFα
Relative mRNA
PBS
VSVΔ51
VSe1-28+VSVΔ51
IL6
IFITM1
B
Relative Tumour Volume
Days post-treatment
Vehicle + PBS (N = 6)
VSe1-28 + PBS (N = 6)
Vehicle + VSVΔ51FLuc (N = 6)
VSe1-28 + VSVΔ51FLuc (N = 6)
C
Percent survival
Days post-treatment
Vehicle + PBS (N = 6)
VSe1-28 + PBS (N = 6)
Vehicle + VSVΔ51FLuc (N = 6)
VSe1-28 + VSV5Δ51FLuc (N = 6)
D
Relative Tumour Volume
Days post-treatment
Vehicle + PBS (N = 7)
VSe1-28 + PBS (N = 7)
Vehicle + VSVΔ51FLuc (N = 8)
VSe1-28 + VSVΔ51FLuc (N = 8)
E
Percent survival
Days post-treatment
Vehicle + PBS (N = 7)
VSe1-28 + PBS (N = 7)
Vehicle + VSVΔ51FLuc (N = 8)
VSe1-28 + VSVΔ51FLuc (N = 8)

Supplementary

Figure S1

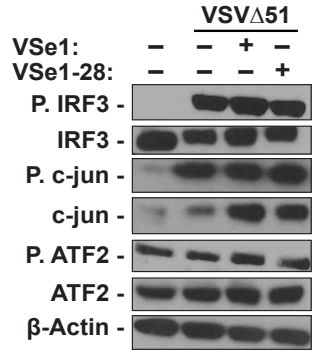

Figure S2

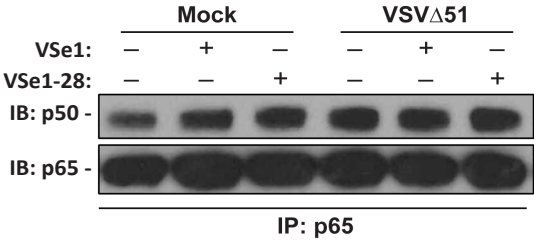

Figure S3

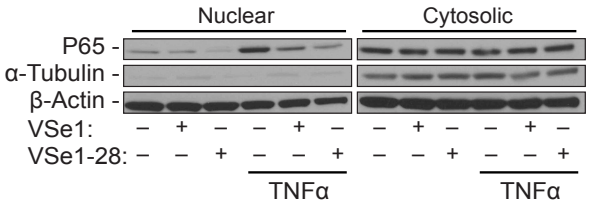

Figure S4

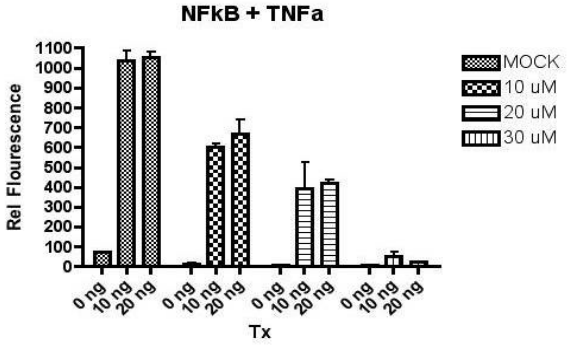

Figure S5

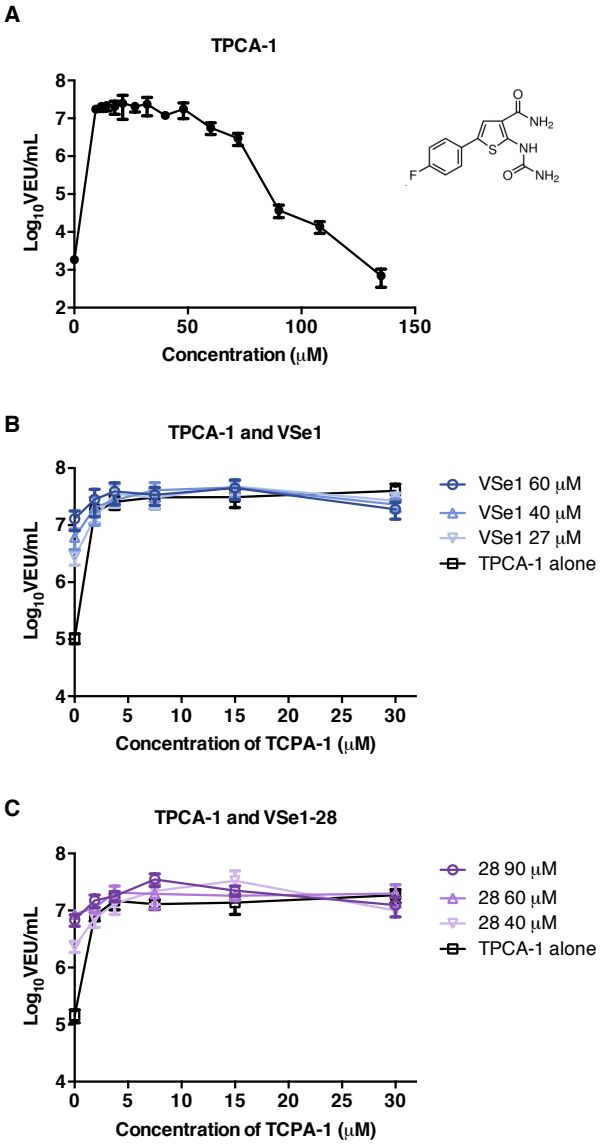

Figure S6

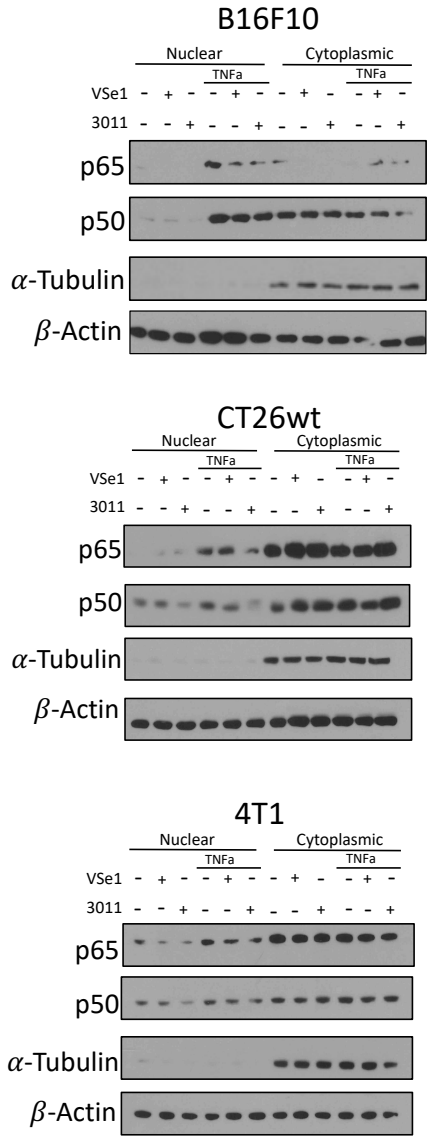

Figure S7

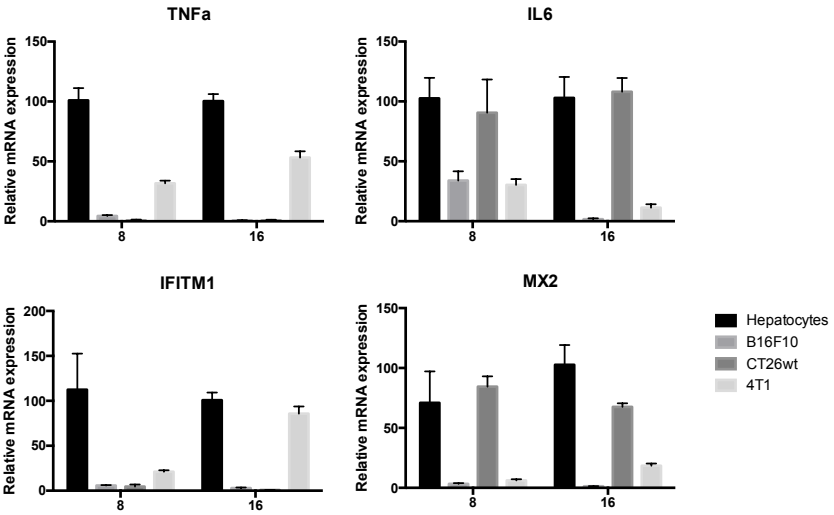

Figure S8

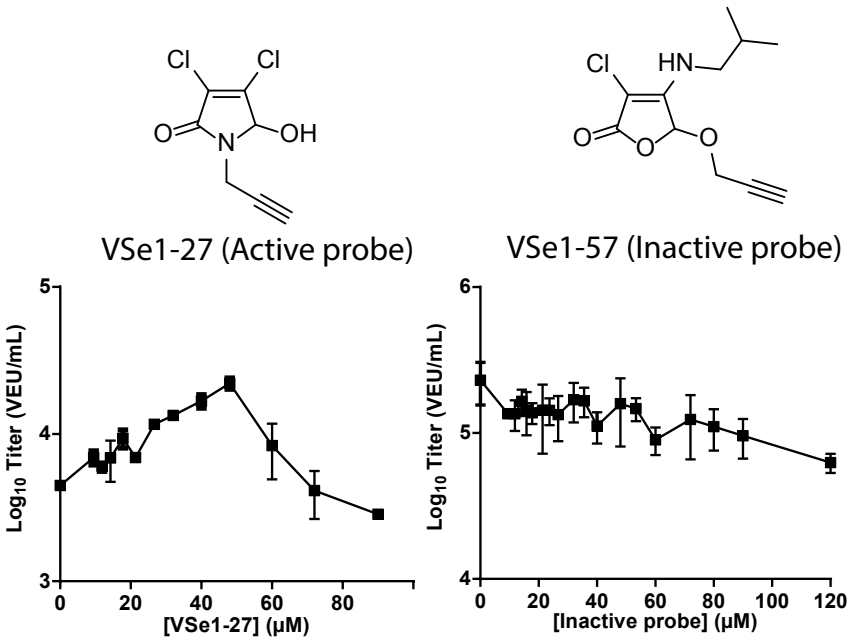

Figure S9

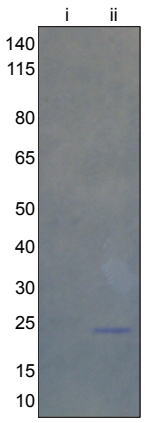

Figure S10

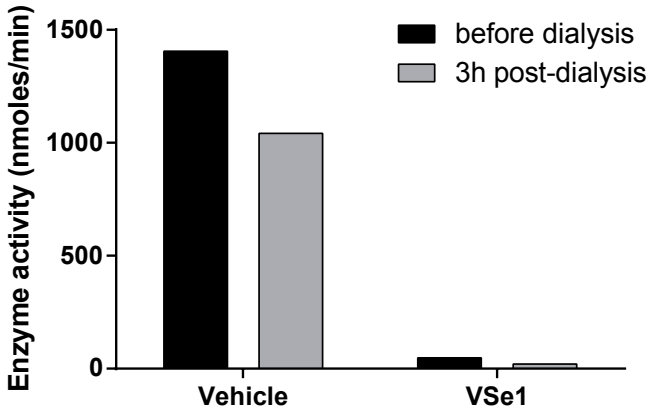

Table S1

Sample	Sequenced hits
Active analog, uninfected lysate	**Glutathione-S-transferase (25 kDa)**
	Peroxiredoxin-1 (25 kDa)
Active analog, infected lysate	**Glutathione-S-transferase (25 kDa)**
	Peroxiredoxin-1 (25 kDa)
	Annexin A2 isoform 2 (20 kDa)
	Thioredoxin (10 kDa)

Figure S11

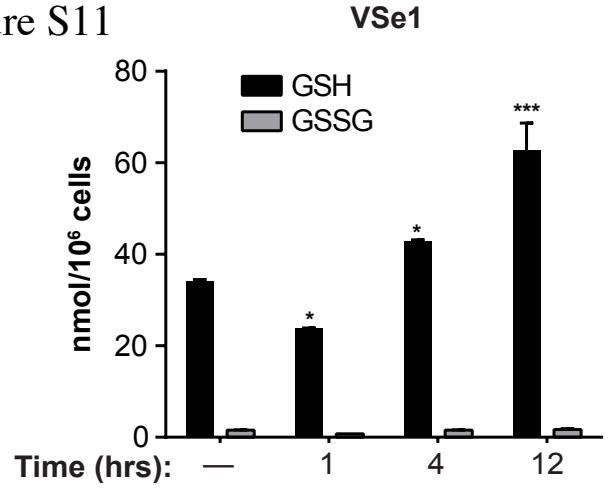

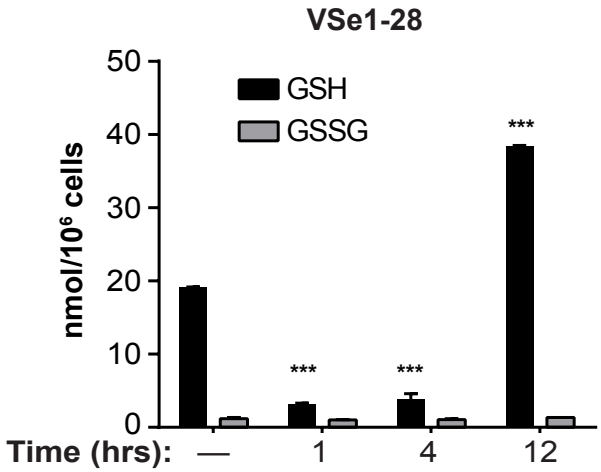

Figure S12

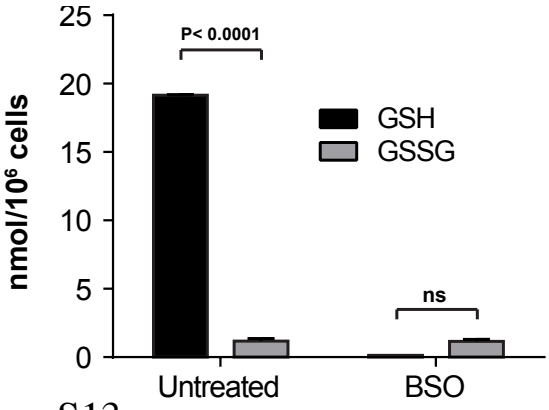

Figure S13

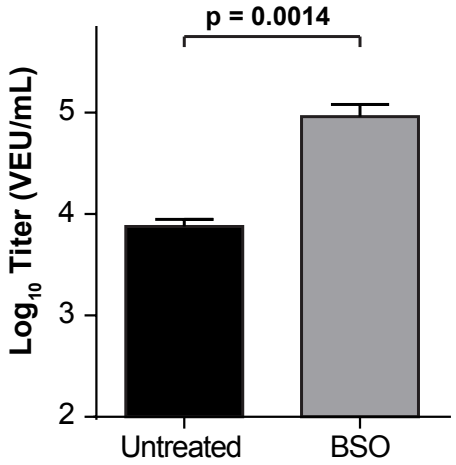

Figure S14

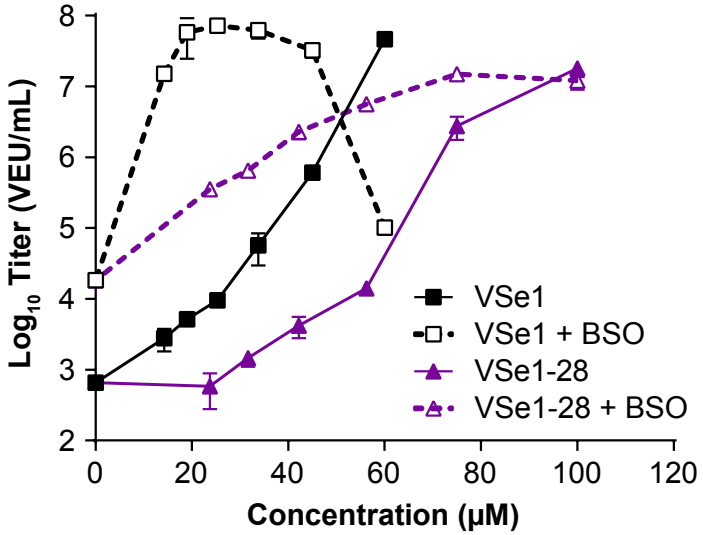

Figure S15

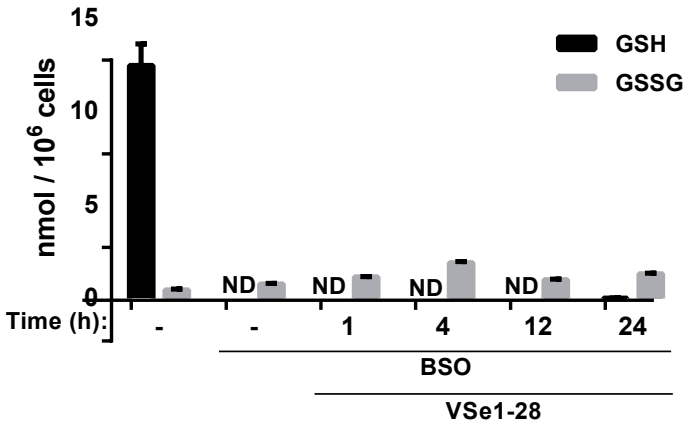

Figure S16

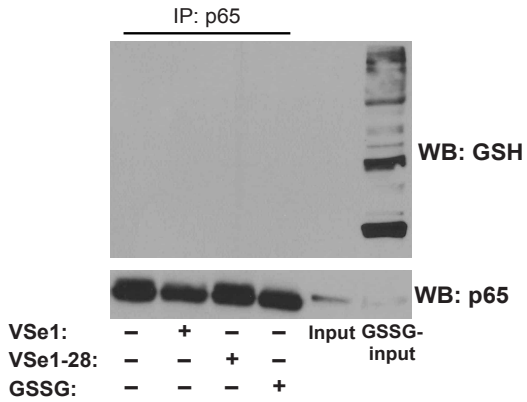

Figure S17

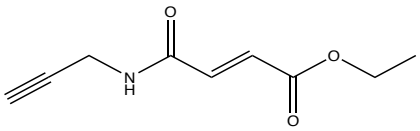

Figure S18

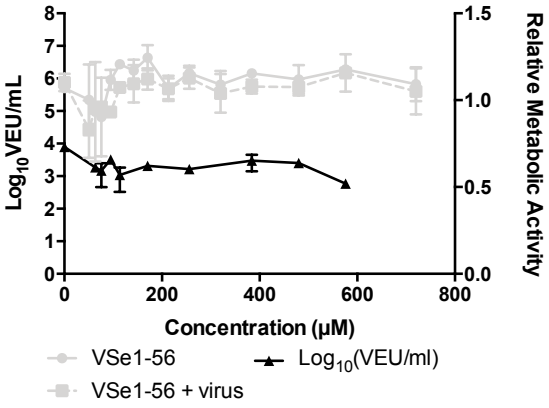

Figure S19

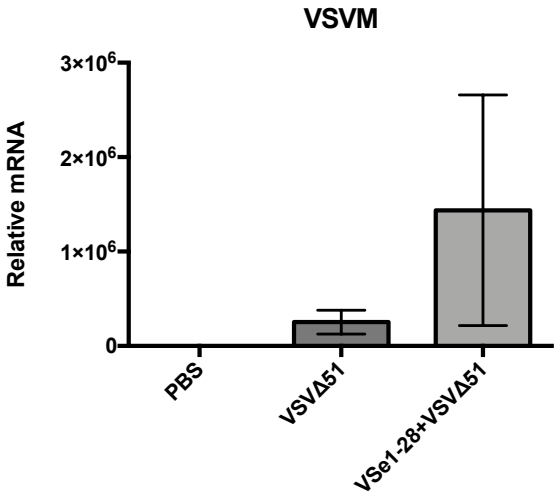

Figure S20

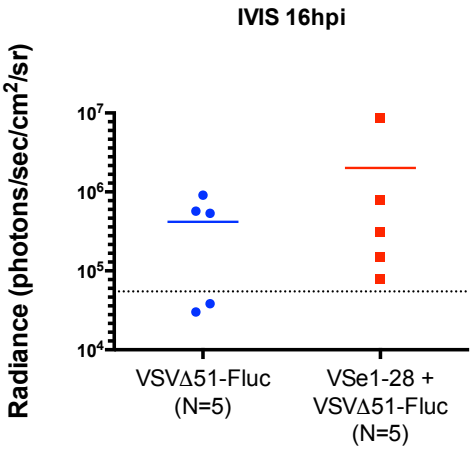

References

(1) Faguet, G. B. A Brief History of Cancer: Age-Old Milestones Underlying Our Current Knowledge Database. *Int. J. Cancer* **2015**, *136* (9), 2022–2036.
(2) Organization, W. H. Cancer.
(3) Committee, C. C. S. A. Canadian Cancer Statistics 2019. *Can. Cancer Soc.* **2019**.
(4) Hanahan, D.; Weinberg, R. A. Hallmarks of Cancer: The next Generation. *Cell* **2011**, *144* (5), 646–674.
(5) Wang, M.; Zhao, J.; Zhang, L.; Wei, F.; Lian, Y.; Wu, Y.; Gong, Z.; Zhang, S.; Zhou, J.; Cao, K.; et al. Role of Tumor Microenvironment in Tumorigenesis. *J. Cancer* **2017**, *8* (5), 761–773.
(6) Mittal, D.; Gubin, M. M.; Schreiber, R. D.; Smyth, M. J. New Insights into Cancer Immunoediting and Its Three Component Phases--Elimination, Equilibrium and Escape. *Curr. Opin. Immunol.* **2014**, *27*, 16–25.
(7) Vesely, M. D.; Schreiber, R. D. Cancer Immunoediting: Antigens, Mechanisms, and Implications to Cancer Immunotherapy. *Ann. N. Y. Acad. Sci.* **2013**, *1284* (1), 1–5.
(8) Ilkow, C. S.; Swift, S. L.; Bell, J. C.; Diallo, J. S. From Scourge to Cure: Tumour-Selective Viral Pathogenesis as a New Strategy against Cancer. *PLoS Pathog.* **2014**, *10* (1).
(9) Welsh, R. M.; Bahl, K.; Marshall, H. D.; Urban, S. L. Type 1 Interferons and Antiviral CD8 T-Cell Responses. *PLoS Pathog.* **2012**, *8* (1).
(10) Seo, Y. J.; Hahm, B. *Type I Interferon Modulates the Battle of Host Immune System against Viruses*, 1st ed.; Elsevier Inc., 2010; Vol. 73.
(11) Teijaro, J. R. Type I Interferons in Viral Control and Immune Regulation. *Curr. Opin. Virol.* **2016**, *16*, 31–40.
(12) Panne, D.; Maniatis, T.; Harrison, S. C. An Atomic Model of the Interferon-Beta Enhanceosome. *Cell* **2007**, *129* (6), 1111–1123.
(13) Liu, Y. C.; Simmons, D. P.; Li, X.; Abbott, D. W.; Boom, W. H.; Harding, C. V. TLR2 Signaling Depletes IRAK1 and Inhibits Induction of Type I IFN by TLR7/9. *J. Immunol.* **2012**, *188* (3), 1019–1026.
(14) Trinchieri, G. Type I Interferon: Friend or Foe? *J. Exp. Med.* **2010**, *207* (10), 2053–2063.
(15) Platanias, L. C. Mechanisms of Type-I- and Type-II-Interferon-Mediated Signalling. *Nat. Rev. Immunol.* **2005**, *5* (5), 375–386.
(16) Lee, A. J.; Ashkar, A. A. The Dual Nature of Type I and Type II Interferons. *Front. Immunol.* **2018**, *9* (SEP), 1–10.
(17) Crameri, M.; Bauer, M.; Caduff, N.; Walker, R.; Steiner, F.; Franzoso, F. D.; Gujer, C.; Boucke, K.; Kucera, T.; Zbinden, A.; et al. MxB Is an Interferon-Induced Restriction Factor of Human Herpesviruses. *Nat. Commun.* **2018**, *9* (1), 1980.
(18) Moynagh, P. N. The NF-KB Pathway. *J. Cell Sci.* **2005**, *118* (20), 4589–4592.
(19) Hoesel, B.; Schmid, J. A. The Complexity of NF-KB Signaling in Inflammation and Cancer. *Mol. Cancer* **2013**, *12* (86).
(20) Sun, S.-C.; Cesarman, E. NF-KappaB as a Target for Oncogenic Viruses. *Curr. Top. Microbiol.* **2011**, *349*, 197–244.
(21) Shih, V. F.-S.; Tsui, R.; Caldwell, A.; Hoffmann, A. A Single NFκB System for Both Canonical and Non-Canonical Signaling. *Cell Res.* **2011**, *21* (1), 86–102.
(22) Oeckinghaus, A.; Ghosh, S. The NF-KappaB Family of Transcription Factors and Its

Regulation. *Cold Spring Harb. Perspect. Biol.* **2009**, *1* (4), a000034–a000034.
(23) Park, M. H.; Hong, J. T. Roles of NF-KB in Cancer and Inflammatory Diseases and Their Therapeutic Approaches. *Cells* **2016**, *5* (2), 15.
(24) Xia, Y.; Shen, S.; Verma, I. M. NF-KB, an Active Player in Human Cancers. *Cancer Immunol. Res.* **2014**, *2* (9), 823–830.
(25) Baud, V.; Karin, M. Is NF-KappaB a Good Target for Cancer Therapy? Hopes and Pitfalls. *Nat. Rev. Drug Discov.* **2009**, *8* (1), 33–40.
(26) Brightbill, H. D.; Suto, E.; Blaquiere, N.; Ramamoorthi, N.; Sujatha-Bhaskar, S.; Gogol, E. B.; Castanedo, G. M.; Jackson, B. T.; Kwon, Y. C.; Haller, S.; et al. NF-KB Inducing Kinase Is a Therapeutic Target for Systemic Lupus Erythematosus. *Nat. Commun.* **2018**, *9* (1), 179.
(27) Plummer, S. M.; Holloway, K. A.; Manson, M. M.; Munks, R. J.; Kaptein, A.; Farrow, S.; Howells, L. Inhibition of Cyclo-Oxygenase 2 Expression in Colon Cells by the Chemopreventive Agent Curcumin Involves Inhibition of NF-KappaB Activation via the NIK/IKK Signalling Complex. *Oncogene* **1999**, *18* (44), 6013–6020.
(28) Podolin, P. L.; Callahan, J. F.; Bolognese, B. J.; Li, Y. H.; Carlson, K.; Davis, T. G.; Mellor, G. W.; Evans, C.; Roshak, A. K. Attenuation of Murine Collagen-Induced Arthritis by a Novel, Potent, Selective Small Molecule Inhibitor of IkappaB Kinase 2, TPCA-1 (2-[(Aminocarbonyl)Amino]-5-(4-Fluorophenyl)-3-Thiophenecarboxamide), Occurs via Reduction of Proinflammatory Cytokines And. *J. Pharmacol. Exp. Ther.* **2005**, *312* (1), 373–381.
(29) Nan, J.; Du, Y.; Chen, X.; Bai, Q.; Wang, Y.; Zhang, X.; Zhu, N.; Zhang, J.; Hou, J.; Wang, Q.; et al. TPCA-1 Is a Direct Dual Inhibitor of STAT3 and NF-KappaB and Regresses Mutant EGFR-Associated Human Non-Small Cell Lung Cancers. *Mol. Cancer Ther.* **2014**, *13* (3), 617–629.
(30) Kwok, B. H.; Koh, B.; Ndubuisi, M. I.; Elofsson, M.; Crews, C. M. The Anti-Inflammatory Natural Product Parthenolide from the Medicinal Herb Feverfew Directly Binds to and Inhibits IkappaB Kinase. *Chem. Biol.* **2001**, *8* (8), 759–766.
(31) Sarveswaran, S.; Gautam, S. C.; Ghosh, J. Wedelolactone, a Medicinal Plant-Derived Coumestan, Induces Caspase-Dependent Apoptosis in Prostate Cancer Cells via Downregulation of PKCε without Inhibiting Akt. *Int. J. Oncol.* **2012**, *41* (6), 2191–2199.
(32) Gilmore, T. D.; Herscovitch, M. Inhibitors of NF-KB Signaling: 785 and Counting. *Oncogene* **2006**, *25* (51), 6887–6899.
(33) Yemelyanov, A.; Gasparian, A.; Lindholm, P.; Dang, L.; Pierce, J. W.; Kisseljov, F.; Karseladze, A.; Budunova, I. Effects of IKK Inhibitor PS1145 on NF-KB Function, Proliferation, Apoptosis and Invasion Activity in Prostate Carcinoma Cells. *Oncogene* **2006**, *25* (3), 387–398.
(34) Li, F.; Zhang, J.; Arfuso, F.; Chinnathambi, A.; Zayed, M. E.; Alharbi, S. A.; Kumar, A. P.; Ahn, K. S.; Sethi, G. NF-KappaB in Cancer Therapy. *Arch. Toxicol.* **2015**, *89* (5), 711–731.
(35) Swinney, D. C.; Xu, Y.-Z.; Scarafia, L. E.; Lee, I.; Mak, A. Y.; Gan, Q.-F.; Ramesha, C. S.; Mulkins, M. A.; Dunn, J.; So, O.-Y.; et al. A Small Molecule Ubiquitination Inhibitor Blocks NF-Kappa B-Dependent Cytokine Expression in Cells and Rats. *J. Biol. Chem.* **2002**, *277* (26), 23573–23581.
(36) Nishimura, D.; Ishikawa, H.; Matsumoto, K.; Shibata, H.; Motoyoshi, Y.; Fukuta, M.; Kawashimo, H.; Goto, T.; Taura, N.; Ichikawa, T.; et al. DHMEQ, a Novel NF-KappaB

Inhibitor, Induces Apoptosis and Cell-Cycle Arrest in Human Hepatoma Cells. *Int. J. Oncol.* **2006**, *29* (3), 713–719.
(37) Umezawa, K. Inhibition of Tumor Growth by NF-KB Inhibitors. *Cancer Sci.* **2006**, *97* (10), 990–995.
(38) García-Piñeres, A. J.; Castro, V.; Mora, G.; Schmidt, T. J.; Strunck, E.; Pahl, H. L.; Merfort, I. Cysteine 38 in P65/NF-KB Plays a Crucial Role in DNA Binding Inhibition by Sesquiterpene Lactones. *J. Biol. Chem.* **2001**, *276* (43), 39713–39720.
(39) Donovan, J. M.; Zimmer, M.; Offman, E.; Grant, T.; Jirousek, M. A Novel NF-KB Inhibitor, Edasalonexent (CAT-1004), in Development as a Disease-Modifying Treatment for Patients With Duchenne Muscular Dystrophy: Phase 1 Safety, Pharmacokinetics, and Pharmacodynamics in Adult Subjects. *J. Clin. Pharmacol.* **2017**, *57* (5), 627–639.
(40) Yamamoto, Y.; Gaynor, R. B. Therapeutic Potential of Inhibition of the NF-KB Pathway in the Treatment of Inflammation and Cancer. *J. Clin. Invest.* **2001**, *107* (2), 135–142.
(41) Jackson, J. D.; Markert, J. M.; Li, L.; Carroll, S. L.; Cassady, K. A. STAT1 and NF-KappaB Inhibitors Diminish Basal Interferon-Stimulated Gene Expression and Improve the Productive Infection of Oncolytic HSV in MPNST Cells. *Mol. Cancer Res.* **2016**, *14* (5), 482–492.
(42) Macdonald, V. Chemotherapy: Managing Side Effects and Safe Handling. *Can. Vet. J.* **2009**, *50* (6), 665–668.
(43) Van Vuuren, R. J.; Visagie, M. H.; Theron, A. E.; Joubert, A. M. Antimitotic Drugs in the Treatment of Cancer. *Cancer Chemother. Pharmacol.* **2015**, *76* (6), 1101–1112.
(44) Johnstone, T. C.; Park, G. Y.; Lippard, S. J. Understanding and Improving Platinum Anticancer Drugs--Phenanthriplatin. *Anticancer Res.* **2014**, *34* (1), 471–476.
(45) Dasari, S.; Tchounwou, P. B. Cisplatin in Cancer Therapy: Molecular Mechanisms of Action. *Eur. J. Pharmacol.* **2014**, *740*, 364–378.
(46) Baskar, R.; Lee, K. A.; Yeo, R.; Yeoh, K.-W. Cancer and Radiation Therapy: Current Advances and Future Directions. *Int. J. Med. Sci.* **2012**, *9* (3), 193–199.
(47) Urruticoechea, A.; Alemany, R.; Balart, J.; Villanueva, A.; Vinals, F.; Capella, G. Recent Advances in Cancer Therapy: An Overview. *Curr. Pharm. Des.* **2010**, *16* (1), 3–10.
(48) Wieder, T.; Eigentler, T.; Brenner, E.; Rocken, M. Immune Checkpoint Blockade Therapy. *J. Allergy Clin. Immunol.* **2018**, *142* (5), 1403–1414.
(49) Postow, M. A.; Callahan, M. K.; Wolchok, J. D. Immune Checkpoint Blockade in Cancer Therapy. *J. Clin. Oncol.* **2015**, *33* (17), 1974–1982.
(50) Bell, J.; McFadden, G. Viruses for Tumor Therapy. *Cell Host Microbe* **2014**, *15* (3), 260–265.
(51) HOSTER, H. A.; ZANES, R. P. J.; VON HAAM, E. Studies in Hodgkin's Syndrome; the Association of Viral Hepatitis and Hodgkin's Disease; a Preliminary Report. *Cancer Res.* **1949**, *9* (8), 473–480.
(52) Russell, S. J.; Peng, K.-W.; Bell, J. C. Oncolytic Virotherapy. *Nat. Biotechnol.* **2012**, *30* (7), 658–670.
(53) Hastie, E.; Cataldi, M.; Marriott, I.; Grdzelishvili, V. Z. Understanding and Altering Cell Tropism of Vesicular Stomatitis Virus. *Virus Res.* **2013**, *176* (1–2), 16–32.
(54) Brown, V. R.; Bevins, S. N. A Review of Virulent Newcastle Disease Viruses in the United States and the Role of Wild Birds in Viral Persistence and Spread. *Vet. Res.* **2017**, *48* (1), 68.
(55) Russell, S. J.; Peng, K.-W. Oncolytic Virotherapy: A Contest between Apples and

Oranges. *Mol. Ther.* **2017**, *25* (5), 1107–1116.
(56) Russell, S. J. Oncolytic Virotherapy. **2014**, *30* (7), 1–29.
(57) Liang, M. Oncorine, the World First Oncolytic Virus Medicine and Its Update in China. *Curr. Cancer Drug Targets* **2018**, *18* (2), 171–176.
(58) Conry, R. M.; Westbrook, B.; McKee, S.; Norwood, T. G. Talimogene Laherparepvec: First in Class Oncolytic Virotherapy. *Hum. Vaccin. Immunother.* **2018**, *14* (4), 839–846.
(59) Hastie, E.; Grdzelishvili, V. Z. Vesicular Stomatitis Virus as a Flexible Platform for Oncolytic Virotherapy against Cancer. *J. Gen. Virol.* **2012**, *93* (Pt 12), 2529–2545.
(60) Melzer, M. K.; Lopez-Martinez, A.; Altomonte, J. Oncolytic Vesicular Stomatitis Virus as a Viro-Immunotherapy: Defeating Cancer with a "Hammer" and "Anvil." *Biomedicines* **2017**, *5* (1), 8.
(61) Stojdl, D. F.; Lichty, B.; Knowles, S.; Marius, R.; Atkins, H.; Sonenberg, N.; Bell, J. C. Exploiting Tumor-Specific Defects in the Interferon Pathway with a Previously Unknown Oncolytic Virus. *Nat. Med.* **2000**, *6* (7), 821–825.
(62) Selman, Mohammed; Ou, Paula; Rousso, Christopher; Bergeron, Anabel; Krishnan, Ramya; Pikor, Larissa; Chen, Andrew; Keller, Brian A.; Ilkow, Carolina; Bell, John C.; Diallo, J.-S. Dimethyl Fumarate Potentiates Oncolytic Virotherapy through NF-KB Inhibition. *Sci. Transl. Med.* **2017**, *Accepted M*.
(63) Arulanandam, R.; Batenchuk, C.; Varette, O.; Zakaria, C.; Garcia, V.; Forbes, N. E.; Davis, C.; Krishnan, R.; Karmacharya, R.; Cox, J.; et al. Microtubule Disruption Synergizes with Oncolytic Virotherapy by Inhibiting Interferon Translation and Potentiating Bystander Killing. *Nat. Commun.* **2015**, *6*, 6410.
(64) Bourgeois-Daigneault, M.-C.; St-Germain, L. E.; Roy, D. G.; Pelin, A.; Aitken, A. S.; Arulanandam, R.; Falls, T.; Garcia, V.; Diallo, J.-S.; Bell, J. C. Combination of Paclitaxel and MG1 Oncolytic Virus as a Successful Strategy for Breast Cancer Treatment. *Breast Cancer Res.* **2016**, *18* (1), 83.
(65) Phan, M.; Watson, M. F.; Alain, T.; Diallo, J.-S. Oncolytic Viruses on Drugs: Achieving Higher Therapeutic Efficacy. *ACS Infect. Dis.* **2018**, *4* (10), 1448–1467.
(66) Tirelli, U.; Errante, D.; Van Glabbeke, M.; Teodorovic, I.; Kluin-Nelemans, J. C.; Thomas, J.; Bron, D.; Rosti, G.; Somers, R.; Zagonel, V.; et al. CHOP Is the Standard Regimen in Patients > or = 70 Years of Age with Intermediate-Grade and High-Grade Non-Hodgkin's Lymphoma: Results of a Randomized Study of the European Organization for Research and Treatment of Cancer Lymphoma Cooperative Study Group. *J. Clin. Oncol.* **1998**, *16* (1), 27–34.
(67) Selman, M.; Rousso, C.; Bergeron, A.; Son, H. H.; Krishnan, R.; El-Sayes, N. A.; Varette, O.; Chen, A.; Le Boeuf, F.; Tzelepis, F.; et al. Multi-Modal Potentiation of Oncolytic Virotherapy by Vanadium Compounds. *Mol. Ther.* **2017**.
(68) Diallo, J. S.; Boeuf, F. Le; Lai, F.; Cox, J.; Vaha-Koskela, M.; Abdelbary, H.; MacTavish, H.; Waite, K.; Falls, T.; Wang, J.; et al. A High-Throughput Pharmacoviral Approach Identifies Novel Oncolytic Virus Sensitizers. *Mol. Ther.* **2010**, *18* (6), 1123–1129.
(69) Dornan, M. H.; Krishnan, R.; MacKlin, A. M.; Selman, M.; El Sayes, N.; Son, H. H.; Davis, C.; Chen, A.; Keillor, K.; Le, P. J.; et al. First-in-Class Small Molecule Potentiators of Cancer Virotherapy. *Sci. Rep.* **2016**, *6*.
(70) Zhang, X.; Yang, W.; Wang, X.; Zhang, X.; Tian, H.; Deng, H.; Zhang, L.; Gao, G. Identification of New Type I Interferon-Stimulated Genes and Investigation of Their

Involvement in IFN-β Activation. *Protein Cell* **2018**, *9* (9), 799–807.
(71) Pahl, H. L. Activators and Target Genes of Rel/NF-KappaB Transcription Factors. *Oncogene* **1999**, *18* (49), 6853–6866.
(72) Townsend, D. M.; Tew, K. D. The Role of Glutathione-S-Transferase in Anti-Cancer Drug Resistance. *Oncogene* **2003**, *22* (47), 7369–7375.
(73) Laborde, E. Glutathione Transferases as Mediators of Signaling Pathways Involved in Cell Proliferation and Cell Death. *Cell Death Differ.* **2010**, *17* (9), 1373–1380.
(74) Tew, K. D.; Manevich, Y.; Grek, C.; Xiong, Y.; Uys, J.; Townsend, D. M. The Role of Glutathione S-Transferase P in Signaling Pathways and S-Glutathionylation in Cancer. *Free Radic. Biol. Med.* **2011**, *51* (2), 299–313.
(75) Ogino, S.; Konishi, H.; Ichikawa, D.; Matsubara, D.; Shoda, K.; Arita, T.; Kosuga, T.; Komatsu, S.; Shiozaki, A.; Okamoto, K.; et al. Glutathione S-Transferase Pi 1 Is a Valuable Predictor for Cancer Drug Resistance in Esophageal Squamous Cell Carcinoma. *Cancer Sci.* **2019**, *110* (2), 795–804.
(76) Liang, M. C.; Bardhan, S.; Pace, E. A.; Rosman, D.; Beutler, J. A.; Porco, J. A.; Gilmore, T. D. Inhibition of Transcription Factor NF-KB Signaling Proteins IKKβ and P65 through Specific Cysteine Residues by Epoxyquinone a Monomer: Correlation with Its Anti-Cancer Cell Growth Activity. *Biochem. Pharmacol.* **2006**, *71* (5), 634–645.
(77) Widen, J. C.; Kempema, A. M.; Villalta, P. W.; Harki, D. A. Targeting NF-KB P65 with a Helenalin Inspired Bis-Electrophile. *ACS Chem. Biol.* **2017**, *12* (1), 102–113.
(78) Kastrati, I.; Siklos, M. I.; Calderon-Gierszal, E. L.; El-Shennawy, L.; Georgieva, G.; Thayer, E. N.; Thatcher, G. R. J.; Frasor, J. Dimethyl Fumarate Inhibits the Nuclear Factor KB Pathway in Breast Cancer Cells by Covalent Modification of P65 Protein. *J. Biol. Chem.* **2016**, *291* (7), 3639–3647.
(79) Claudino, M.; Zhang, X.; Alim, M. D.; Podgórski, M.; Bowman, C. N. Mechanistic Kinetic Modeling of Thiol-Michael Addition Photopolymerizations via Photocaged "Superbase" Generators: An Analytical Approach. *Macromolecules* **2016**, *49* (21), 8061–8074.
(80) Diallo, J.-S.; Vaha-Koskela, M.; Le Boeuf, F.; Bell, J. Propagation, Purification, and in Vivo Testing of Oncolytic Vesicular Stomatitis Virus Strains. *Methods Mol. Biol.* **2012**, *797*, 127–140.
(81) Fullerton, M. D.; Hakimuddin, F.; Bonen, A.; Bakovic, M. The Development of a Metabolic Disease Phenotype in CTP:Phosphoethanolamine Cytidylyltransferase-Deficient Mice. *J. Biol. Chem.* **2009**, *284* (38), 25704–25713.
(82) Yang, P. Y.; Liu, K.; Zhang, C.; Chen, G. Y. J.; Shen, Y.; Ngai, M. H.; Lear, M. J.; Yao, S. Q. Chemical Modification and Organelle-Specific Localization of Orlistat-like Natural-Product-Based Probes. *Chem. - An Asian J.* **2011**, *6* (10), 2762–2775.
(83) Yang, P. Y.; Liu, K.; Ngai, M. H.; Lear, M. J.; Wenk, M. R.; Yao, S. Q. Activity-Based Proteome Profiling of Potential Cellular Targets of Orlistat - An FDA-Approved Drug with Anti-Tumor Activities. *J. Am. Chem. Soc.* **2010**, *132* (2), 656–666.
(84) Pfaffl, M. W. A New Mathematical Model for Relative Quantification in Real-Time RT-PCR. *Nucleic Acids Res.* **2001**, *29* (9), e45–e45.
(85) Garcia, V.; Krishnan, R.; Davis, C.; Batenchuk, C.; Le Boeuf, F.; Abdelbary, H.; Diallo, J.-S. High-Throughput Titration of Luciferase-Expressing Recombinant Viruses. *J. Vis. Exp.* **2014**, No. 91, 51890.
(86) Blais, D. R.; Nasheri, N.; McKay, C. S.; Legault, M. C. B.; Pezacki, J. P. Activity-Based

Protein Profiling of Host-Virus Interactions. *Trends Biotechnol.* **2012**, *30* (2), 89–99.
(87) Hein, C. D.; Liu, X.-M.; Wang, D. Click Chemistry, a Powerful Tool for Pharmaceutical Sciences. *Pharm. Res.* **2008**, *25* (10), 2216–2230.
(88) Hermanson, G. T. Chapter 11 - (Strept)Avidin–Biotin Systems; Hermanson, G. T. B. T.-B. T. (Third E., Ed.; Academic Press: Boston, 2013; pp 465–505.
(89) Millipore Sigma. Azide-fluor 488.
(90) Novick, D.; Rubinstein, M. Ligand Affinity Chromatography, an Indispensable Method for the Purification of Soluble Cytokine Receptors and Binding Proteins. *Methods Mol. Biol.* **2012**, *820*, 195–214.
(91) Sánchez-Gómez, F. J.; Díez-Dacal, B.; García-Martín, E.; Agúndez, J. A. G.; Pajares, M. A.; Pérez-Sala, D. Detoxifying Enzymes at the Cross-Roads of Inflammation, Oxidative Stress, and Drug Hypersensitivity: Role of Glutathione Transferase P1-1 and Aldose Reductase. *Front. Pharmacol.* **2016**, *7*, 237.
(92) Peklak-Scott, C.; Smitherman, P. K.; Townsend, A. J.; Morrow, C. S. Role of Glutathione S-Transferase P1-1 in the Cellular Detoxification of Cisplatin. *Mol. Cancer Ther.* **2008**, *7* (10), 3247–3255.
(93) Checa-Rojas, A.; Delgadillo-Silva, L. F.; Velasco-Herrera, M. del C.; Andrade-Domínguez, A.; Gil, J.; Santillán, O.; Lozano, L.; Toledo-Leyva, A.; Ramírez-Torres, A.; Talamas-Rohana, P.; et al. GSTM3 and GSTP1: Novel Players Driving Tumor Progression in Cervical Cancer. *Oncotarget* **2018**, *9* (31), 21696–21714.
(94) Lu, H.; Lei, X.; Zhang, Q. Moderate Activation of IKK2-NF-KB in Unstressed Adult Mouse Liver Induces Cytoprotective Genes and Lipogenesis without Apparent Signs of Inflammation or Fibrosis. *BMC Gastroenterol.* **2015**, *15*, 94.
(95) Jones, J. T.; Qian, X.; van der Velden, J. L. J.; Chia, S. B.; McMillan, D. H.; Flemer, S.; Hoffman, S. M.; Lahue, K. G.; Schneider, R. W.; Nolin, J. D.; et al. Glutathione S-Transferase Pi Modulates NF-KB Activation and pro-Inflammatory Responses in Lung Epithelial Cells. *Redox Biol.* **2016**, *8*, 375–382.
(96) Crispe, I. N. Hepatocytes as Immunological Agents. *J. Immunol.* **2016**, *196* (1), 17–21.
(97) Blair, H. A. Dimethyl Fumarate: A Review in Moderate to Severe Plaque Psoriasis. *Drugs* **2018**, *78* (1), 123–130.
(98) Yadav, S. K.; Soin, D.; Ito, K.; Dhib-Jalbut, S. Insight into the Mechanism of Action of Dimethyl Fumarate in Multiple Sclerosis. *J. Mol. Med. (Berl).* **2019**, *97* (4), 463–472.
(99) Bruck, J.; Dringen, R.; Amasuno, A.; Pau-Charles, I.; Ghoreschi, K. A Review of the Mechanisms of Action of Dimethylfumarate in the Treatment of Psoriasis. *Exp. Dermatol.* **2018**, *27* (6), 611–624.
(100) Carlström, K. E.; Ewing, E.; Granqvist, M.; Gyllenberg, A.; Aeinehband, S.; Enoksson, S. L.; Checa, A.; Badam, T. V. S.; Huang, J.; Gomez-Cabrero, D.; et al. Therapeutic Efficacy of Dimethyl Fumarate in Relapsing-Remitting Multiple Sclerosis Associates with ROS Pathway in Monocytes. *Nat. Commun.* **2019**, *10* (1), 3081.
(101) Mills, E. A.; Ogrodnik, M. A.; Plave, A.; Mao-Draayer, Y. Emerging Understanding of the Mechanism of Action for Dimethyl Fumarate in the Treatment of Multiple Sclerosis. *Front. Neurol.* **2018**, *9*, 5.
(102) Erstad, D. J.; Cusack, J. C. J. Targeting the NF-KappaB Pathway in Cancer Therapy. *Surg. Oncol. Clin. N. Am.* **2013**, *22* (4), 705–746.

Contributions from Collaborators

Jesse Brown, André Paquette and members of Dr. Christopher Boddy's lab (Department of Chemistry, University of Ottawa) synthesized VSe1, VSe1-28 and the analog probes (VSe1-54: active probe and VSe1-56: inactive probe).

Dr. Ramya Krishnan performed the plaque assay experiments in figure 7a (section 3.1).

The primary hepatocytes used in figure 11-13 (section 3.2) were isolated by Conor O'Dwyer from Dr. Morgan Fullerton's Lab (Department of Biochemistry, Immunology, and Microbiology, University of Ottawa).

Anabel Bergeron assisted with the experiment in figure 11 (section 3.2).

Dr. Ramya Krishnan assisted with the experiments in figure 15b and c (section

Naveen Haribabu conducted the experiment in figure 15d (section 3.3).

The click-chemistry experiments in figures 16-18 (section 3.3) were performed using protocols developed by members of Dr. John Pezacki's lab (Department of Chemistry, University of Ottawa).

Andrew Chen and Anna Jirovec assisted in the *in vivo* experiment in figure 19-20 (section 3.4).

Dr. Rozanne Arlunanadam assisted with the IVIS analysis in figure 20 (section 3.4)

Curriculum Vitae

EDUCATION

‘17/9-present **Master’s of Science in Microbiology and Immunology**, University of Ottawa
*Queen Elizabeth II Graduate Scholarship in Science and Technology***:** $15,000 per year
Admission Scholarship: 85% average in Undergraduate Studies, $7500 per year
Mitacs CanPRIME Intern
Degree Status: In Progress

Masters thesis title: “Viral Sensitizers Potentiate Infection of Cancer Cells via NF-kappaB.” Investigating the mechanism of action of small chemical molecules termed “Viral Sensitizers” that potentiate the infection of cancer cells by oncolytic viruses. P.I: Dr. Jean-Simon Diallo

‘12/9-17/4 **Honours B.Sc. in Biomedical Science**, University of Ottawa
Entrance Scholarship: 90% average in grade 12, $12 000 value
Undergraduate Research Scholarship: Demonstrated research skills and involvement in extracurricular activities of a scientific nature, $10,000 value
Loblaws Scholarship: Demonstrated exceptional roles in volunteer activities and hold a minimum academic average of 70%: $1500
Degree Status: Complete

Honours thesis title: “Optimization of Cytoviva Hyperspectral Live Cell Imaging System.” Developed a new technique adapting the Cytoviva Hypspectral Microscope used for detection of nanoparticles in cells and tissue to include live cell imaging capabilities to allow for real-time imaging of nanoparticle interactions with living systems. P.I.: Dr Sabina Halappanavar

Publications

2020/01 Clarke L., Pelin A., Phan M., Wong A., *The effect of environmental heterogeneity on the fitness of antibiotic resistance mutations in Escherichia Coli*, Evolutionary Ecology 2020, doi: https://doi.org/10.1007/s10682-019-10027-y. Epub 2020 Jan 7

2018/09 Phan M.[*] and Watson M. F.[*], Alain T.[$] and Diallo JS[$] *Oncolytic Viruses on Drugs – For Higher Therapeutic Efficacy*, ACS Infect Dis. 2018 Oct 12;4(10):1448-1467. doi: 10.1021/acsinfecdis.8b00144. Epub 2018 Sep 12

EMPLOYMENT

’16/9 – ‘16/12 **Biosafety Risk/ Policy Analyst -**
Duties include performing literature reviews for risk assessment of biological pathogens as well as coordinating PHAC resources to meet WHO collaboration objectives.
Supervisor: Dr. Anastasia Rogaeva
Public Health Agency of Canada Center for Biosecurity

‘16/5-’16-/9 **Research Assistant** –
Optimization of HPAEC-PAD system for quantification of conjugated and unconjugated

polysaccharide content for Haemophilus influenza B vaccine samples P.I.: Dr. Richard Siggers
Health Canada Bacterial and Combination Vaccines Division

‘15/01 – ‘15/08 **Research Assistant-**
Studied the Mechanism of Toxicity of 14 SiO2 particles that were different sizes and contained different surface modifications after exposure to cells in-vitro. Looked at gene expression data to determine biological pathways that were affected,
P.I.: Dr. Sabina Halappanavar
Health Canada Mechanistic Studies Division

‘12/06-‘13/08 **Research Assistant-**
Studied protein interactions and deducing structure activation of DGKz binding capabilities to other proteins including Rho family proteins.
P.I.: Dr. Stephen Gee
University of Ottawa Cellular and Molecular Medicine

EVENT PARTICIPATION

Poster Presentation, BiocanRx: Summit4CI 2019/10/22 Presented abstract and poster on Viral Sensitizers Potentiate Infection of Cancer Cells via NF-kappaB

Oral Presentation, BMI Seminar Day, University of Ottawa, 2019/02/21
BMI Seminar Day oral presentation on Viral Sensitizers Potentiate Infection of Cancer Cells via NF-kappaB

Poster Presentation, Ottawa Hospital Research Institute Research Day, 2018/11/08
Presented abstract and poster at Research day on Viral Sensitizers Potentiate Infection of Cancer Cells via NF-kappaB

Poster Presentation, BiocanRx: Summit4CI 2018/10/28 Presented abstract and poster on Viral Sensitizers Potentiate Infection of Cancer Cells via NF-kappaB

2 Minute Speed Poster Presentation, BiocanRx: Summit4CI 2018/10/28 Presented a 2 minute oral presentation on Viral Sensitizers Potentiate Infection of Cancer Cells via NF-kappaB

Poster Presentation, BMI Poster Day, University of Ottawa, 2018/05/03
Presented abstract and poster on Viral Sensitizers Potentiate Infection of Cancer Cells via NF-kappaB

Poster Presentation, Keystone Symposia: Cancer Immunotherapy, Combinations, 2018/03/27
Presented abstract and poster on Viral Sensitizers Potentiate Infection of Cancer Cells via NF-kappaB

Poster Presentation, Ottawa Hospital Research Institute Research Day, 2017/11/09
Presented abstract and poster at Research day on Viral Sensitizers Potentiate Infection of Cancer Cells via NF-kappaB

Poster Presentation, Health Canada Science Forum, 2016/02/26-2016/02/27
Presented abstract and poster at the Science forum on Mechanisms of Toxicity of exposure of SiO2 nanoparticles to cells in-vitro

Participant, Scinapse, 2015/11
Participated in an undergraduate science case competition developing an innovative technology for the agricultural industry to improve crop yields and pest management.
Participant, Health Canada Science Forum, 2015/02/26-2015/02/27
Attended the conference where researchers and students in Health Canada presented their research findings that are

fuelling regulatory action.

Participant, Sanofi Aventis BioGENEius Competition, 2011/09/01-2012/03/01
Science competition that involved the development of a proposal as well as testing portential chemotherapeutic properties of two compounds extracted from Devil's Club, a plant related to North American Ginseng on various human cancer cell lines including lung, colon and ovarian cancers.

AWARDS

- 5th Place, Sanofi BioGENEius Competition, St. Joan of Arc Secondary School, **2012**
- Undergraduate Research Scholarship, University of Ottawa, $10,000, **2012-2013**
- Admission Scholarship, Undergraduate Studies, University of Ottawa, $12,000, **2012-2017**
- Dean's Honour List, University of Ottawa, **2012-2017**
- Admission Scholarship, Graduate Studies, University of Ottawa, $7500, **2017-2018**
- Excellence Scholarship, Graduate Studies, University of Ottawa, $7500, **2018-2019**
- Queen Elizabeth II Graduate Scholarship in Science and Technology (QEII-GSST), Graduate Studies, University of Ottawa, $15,000, **2018-2019**
- 3rd Place, Oral Presentation, BMI Seminar Day, University of Ottawa, **2019**

COMMUNITY AND VOLUNTEER ACTIVITIES

- '18/03 – present Operations, Logistics and Advanced First Aid Provider, Canadian Ski Patrol
    - '19/04 Mont Cascade Male Recruit of the Year (2018-2019)
- '16/09 – 2018/09 Let's Talk Science, University of Ottawa
- '15/5 – '09/17 Volunteer, Ottawa Hospital General Campus
- '15/9 – '17/04 Volunteer, University of Ottawa Office of Campus Sustainability